Cell Settling, Migration, and Stochastic Cancer Expression Suggest Potassium Flux Per H^+- Sensitive KCN Members Associated with Oncogenes and Histone/DNA Modulators Potentially Initiates pH-Reversal

Marie E. Beckner[1]*

1 Brain Health Research Institute at Kent State University; mbeckne1@kent.edu
* Correspondence: mbeckne1@kent.edu

ABSTRACT

Attraction of glioblastoma cells to potassium was suspected when cells clustered around dying cells and they migrated towards serum (high [K^+]) and a positive potassium gradient. Potassium channel proteins (KCN family, 90 members) mediating altered transmembrane flux may provide K^+ that releases H^+ bound to inner membranes in cancer cells for cytosolic proton transfer (possibly Grotthuss) to extrusion sites. Cell settling and migration assay results led to collection of 70 studies, unbiased by authors for inclusion of KCN genes, that detected KCN differentially expressed genes (DEG). Of 53 KCN DEG found among 29 malignancies, 62.3% encoded H^+-sensitive proteins. KCN DEG encoding H^+-sensitive proteins were more prevalent in 50 studies involving one or more of 8 categories (7 oncogenes and histone/DNA modifiers) versus those with none, p = 0.0325. Pertinent genes for lactate outflow, etc. had relatively normal expressions. Brain tumors in REMBRANDT (database) showed altered expression of KCN genes encoding H^+-sensitive proteins in glioblastomas versus less invasive oligodendrogliomas of patients on anti-seizure medications, with less *KCNJ16* /Kir5.1, $p = 5.32 \times 10^{-8}$. Altered H^+-sensitive potassium flux via the KCN family downstream of oncogenes and histone/DNA modifiers putatively incites proton transfers for H^+ release during pH reversal in cancer.

Keywords: Potassium Channels, Potassium, *KCNJ16, KCNN4, KCNMA1*, H^+-sensitivity, pH-reversal, Differential Gene Expression, Grotthuss Proton Transfer, Oncogenes

Graphical Abstract

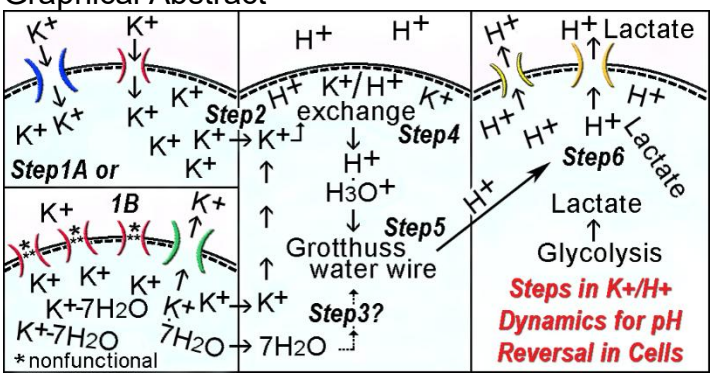

Graphical Abstract Legend: Steps in K^+/H^+ Dynamics for pH Reversal in Cells. Step1. Potassium ions accumulate near cell membranes if (A) inward flow channels bring in more

K^+ than normal or (B) if the diffuse low outward flow channels are nonfunctional with compensation by channels in a few locations that are high flow requiring contributions of solvated potassium (K^+-$7H_2O$) from deeper cell regions. Step2. K^+ reaches the inner cell membrane where H^+ is bound diffusely to its negative charges. Step3. As K^+-$7H_2O$ desolvates (for channel exit or membrane binding), the release of $7H_2O$ may augment or form Grotthuss water wires near inner membrane surfaces. Step4. At the inner membrane K^+ exchanges with H^+. As H^+ is released, it becomes H_3O^+ and diffuses into the cytosol. Step5. H_3O^+ enters a Grotthuss water wire that enables rapid proton transfer (conformational) to H^+ exit sites. Step6. H^+ leaves the cell with lactate or it exits via other H^+ extruders. The cytosolic pH increases and the external pH decreases for pH reversal.

1. Introduction

1.1. General

Potassium flux is already known to maintain cell membrane potential in all cells, to assist volume changes in migrating cells, and permits neurons to fire action potentials as they release potassium that is buffered by glial cells. Potassium, as cytoplasmic monovalent cations, is now proposed to also exchange with fixed H^+ on inner membranes to incite proton transfer and extrusion for shifts in pH that favor tumor cell survival and invasion. If so, then K^+/H^+ cation exchange may help to explain the attraction of glioblastoma cells (highest grade malignant glial tumors) to axons in CNS white matter tracts and peripheral nerve fibers [1,2] that release K^+ via axonal action potentials as well as their growth factors. Experiments performed to study cell morphology and viability in a microaqueous environment suggested malignant cell attraction to K^+. Glioblastoma cells tightly clustered around single dying cells, putatively releasing their cytoplasmic stores of K^+. It had already been observed that glioblastoma cells migrated towards fetal bovine serum, known to have levels of 5-15 mM K^+ [3]. This clustering behavior was similar to how glioblastoma cells rim necrotic foci (pseudopalisading) which is a typical histologic feature of these tumors [4-6]. Also, pseudopalisading glioblastoma cells have an enhanced migratory phenotype [6,7]. Additionally, in regard to reversal of pH, i.e. intracellular pH (pHi) is greater than extracellular pH (pHe), there are related metabolic features reported for benign astrocytic cells, such as (*i*) an increase of their intracellular pH with neuronal stimulation, possibly triggered by membrane K^+ redistribution during depolarization [8,9]. Also, intracellular alkalinization detected in benign mammalian astrocytes has been attributed to their uptake of potassium released by repetitive neuronal firing of action potentials *in vivo* [10] as astrocytic cell membranes depolarize. Also, (*ii*) the rate of glycolysis (inhibited by lactic acid produced in hypoxia) is stimulated by changes in intracellular [H^+] rather than [HCO_3^-] in astrocytes [11]. Cytoplasmic alkalinization in malignant and transformed cells occurring via efflux of protons resulting in extracellular acidosis has been attributed to mechanisms involving ion transporters, pumps, exchangers, etc. with the “active” ones requiring ATP [12-19]. Redistribution of K^+ has been previously suggested as being a contributing factor in tumor cell alkalinization [12] and pH-sensitive ion channels, including those for K^+, have been mentioned as “sensors” in descriptions of pH reversal [13,14,16,17]. Data in this study suggests the possibility of potassium flux as playing a role in glioblastoma cell behavior.

The large size of the KCN (potassium channel) family with its complex interactions among family members, an extensive complement of non-family regulators, functional reliance on contents of biological milieus, and a wide distribution across the genome serving as a relatively large target for genetic damage, were characteristics that supported further investigation of potential anomalous potassium flux in cancer through gathering data on this family in a stochastic manner. Retrieval of reported data unbiased for KCN gene expression in tumors allowed retrieval of data on differentially expressed genes (DEG) of KCN family members and associated non-KCN DEG in 70 studies of many types of cancer to provide an overall view of anomalous potassium flux in cancer. Also, a brain tumor database REMBRANDT [20,21], and a published whole genome analysis of 6 glioblastoma cell lines, Patil, et al. [22], were queried for data on KCN genes. The H^+-sensitivity of a large proportion of the KCN family members detected and the high likelihood of K^+ as a replacement cation for H^+ suggest that potassium ion flux across plasma membranes or accumulation near them may play a role in the pH reversal commonly seen in malignancy. Deregulated, passive inward channel flux (without requiring ATP) or loss of normal diffusely distributed outward K^+ flow (necessitating focally concentrated outward flow as needed) leading to accumulations of K^+ ions at inner cell membranes with H^+ bound to fixed anions potentially leads to K^+/H^+ exchange to release H^+ as an initial step leading to pH reversal.

1.2. Cytosolic Proton Transfer Related to K^+ and Hydration

The proposed K^+ replacement of bound H^+ would augment adjacent hydronium ion (H_3O^+) accumulation which can be seen at water-lipid interfaces [23], such as along inner cell membranes. This putatively sets the stage for pH reversal via subsequent steps. The mobility of unbound H^+ (H_3O^+ at 36.2×10^{-4} cm^2 $V^{-1}s^{-1}$) is very high compared to other univalent cations such as K^+ and Na^+ [24]. In immortalized human embryonic kidney cells, H^+ diffusion through the cytosol occurred 60-fold faster than when limited to the inner plasma membrane surface, i.e. 0.6 $\mu m s^{-1}$ versus 0.01 $\mu m s^{-1}$ [25]. In cardiac myocytes a comparable high speed of cytoplasmic H^+ distribution, 0.7 $\mu m s^{-1}$, has been detected. This was based on using HCl in KCl (140 mM) solutions (pH 3.0) for acid diffusion studies with membrane acid transport simultaneously inhibited [26]. Another study has shown dissociation of HCl in a microaqueous environment so that the acid's protons were each transferred to a neighboring water molecule and then another in clusters of $HCl(H_2O)_n$, where n=1 to 5 and 7. With the addition of a fifth and sequential seventh water molecule, the covalent H-Cl bond transitioned to the contact ion pair, $H_3O^+Cl^-$, plus free hydrogens. The $HCl(H_2O)_5$ and $HCl(H_2O)_7$ clusters were spontaneously dissociated structures with contact ionic bonds [27]. Thus, H_3O^+ may be distributed to the cytosol after putative K^+/H^+ exchange on inner membranes and after spontaneous dissociation of acids (multiple types in cancer cells) within cytosols, possibly microaqueous in nature.

Cytosolic proton transfer has been previously attributed to small molecules, such as taurine, carnitine, carnosine, or homocarnosine, behaving as mobile buffers that shuttle H^+ to enable cytosolic proton transfers [26]. However, proton transfers from H_3O^+ may also be enabled by a rapid mechanism consistent with behavior described originally by C.J.T. Grotthuss in 1806 [28] that fits with this scenario. Proton transfers may occur within the cytoplasm via H-bonded complexes, possibly involving Eigen and Zundel cations,

$H_9O_4^+$ and $H_5O_2^+$, respectively, or by wires of protonated water molecules linked by interconversions in a manner that is consistent with the behavior of salts and water observed between electrodes in the early 1800s. According to the Grotthuss mechanism, due to interconversions, a proton that enters a chain or matrix of water molecules is not the same proton that exits elsewhere [24,28-34]. The conformational changes for proton transfer in water can occur as a rapid falling domino effect. Thus, a wide-reaching, flexible delivery of cytoplasmic protons to membrane extruders may result. Putative K^+/H^+ exchange that frees bound H^+ from cell membranes would generate water cations because free H^+ becomes H_3O^+ almost immediately which then potentially interacts with cytosolic chains of $H_9O_4^+$ and $H_5O_2^+$ or protonated water wires for distribution. Extended hydrogen bonded chains that undergo rapid conformational changes potentially mediate proton release distal from the point of proton entry much faster than by simple diffusion. H^+ can be transferred in this manner to cell exit sites, such as exchangers swapping out H^+, monocarboxylate transporters venting lactate that requires accompanying protons, one for one, exiting through gap junctions, etc. This type of rapid transfer of H^+ in water has also been referred to as a "proton jump" [35]. Although in a previous study, the Grotthuss mechanism was not thought to mediate extracellular tumor acidity [36], it was not ruled out as occurring intracellularly. The Grotthuss mechanism describes a potential almost "everywhere, all at once" strategy for delivery of free protons to cell exit sites as needed. Therefore, putative inner membrane proton replacement by K^+ to initiate formation of H_3O^+ is probably a highly regulated process in normal cells, consistent with the large, complex KCN family controlling K^+ flux. Loss of regulation with differential expressions of KCN genes in malignant cells offers one approach to begin investigating the potential ionic dynamics of tumor cells related to pH reversal. Genetic damage of the KCN family members or altered regulation by activated oncogenes and/or modified histones/DNA putatively plays a role in pH reversal for tumor cell survival in glycolytic cells producing lactate if it cannot be removed in another way (such as by forming intracellular glycogen).

Also, potassium has a relationship with water that is important. A lack of water due to poor circulation, cell crowding, pressure from fibrotic, stiff surroundings, etc., especially during invasion, produces generalized microaqueous conditions within cancer cells. Regional hydration may be possible by redistribution of water molecules loosely associated with solvated ions, such as potassium, K^+-$7H_2O$. Redistribution of water via its association with potassium may enhance Grotthuss type protonated water structures close to the inner surface of cell membranes but this is unknown.

Volume changes related to ions are known to occur in malignant cells during division and migration. Protrusion of pseudopodia or invadopodia (increased volume in cell projections) and shrinkage of their retracted rear cell bodies that are accomplished with oscillations of cell membrane potential and osmotic changes via KCl uptake and release per potassium and chloride channels, along with aquaporin participation, and possibly with K^+ refilling/recycling [37-42]. The spontaneous dissociation of acids generated in a microaqueous environment undergoing changes in the number of water molecules available for solvation of acids into ion pairs [27], along with rapid proton transfers via the Grotthuss mechanism, putatively enhance proton delivery to the leading edge of migrating cells for efflux to preserve glycolysis from lactate inhibition. Pseudopodia are glycolytic as indicated by proteomic analysis [43]. Also, enhanced proton release from cancer cells

leads to extracellular acidosis that aids tumor invasion via activation and induced expression of metalloproteases for matrix degradation [44-50]. Thus, tumor cells can escape poorly perfused or crowded, microaqueous tissue regions via pH reversal relying on proton release putatively following K^+/H^+ exchange as the initiating step.

1.3. Need for Proton Extrusion in Cancer

The metabolism of cancer cells produces excess protons [51]. In addition to acids produced by metabolic pathways, free radicals generated are also acidic [52-54]. Extrusion of protons avoids cytoplasmic acidosis within tumor cells, so this not only protects glycolysis via lactate release but also prevents cytochrome c-mediated activation of caspase-3 to stop apoptosis [55], protects gap junctions to maintain cell to cell exchange of ions and metabolites [56-59], and increases the activity of ATP citrate lyase (ACLY) that connects lipid and carbohydrate metabolism. The optimal pH of ACLY is in the 8.5 - 8.7 range [60,61]. ACLY's removal of citrate (inhibitor of glycolysis) is protective in glioblastomas [62]. ACLY also regulates histone acetylation in response to growth factor stimulation [63,64]. Thus, proton removal from the cytoplasm favors cell fitness in tumor cells [65] as well as enabling migration for their escape from adverse conditions.

1.4. Complexity of K^+ Flux

As mentioned earlier, direction (inward or outward) and strength of K^+ channel flow is complex. The KCN family has more than 90 members [66,67]. Complexity is also due to numerous regulators (in addition to those encoded by KCN genes) present in biological milieus. Regulators, gating agents, and cofactors, include polyamines, voltage, H^+, Ca^{2+}, Mg^{2+}, Zn^{2+}, Na^+, ATP, miR-133b, reactive oxygen species (ROS), reactive nitrogen species, reactive sulfur species, nitric oxide, hydrogen sulfide, hypoxia, hyperglycemic levels of glucose, nucleotides, protein kinase A, protein kinase C, protein kinase G, guanosine-triphosphate-binding proteins (G-proteins), regulator of G protein signaling (RGS) proteins, phosphatidyl inositol 4,5 bisphosphate (PIP2), steroids (estrogen, testosterone, etc.), cholesterol, sulfonylurea, β-hydroxybutyrate, hypoxia inducible factor 1α, the 14-3-3 protein, β-coat protein, dipeptidyl aminopeptidase-like proteins, the neurotransmitter GABA, NAD(+), NADP(+), NADH, NADPH, glutathione, glutathione disulfide, mechanical stimulation, cell cycle progression, products of *LINGO1, 2*, and BKγ1-4 encoded by *LRRC26*, *52*, *55*, and *38* [68-90]. Also, 19% (or more) of proteins targeted by small-molecule drugs used to treat numerous diseases include ion channels [91-93]. Thus, the complexity of K^+ channel flux hinders planning studies to identify specific regulatory mechanisms lost in cancer.

Complexity is further enhanced because the ROS affecting potassium channels are generated via multiple sources such as (*i*) mitochondrial respiratory chain electron transport redox reactions [84,94-97], as well as (*ii*) the NOX family (6 members) of NADPH oxidases [71,94,95,98]. ROS from these sources can reach the cytoplasm [95]. Colon carcinoma cell lines with acid-resistant growth showed significantly upregulated mRNA levels of *NOX1* encoding NADPH oxidase 1 [99] that produces ROS. Interestingly, isolated intact respiring rat brain mitochondria increased ROS production when their

medium was alkalinized which raises the possibility that this could also happen in alkaline cytosol of cancer cells as pH reversal develops [100].

The widespread chromosomal distribution of the 90 (or more) KCN genes plus those of the numerous non-family regulators suggests that failsafe redundancies for genomic damage may exist that increase the chances of selecting cells that can maintain levels of K^+ for survival but not in a manner that is optimal for differentiation and normal activity. Numerous genomic/expression scenarios selected in rapidly dividing tumor cells may work around mutational losses or gains with adaptations so that cells maintain their K^+ levels for supporting membrane integrity and are putatively also able to exchange with fixed H^+ on inner membranes in invasive cells to incite pH reversal. Not only do the monocarboxylate transporters, MCT1 and MCT4, transport negatively charged lactate molecules coupled one-for-one with protons across the cell membrane [101], protons can also be extruded from cancer cells via Na^+/H^+ exchanger family members, ATP driven pumps, etc. as detected in numerous studies [102] and in earlier cited studies. Therefore, pertinent genes among the non-KCN DEG are also of stochastic interest in this study.

Mediators of potassium flux, despite their complexity, and the relationship of K^+ and H^+ at cell membranes should be clarified. K^+ accumulation due to a lack of normal diffuse K^+ efflux or buildup of K^+ around large outwardly conducting potassium channels, could putatively exchange with bound protons on inner membranes or it could happen with deregulated inwardly channeled K^+ flux (possibly with K^+ being recycled for refilling as needed if efflux becomes excessive). These events with K^+ could occur without affecting the functions of key structural proteins that would be seen if Na^+ was used [103]. Although both potassium and sodium are the available monovalent cytoplasmic cations to potentially replace membrane bound H^+, there should be a preference for potassium due to its weaker binding of water compared to sodium ions. Less energy is required to displace water from potassium than sodium [104,105]. K^+ ions permeate their membrane channels in a desolvated ('naked') state rapidly so at this point they release their associated water molecules. Also, there is exclusion of smaller Na^+ ions that have stronger water binding from the channels selective for potassium [106-108]. Also, compared to Na^+, K^+ is better at maintaining solubility of cell components containing carboxylates and phosphates to help explain its higher concentration in the cytoplasm [105,109]. Numerous KCN family scenarios may be involved with anomalous potassium flux in cancer. Deregulated diffuse, passive K^+ entry, such as the *KCNJ*/Kir (inwardly rectifying, also bidirectional, flux), or disrupted K^+ outflow via KCN family members, such as the numerous members of the Kv (voltage dependent) KCN subfamily and the *KCNK*/K2P (tandem two pore "leak") subfamily members, may be important. Also, Ca^{2+} activated potassium channel families, *KCNM*/BK for *MA1* plus other members that regulate it, and the *KCNN*/SKs and *KCNN4*/IK family members that mediate outward flow, with BK and IK providing large and medium flux, respectively, likely play important roles due to their relatively high flow rates. High flow rates may indicate localized versus diffuse K^+ release and in addition these channels can be affected by the release of calcium from cancer cells. However, all types of K^+ transits may be involved and a role for Na^+ in releasing H^+ cannot be ruled out given the abnormally high levels of Na^+ found in tumor cells [110-112]. Additionally, some K^+ channels are influenced by Na^+.

Loss of normal cellular responses to pH via loss of KCN channels that function with H^+-sensitivity may alter cells in cancer. Malignant cell behavior suggests that tumor cells

respond opportunistically to sources of K^+, thus achieving levels of K^+ ions at inner membrane surfaces or flow rates that force K^+/H^+ exchanges that initiate pH reversal to improve tumor cell survival and invasion. Deregulated potassium uptake by glioblastoma cells may occur from the available sources *in vivo* as briefly mentioned earlier. These (with additional information) include (*i*) neurons and axons firing action potentials where K^+ is released to maintain electroneutrality, (*ii*) dying cells, including red cells (K^+, 80 - 120 mmol/L) and necrotic tissue releasing cytoplasmic K^+ [113-116], and (*iii*) damaged blood vessels leaking plasma (potassium, 3.8 - 5.0 mmol/L [117]). Importantly, deregulation via loss of a K^+ channel is illustrated by showing in an experimental mode that the loss of H^+-sensitive *KCNK1* (among a small group of genes identified) was advantageous for breast cancer cell survival of induced necrosis I [118].

1.5. Biological Milieu Constituents to Consider in Studying K^+ Flux

Biological milieus contain many factors regulating potassium channels as described earlier. More details to consider in studying these channels in cancer are listed here. Serum includes calcium (2.30 - 2.74 mmol/L), magnesium (0.74 - 1.23 mmol/L), phospholipids (1.50 - 3.80 g/L), sodium (136 - 142 mmol/L, adult plasma value) [117], and polyamines (0.1 - 1.0 μM, fetal bovine serum [3]). Magnesium and polyamines (positively charged) are important gating molecules of inwardly-rectifying *KCNJ*/Kir family channel members [119]. Removing fetal bovine serum from the medium of cultured fibroblasts resulted in decreased potassium intracellularly [120]. Also, fetal bovine serum lost the ability to depolarize the resting membrane potential of airway smooth muscle cells after dialysis against distilled water but its freeze-dried dialysate retained this ability after reconstitution [121], consistent with potassium as the responsible constituent. Elevations of polyamines have been reported in cerebrospinal fluid in instances of brain tumors [122] and are in the tumor-associated myeloid cells that infiltrate glioblastomas [123]. Also, polyamines are formed when L-arginine, released from apoptotic bodies, is metabolized by Arg1 [124]. Other agonists and modifiers in biological milieus within regions of necrosis include heme and other hemoglobin break-down products [125,126]. Tumor associated macrophages are influenced to promote malignancy (increased expression of *ARG1, VEGF*, *TGFB*, etc.) by lactate, presumably shuttled from cancer cells, such as seen in transitional cell carcinoma of the bladder, gastric cancer, and others [127-129]. As mentioned earlier, many types of tumors outside of the CNS exhibit perineural invasion [130-133].

There may be reciprocal gain of potassium by tumor cells from nerves and axons as the tumor cells provide lactic acid back to neurons and axons as energy substrate for a mutually beneficial metabolic interchange. If constituents of biological milieus modulate K^+ transits indirectly via their effects on downstream potassium channel activity, then sources of extracellular potassium may attract tumor cells to fulfill their needs. Although specific sources of K^+ *in vivo* have not been generally appreciated for influencing the behavior of cancer cells, they may be important as loss of regulation required for complex normal cell functions occurs in dedifferentiation.

1.6. Highlighted Findings in This Study

Fetal bovine serum (with and without hepatocyte growth factor (HGF)) had been seen previously to promote glioblastoma cell migratory behavior, including protrusion of pseudopodia through 3 μm filter pores, migration of whole cells through 8 μm filter pores, and invasion through a Matrigel matrix and rat brain tissue slices, often under glycolytic conditions [43,62,134-136]. Glioblastoma cell clustering around dying cells and their migration to serum, with compelling background information on astrocytes, suggested that anomalous potassium flux could play a role in tumor cell behavior. Cell migration of multiple glioblastoma cell lines to serum among eight tested in this study and the response in a separate assay to a positive gradient of potassium supported abnormal membrane flux or lack of it via some of the potassium channels as a putative aid for tumor cells.

The large scope of K^+ channel candidates for loss or gains in expression and the potential influence of numerous known modulators were daunting. However, stochastic analysis of numerous published studies to gather unbiased data was reasonable to survey as many contributing factors as possible at this point. Incidentally detected KCN DEG and related non-KCN DEG in genomic landscapes of experimental cancer scenarios and databases permitted a search for pertinent functional similarities among the DEG of the large KCN family. Meta-analysis of 70 malignant (or models related to cancer) expression studies found that the studies fell into 8 categories of 7 oncogenes and histone/DNA modifiers. These categories were determined by the authors of the expression (E), E1-E70, studies if related DEGs were also detected in any of the 70 studies. The studies included 29 types of malignancy (breast, lung, brain, etc.) that incidentally detected one or more KCN DEG. *KCNMA1* and *KCNN4* were the most frequently detected KCN DEG. The encoded products of the 53 detected KCN DEG are predominantly H^+-sensitive (62.26%) and 52 (74.3%) of the 70 studies identified at least one H^+-sensitive KCN DEG. There was a significant propensity for KCN DEG to encode H^+-sensitive family members in the studies among the 8 categories of 7 oncogene and histone/DNA modifier related scenarios compared to the 20 studies in “no category”. A concurrent search of the National Institutes of Health REpository of Molecular BRAin Neoplasia Data (REMBRANDT) database for expression levels of KCN genes in invasive glial brain tumors (glioblastomas versus oligodendrogliomas that are less invasive) of patients on anti-seizure medications showed a significant decrease in *KCNJ16* and trends in three other KCNs also encoding H^+-sensitive proteins in glioblastomas. Correlation with a genomic study of 6 glioblastoma cell lines [22] confirmed relatively decreased RNA expression of *KCNJ16* among KCN genes and provided additional relevant genomic data. Altered expression of KCN family members, possibly with compensatory activities of other KCNs and non-KCN factors, may provide quantities of K^+ sufficient for preservation of cell membrane integrity and putative K^+/H^+ exchange on inner membranes to release bound H^+. As an initial step K^+/H^+ exchange may incite pH reversal and invasive behavior.

2. Materials and Methods

2.1. Materials and Cell Culture

All chemicals and reagents were from Sigma-Aldrich (RRID:SCR_008988), St. Louis, MO, USA, unless otherwise stated. Anti-Met was from Cell Signaling Technology, Beverly, MA, USA, Cat# 4560, RRID:AB_2143887), 1:1000 dilution, for the beta Met

subunit (145 kDa). Diff Quik (Allegiance, McGaw Park, IL, originally developed by Harleco, now a product line of Sigma-Aldrich (RRID:see above) is sold as Hemacolor Solutions I, II, and III. It is also sold by many medical suppliers with reference to Harleco and/or the cytology literature [137]. A172 (RRID:CVCL_0131), C6 (TKG Cat# TKG 0242, RRID:CVCL_0194), F98 (ATCC Cat# CRL-2397, RRID:CVCL_3510), LN18 (RRID:CVCL_0392), LN229 (RRID:CVCL_0393), T98G (RRID:CVCL_0556), U87 (RRID:CVCL_0022), and U373 (RRID:CVCL_2219) glioblastoma/astrocytoma cell lines (human (A172, LN18, LN229, U87, U373) and rat (F98 and C6)) were obtained from the American Type Culture Collection, Manassas, VA, USA RRID:SCR_021346. No cell lines were generated from live animals for this study by the author. The cells were maintained in Minimal Essential Media (MEM) Eagle(138) or alpha-MEM (Cellgro, Mediatech, Herndon, VA, USA) with 10% fetal bovine serum, FBS, (Invitrogen, Carlsbad, CA, USA).

2.2. Statistics Section

Pearson product-moment correlation, R, also termed cor (with *p* values for a true correlation being greater than 0), the Student's t-Test, paired and unpaired, and Fisher's Exact Test for Count Data, in either Excel Statistics (RRID:SCR_017294) or the R Project for Statistical Computing (RRID:SCR_001905) were used.

2.3. Databases

For general gene information, the National Institutes of Health database, https://www.ncbi.nlm.nih.gov , the Online Mendelian Inheritance in Man (OMIM) database, OMIM (RRID:SCR_006437), https://omim.gov , and GeneCards (RRID:SCR_002773) https://www.genecards.org/ were used. GeneCards was also used to obtain protein-protein interaction data. The Ensembl https://www.ensembl.org/ database (RRID:SCR_002344) was used to obtain information on the structure of genes, including features of exons and introns. The National Library of Medicine's PubMed database, https://pubmed.ncbi.nlm.nih.gov/ , was searched for the numbers of publications available using 2 and 3 word searches for subjects of interest. The Online Mendelian Inheritance in Man (OMIM) database was searched for KCN family member genes expressed in the nervous system with exclusion of genes uniquely expressed in heart, kidney, and other non-neural sites, and to identify their chromosomal loci (March 2019). The REpository for Molecular BRain Neoplasia DaTa (REMBRANDT) (RRID:SCR_004704), originally at the NIH, became part of the Georgetown Database of Cancer (G-DOC), https://sites.google.com/georgetown .edu/g-doc/home or via the G-DOC Hub platform at https://gdochub.georgetown.edu/ as a project of the Georgetown Lombardi Comprehensive Cancer Center, Washington, D.C., designed to provide translational research tools to the scientific community [20,21]. It was queried for gene expression on microarrays of KCN family members, selected genes important in cancer and brain tumors, and housekeeping genes. Medians of reporter probes for each gene were available in Adobe Flash (RRID:SCR_017258) readouts through 12/31/2020 (date of last service). Genomic sequence and expression results of 6 glioblastoma cell lines were obtained from the Supplemental Materials of Patil et al. [22].

2.4. Ethics Statement

No human subjects or animal experiments were used by the author in this study. Only commercially available human and rat cell lines were used i*n vitro* for laboratory studies. Published medical science manuscript information, mostly open access, with the authors of the studies following the guidelines of each their institutions, was also used for data.

2.5. Cell Settling with Fluid Removal Assays

Human glioblastoma cells (U87, LN229, A172, T98G) were maintained in routine culture conditions. On the day of each assay, cells were detached with trypsin and allowed to recover for 4 hours in MEM with 10% FBS at 37° C in a CO_2 tissue culture incubator. For each assay, a Cell Settling Chamber Kit (Neuro Probe, formerly Gaithersburg, MD, USA, Ph: (301) 417-0014, email info@neuroprobe.com), with 8 wells, each 7 mm in diameter, was assembled. A provided glass slide, 1 mm thick, 25 x 75 mm, was placed in the recessed bottom plate. A provided pre-punched piece of blotting paper, pre-moistened with PBS, a gasket, and the upper plate were stacked on top of it. Thumbnuts fitted on the top plate were securely hand tightened. Cells were centrifuged (500 rpm, 5 min) and resuspended with gentle pipetting, 500,000 cells per ml in culture media with 10% FBS. Cell suspensions were added, 50 microliters per well. After 30 minutes with media visibly absorbed out of the wells by the blotting paper, the chamber was disassembled, the slide was removed and stained with Diff Quik solutions, I, II, and III followed by 3 quick rinses in tap water in beakers. At least two replicate wells per cell line were prepared. Stained cells were examined microscopically. Cell vacuoles in U87 cells (single and clustered) were counted in the settled cellular monolayers. When vacuoles collectively had a diameter of at least one third of an average nuclear diameter in the same 100X microscopic field, the cell was counted as positive for vacuolization (surrogate indicator of degeneration). Cells were analyzed in a midline sweep of the 100X microscopic fields across the 7 mm width of each well. Pearson product moment correlation coefficient, R, determinations, were performed for the percentage of cells vacuolated versus the number of cells in each cluster. Morphological features, such as cell clustering, were noted. An Olympus BH2 microscope (Olympus Corp., Lake Success, NY, USA) with an Olympus FV II digital camera using Olympus Microsuite Five Software for Imaging Applications (Soft Imaging System, Lakewood, CO, USA) was used to capture the black and white images. An American Optical Spencer Microscope (Buffalo, NY, USA, sold to Reichert Technology, then Leica Microsystems, Inc. (Deerfield, IL (RRID:SCR_008960)) with an OptikamB9 Digital Camera 10 MegaPixels (Optika, www.optikamicroscopes.com, Via Rigla 32, 24010 Ponteranica (BG), Italy) with Adobe Photoshop v5.1 and Adobe Photoshop Elements 2024 for Windows (Adobe Systems Incorporated, San Jose, CA, USA (RRID:SCR_014199) was used to generate the color microscopic images.

2.6. Cell Migration Assays

Cells of A172, C6, F98, LN18, LN229, T98G, U87, and U373 glioblastoma cell lines were maintained in normal tissue culture conditions with half volumes of culture media

changed one day prior to each assay. Confluent cells were detached with trypsin on the day of assay and allowed to recover in media with 10% FBS for 2 hours at 37°C in a CO_2 tissue culture incubator. Cells were centrifuged (<500 rpm, 5 min) and resuspended at 2 million/ml with gentle pipetting in media for migration, MEM (includes 5.4 mM KCl [138] but it is 5.3 mM according to Thermo Fisher among its inorganic salts), with 0.1% bovine serum albumin (BSA). Chemoattractant/chemokinetic stimulants, recombinant hepatocyte growth factor (HGF) and/or FBS were added to the bottom wells (29-30 μl total volume) as indicated in Figure 2. The 48-well modified Boyden Chambers (Neuro Probe) were assembled with porous (8 μm diameter pores, 1,000 pores/mm^2, laser generated), air-dried polycarbonate filters, 8 μm thick (Neuro Probe), coated with 0.01% porcine gelatin (solution of 1 ml 10% acetic acid, 1 ml 1% gelatin (fully dissolved, no floating globules) from refrigerated stock (10%, gently warmed to liquify), and 98 ml H_2O). One corner of each filter was diagonally cut off sufficient for orientation before each assay. Cell suspensions were added to the upper wells, 60 μl each well. The chambers were incubated at 37°C for 5 hours in a CO_2 (5%) tissue culture incubator. Upon completion of the assay, each filter (easily disturbed by air flow) was removed by lifting one end with a pair of fine, curved tip tweezers, and then clamped into a large square plastic clip at the other end of the filter and then releasing the tweezers without disturbing any cell pellets. The filter attached to the large clip was stained with Diff Quik solutions (I-III) by hanging the filter by its attached clip on a metal weighing spatula placed over tops of beakers with Diff Quik solutions, followed by rinses in 3 different beakers of water using quick dips, and then carefully placed on a large glass slide (2" x 3") using tweezers and the clip with migrated cells on the downside of filters. Unmigrated cells were gently removed from the upper side of a filter with cotton swabs or Kimwipes so that only the stained migrated cells remained, located between the filter and glass slide. There were 4 replicates per data point unless pre-assay cell harvests only allowed fewer replicates. Slides with migrated cells were digitized using a regular scanner (HP OfficeJet Plus 8715 printer/scanner (Hewlett Packard (formerly RRID:SCR_011873), Spring, TX, USA). Densitometry (UN-SCAN-IT Gel Analysis Software, 7.1 (RRID:SCR_017291) Silk Scientific, Inc., Provo, UT, USA) with correction for background filter staining density to quantify cell migration results. An Epson Perfection 2450 PHOTO (Epson America, Long Beach, CA, USA) was also used for obtaining some of the images of migration assays. The first two rows of migrated cell pellets, digitized for densitometry, were the results used to calculate cell migration specifically to HGF, i.e. HGF cell migration, defined as the 2nd rows of cells which had migrated to HGF divided by the 1st rows of cells representing background (unstimulated) migration because they migrated to media without the added chemoattractants, HGF and/or FBS. HGF cell migration results are stated as times(X) the corresponding unstimulated, background cell migration for each cell line. Additional migration assays of U87 cells evaluated the motogenic/chemokinetic properties of FBS and HGF by placing them in either the bottom or both top and bottom wells and also separately, MEM versus Dulbecco's PBS was evaluated in the bottom wells in a small dose curve of FBS with Migration media (Dulbecco's PBS (contains 2.7 mM KCl, 1.8 mM KH_2PO_4, 137.9 mM NaCl, 10 mM Na_2HPO_4) with added 0.210 mM $MgCl_2$, 0.243 mM $CaCl_2$, 5 mM pyruvate, 5.551 M glucose, and 0.1% bovine serum albumin) in all of the top wells.

2.7. Immunoblot of Met, Receptor for HGF

One dimensional gel electrophoresis was performed for immunoblotting. Lysates of unmigrated cells from 8 cell lines, equalized for total protein content (10 µg per lane), were electrophoresed in separate lanes of 10% polyacrylamide gels under reducing conditions. Protein standards (MagicMark, MultiMark, Invitrogen (now merged with Thermo Fisher Scientific (RRID:SCR_008452)) were loaded 8 µg per lane. The gel was stained with Coomassie blue (Novex Colloidal Blue Stain Kit, Invitrogen, now merged with Thermo Fisher Scientific (RRID:SCR_008452)), as shown, and destained with tap water. Gel contents were transferred onto polyvinylidene difluoride membranes (Invitrogen, now merged with Thermo Fisher Scientific (RRID:SCR_008452)), blocked (Detector Block, Protein Detector Western Blot Kit Lumi-GLO System, Kirkegaard & Perry Laboratories, Gaithersburg, MD, USA, now merged with SeraCare Lifesciences:(RRID:SCR_004535)) and reacted with anti-Met (1:1000), reactive with a 145 kDa band. The secondary antibody 1:1000 (Kirkegaard & Perry Laboratories, now merged with SeraCare Lifesciences:(RRID:SCR_004535)) was horseradish peroxidase-labeled anti-mouse. Immunoreactive bands were visualized via horseradish peroxidase's conversion of a luminol-based solution to produce chemiluminescence, and the reactive blot was scanned to generate a digital image. An Epson Perfection 2450 PHOTO was used for obtaining digital images with densitometry obtained using UN-SCAN-*It* gel, early version 5.1.

2.8. Differentially Expressed Genes of Potassium Channels

Potassium channel (KCN) family members were found as differentially expressed genes (DEG) in cancer genomic landscapes described in 70 studies (1301 authors) recently published (2007-24) in 15 journals through subscriptions and open access. The KCN DEG were detected with non-KCN DEG in at least one published figure (heatmap, Venn diagram, volcano plot, etc.) or table (none from Supplemental Materials of the manuscripts) in each publication. Detection of one or more KCN genes in a group of genes designated as DEG by the authors (with no initial focus on KCN genes) was used for selecting these studies. Types of studies included mostly common malignancies, such as breast, lung, gastrointestinal, brain, bone marrow, liver, soft tissue sarcomas, etc. Categories (determined after all E1-E70 studies were completed) were according to descriptions by the authors of each paper with the caveat that there had to also be a relevant DEG reported in at least one of the E1-E70 studies.

2.9. Expression of Potassium Related Genes in Glial Tumors

REMBRANDT (G-DOC) contained tumor expression data on 67 oligodendrogliomas (Oligo) and 220 glioblastoma (GBM) patients, including subgroups treated with anti-seizure (AS) medications, i.e. 24 Oligo-AS and 75 GBM-AS. Gene expressions were determined by reporter probes on microarrays with their median values provided. Differences in median values for multiple probes (when available) were found with t-tests, paired via reporter probes for the two comparison groups when possible, and otherwise, unpaired t-tests were performed. Housekeeping genes (HKG) that lacked relevance for glial tumors via literature searches were also analyzed for comparisons. Additionally,

Oligo-minus-GBM (OMG) differences were calculated for each probe. OMG differences for each gene of interest were compared to the OMG differences for HKG (*B2M*, *PPIA*, *RRLP0*, and *YWHAZ*). The *t*-tests were performed for unpaired samples with unequal variance in OMG comparisons. Published studies [22,139,140] were used for confirmation of REMBRANDT results.

3. Results

3.1. Settled Glioblastoma Cells with Fluid Removed

At the end of each cell settling assay, the extracellular fluid had been wicked away. Cell groups could be seen macroscopically in some as viewed in Appendix A (Figure. A1). For each cell line (A172, LN229, T98G, and U87) a striking feature was the clustering of robustly viable tumor cells around single degenerating cells of the same lineage on slide surfaces in low numbers. Cell surfaces were exposed to ambient air, glass, or surfaces of other cells by the end of the assays. The tight clustering of viable cells suggested an opportunistic attraction to the dying single cells by possibly taking up released contents from moribund cells to enhance fitness. Although the tint of staining varied, some viable cells clustered around single dying cells displayed basophilic cytoplasmic staining (Figure 1A-B). Although some faint, thin connecting strands between cells may have been present, mostly there was a narrow linear open space between the apposed cells, best seen in black and white photographs. Cells, single and in groups without visible degenerating central cells, and scattered debris were also seen. Cytoplasmic vacuolization was most prominent in the U87 cells (Figure 1A-C). The number of vacuoles was highest in single cells and decreased as the size of cell clusters increased. Representative U87 cells, single and in groups, were layered together into one image with a broad white stroke added around each layer for delineation and contrast with the added pink background (Figure 1C). In counts of vacuolated settled cells performed on the cell monolayers from two separate wells, 15% and 72% of single cells were vacuolated whereas vacuolated cells were only 11% and 18% in cell groups comprised of greater than twenty cells in the 1st and 2nd wells, respectively. Pearson regressions of the cells in clusters with vacuoles for the two wells had significant R^2 values of 0.266 (p = 0.0410) and 0.544 (p = 0.0062), 1st and 2nd wells, respectively, as seen in scatterplots (Figure 1D). The cells in clusters exhibited less vacuolization as a sign of less degeneration possibly due to sharing their cytoplasmic contents as needed and also

possibly due to the contributions of contents from dying cells of the same lineage.

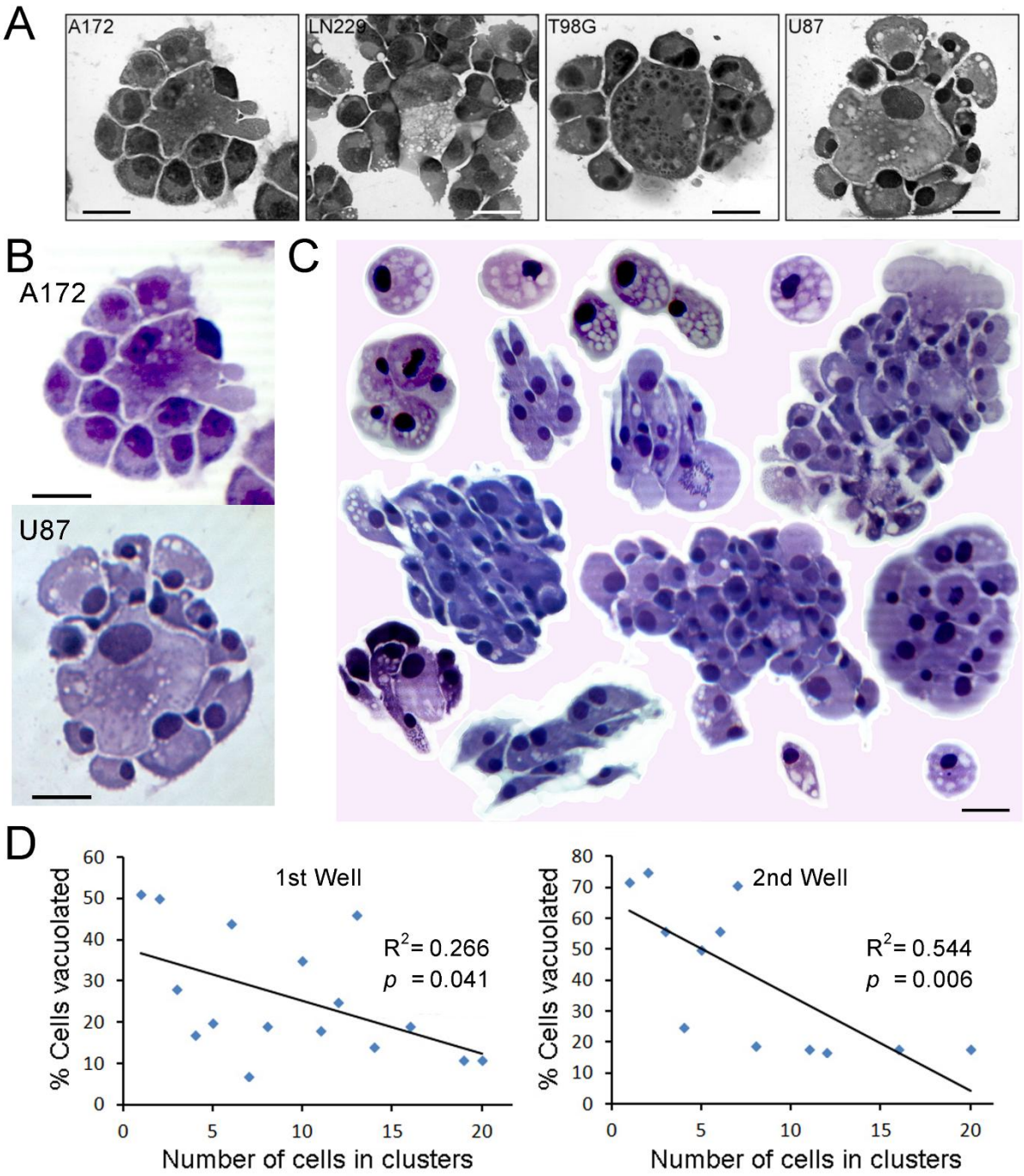

Figure 1. Settled glioblastoma cells deprived of extracellular fluid. (A and B) The morphology of each cell line (A172, LN229, T98G, and U87) after cell settling with fluid wicked away, included a few clumps of robust appearing, viable tumor cells clustered around single degenerating cells of the same lineage. Cell surfaces, after settling and withdrawal of suspension media, were exposed to ambient air, glass, or surfaces of other cells. Although the tint of Diff Quik staining varied, some viable clustered cells' cytoplasm stained relatively basophilic. The black and white photographs suggest some thin connections between cells

crossing the narrow linear open spaces separating them. Single and grouped cells without a visible degenerating central cells and scattered cell debris were also seen in wider views. (C) Cytoplasmic vacuolization, most prominently seen in U87 cells, is shown in the representative single and grouped cells that were outlined with digital white strokes around each merged layer for delineation and contrast with the added pink background. More basophilic cytoplasmic staining with Diff Quik seen in some cell groups would be consistent with an alkaline pH but no pH measurements were made. The numbers of vacuoles were highest in single cells and decreased as the numbers of cells in the cellular groups increased. (D) In counts performed on the cell monolayers from two separate wells, 51% of 75 and 72% of 25 single cells were vacuolated, 1st and 2nd wells, respectively. However, vacuolated cells in groups were only 11% of 122 and 18% of 39 cell groups comprised of greater than twenty cells, 1st and 2nd wells, respectively. As shown in the 2 scatterplots, Pearson regressions of the numbers of cells contiguous in groups or clusters that had vacuoles had R^2 values of 0.266 (p = 0.0410) and 0.544 (p = 0.0062), 1st and 2nd wells, respectively. Scale bars, 25 μm.

3.2. Cell Migration with HGF and Serum Chemoattraction

Earlier studies of U87 and LN229 glioblastoma cell lines and fresh glioblastoma cells from a clinical specimen reported chemoattraction to HGF and serum [43,62,134-136]. Testing additional glioblastoma cell lines for migration to HGF and FBS, their chemokinetic effects (more extensively than previously), comparing cellular levels of HGF's receptor, Met, and including a comparison of MEM versus Dulbecco's PBS as the media in bottom wells for chemoattraction in a FBS dose curve with U87 cells are reported here. Boyden chamber assays (48 well chambers), 3 per cell line, for 2 rat astrocytoma cell lines (C6 and F98) and 5 human glioblastoma cell lines (T98G, LN18, U87, LN229, and U373) showed cell migration to HGF alone as a chemoattractant (row 2), HGF and FBS together as chemoattractants (rows 3-9), and to FBS alone as a chemoattractant in a dose curve (rows 10-12) compared to background (unstimulated) cell migration in the top rows. Concentrations of chemoattractants are indicated in the left columns. Notably, with the same amount of HGF present, adding increased amounts of FBS increased cell migration in 7 of the 8 cell lines (Figure 2A).

Portions of scanned assay images of FBS alone as the chemoattractant in a dose curve are shown as migrated cell pellets with densitometry results in bar charts below their images. All cell lines, except A172, showed significant migration to FBS alone. U87 and U373 results showed the most impressive stepwise increase in chemotactic migration at all 3 concentrations of FBS versus background migration with all p values < 0.0005 and 0.000005, respectively. U373 chemotaxis to 0.5% FBS, 3.8 times the background (unstimulated) migration, was the highest level for all cell lines. A172 cells showed a trend for increased migration to 0.5% FBS, p = 0.0638. Some of the cell lines showed flattening of their responses as levels of FBS increased (Figure 2B). All assays (3 per cell line) are shown in Appendix A for C6, F98, T98G, and LN18 (Figure A2) and U87, LN229, A172, and U373 (Figure A3). Cell migration specifically for HGF in each cell line is stated as a multiple (X) of the background cell migration, obtained by dividing the 2nd row of assays' cell pellets densitometry results by the corresponding 1st row of

background cell migration, bottom row (Figure 2C). The immunoblot shows reactivity for HGF's receptor, Met (β subunit, 145 kDa). The Met reactivity with U87 and LN229 has been published previously [134] but here the relative amounts of Met in 8 cell lines are reported, including rat (C6 and F98) and human glioblastomas (T98G, LN18, U87, LN229, A172, and U373). As shown in the bar chart there was a lack of correlation with the cell motility results shown below it (Figure 2C). In Appendix A, the gel image showing equalized protein loading for all 8 cell lines in the immunoblot is available (Figure A4A). The order for HGF cell migration from highest to lowest results for all 3 assays of each cell line was T98G (2.11X), U373 (1.93X), LN229 (1.52X), U87 (1.49X), C6 (1.33X), A172 (1.30X), LN18 (1.15X), and F98 (1.13X). Twelve of the 92 data points of visibly migrated HGF cell pellets had densitometry results showing slightly less than 1X background cell migration and were rounded up to 1X for these results. A few replicates did not show visible unstimulated or stimulated cell pellets.

Earlier studies had noted chemokinesis with HGF and 0.1% FBS in U87 cell migration assays [136] and also chemokinesis with 5% FBS alone in LN229 cell invasion assays [135]. The dose curve for FBS includes additional data points as shown in Figure 2D. A dose curve was also published earlier with fewer data points for chemoattraction using HGF, FBS, and both for U87 and LN229 cells previously (134) but the assays here include additional data points and 6 more cell lines. The chemoattractant strength of HGF alone (row 2), and with 0.1% and 1% FBS (rows 5 and 8, respectively) was enhanced by both FBS concentrations in the U87 cells. Chemokinetic strength of HGF alone (row 3), with 0.1% and 1% FBS (rows 6 and 9, respectively) was also enhanced by FBS. Chemotaxis and chemokinesis at 0, 0.1, and 1% FBS demonstrated strong enhancement of FBS versus HGF alone for either type of U87 cell migration. The combination of HGF, 2.5 ng/ml, and 1% FBS for chemoattraction significantly, p= 0.012, outperformed their chemokinetic effects on cell migration (Figure 2D). A scanned image of the assay is also available in Appendix A (Figure A4B). A portion of the immunoblot for Met in U87 and LN229 cells with the gel was published previously (134) but without the entire immunoblot for U87 and LN229 cells plus 6 additional cell lines and all standards as included in this study

Another assay to evaluate MEM for migration studies included gradients of K^+ and Cl^- in migration assays of U87 cells. Both ions are redistributed with volume changes during cell migration. In the absence of FBS, Dulbecco's PBS in the bottom wells provided K^+ as 2.7 mM KCl + 1.8 mM KH_2PO_4 (**4.5 mM K^+**) and Cl^- as 2.7 KCl + 137.9 mM NaCl (**140.6 mM Cl^-**). MEM in the lower wells provided K^+ as 5.3 mM KCl (**5.3 mM K^+**) and Cl^- as 5.3 mM KCl + 1.8 mM $CaCl_2$-$2H_2O$ (**8.9 mM Cl^-**). See Methods for a minor issue with KCl molarity in MEM. For all upper wells without FBS, the Migration media provided K^+ as 2.7 mM KCl + 1.8 mM KH_2PO_4 (**4.5 mM K^+**) and Cl^- as 2.7 KCl + 137.9 mM NaCl + 0.21 mM $MgCl_2$ + 0.243 mM $CaCl_2$ (**141.5 mM Cl^-**). Potassium did not generate any gradient for cells migrating from upper to lower wells when Dulbecco's PBS was used in the bottom wells and there was almost no gradient for chloride either. However, when MEM was used in the lower wells a reverse gradient for Cl^- was generated with more Cl^- in the upper versus the lower wells. With MEM in the lower wells there was a positive gradient to potassium for migrating cells (5.3 mM in the lower

wells versus 4.5 mM in the upper wells). Chloride ions present in a negative gradient are probably not responsible for the 1.7X increase in cell migration when MEM was used in the bottom wells. However, the positive gradient for K^+ may have contributed to the significantly increased migration, $p = 0.0144$, without FBS present. MEM as the media in the lower wells was also associated with significantly increased cell migration when 0.1 and 1% FBS were present, $p = 0.0136$ and $p = 0.000442$, respectively, compared to using Dulbecco's PBS for the media in the lower wells having the same FBS concentrations (Figure 2E). MEM contains 5.6 mM dextrose, 1 mM pyruvate, and 2 mM l-glutamine, whereas Migration media contained 5.6 M glucose and 5 mM pyruvate. Therefore, MEM as a source of fuel in the bottom wells was probably not a significant differentiating factor in the results. MEM also contains 17.856 mM sodium bicarbonate, 0.8 mM magnesium sulfate (more Mg^{2+} than Migration media (0.21 mM $MgCl_2$), less sodium than Dulbecco's PBS and Migration media, amino acids, vitamins, etc. A scanned image of the assay is available in Appendix A (Figure A4C). These results support the role of K^+ in enhancing cancer cell migration. Variable background migration, as shown in the top rows of representative assays (Figures 2A-B) and assay-to-assay variation for each cell line as shown in Appendix A files (Figures A2 and A3) are routine for cell migration assays.

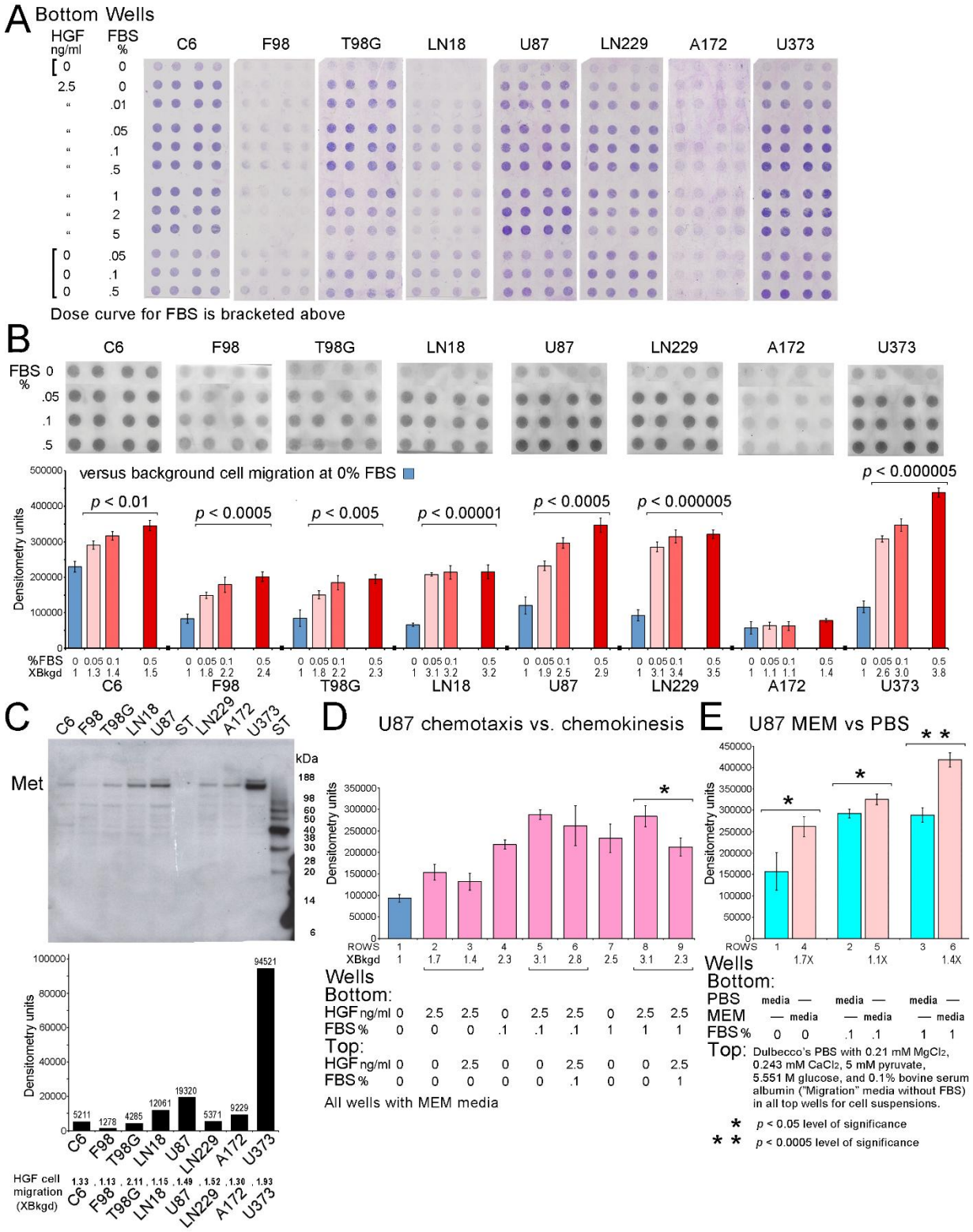

Figure 2. Migration of glioblastoma cell lines to hepatocyte growth factor (HGF) and fetal bovine serum (FBS). (A) Representative Boyden chamber assays of 2 rat astrocytoma (C6 and F90) and 6 glioblastoma

cell lines (T98G, LN18, U87, LN229, A172, and U373) showed unstimulated (background) cell migration (row 1, at the top), cell migration to HGF (row 2), HGF and FBS (rows 3-9), and to FBS alone (rows 10-12) using concentrations in the bottom wells as indicated in the left columns. All cell lines, except for A172, migrated to FBS alone. With the same amount of HGF present, adding increasing amounts of FBS increased chemotactic cell migration in the other 7 cell lines. These images were obtained by using a transparency scanner. (B) Portions of scanned (regular scanner) assay images using FBS alone as the chemoattractant were digitized for densitometry (total pixels for units) with results shown as bar charts. All cell lines showed significant migration to FBS except for A172 which only had a trend, $p = 0.0638$, for 0.5% FBS. The entire collection (3 assays per cell line) is available in Appendix A for C6, F98, T98G, and LN18 (Figure A2) and U87, LN229, A172, and U373 (Figure A3). The first assays for C6, F98, LN18, and LN229, the second assay for T98G, and the third assays for U87, A172, and U373, were digitized for densitometry. (C) An immunoblot with a bar graph of densitometry results underneath shows the relative amounts of HGF's receptor, Met (β subunit, 145 kDa) in each cell line. Also, HGF-stimulated cell migration is listed below the bar graph. HGF-stimulated cell migration (digitized densitometry of row 2 of the migration assays divided by background (no stimulation) migration for row 1 cell pellets in B) is stated in units of times(X) background cell migration. The HGF-stimulated cell migration compared with levels of Met lacks notable correlation. The gel for the immunoblot showing equalized protein loading is available in Appendix A (Figure A4A). (D) Unstimulated cell migration (blue bar representing the average of the assay replicates) in U87 cells is shown for contrast with the chemotactic and chemokinetic strength of HGF and FBS (pink bars representing averages of replicates in each row of the assays using HGF alone or HGF and FBS) that were both greater than unstimulated cell migration. The chemoattractant strength of HGF alone (bar for row 2) and with 0.1% and 1% FBS (bars for rows 5 and 8, respectively) shows impressive enhancement by FBS. Chemokinetic strength of HGF alone (bar for row 3), with 0.1% and 1% FBS (bars for rows 6 and 9, respectively) also showed impressive enhancement by FBS. The combination of HGF, 2.5 ng/ml, and 1% FBS for chemoattraction (bar for row 8) significantly, $p = 0.012$, outperformed their chemokinetic effects (bar for row 9) on cell migration. The scanned image of the assay is also available in Appendix A (Figure A4B). (E) An assay that evaluated MEM for U87 migration studies included gradients for K^+ and Cl^-. In the absence of FBS, Dulbecco's PBS in the bottom wells provided K^+ as 2.7 mM KCl + 1.8 mM KH_2PO_4 and Cl^- as 2.7 KCl + 137.9 mM NaCl. MEM in the lower wells provided K^+ as 5.3 mM KCl, and Cl^- as 5.3 mM KCl + 1.8 mM $CaCl_2$-$2H_2O$. For all upper wells without FBS, the Migration media provided K^+ as 2.7 mM KCl + 1.8 mM KH_2PO_4 and Cl^- as 2.7 KCl + 137.9 mM NaCl + 0.21 mM $MgCl_2$ + 0.243 mM $CaCl_2$. See text for total mM for each ion. When the bottom wells contained Dulbecco's PBS there was no significant gradient created for K^+ or Cl^-. However, when MEM was in the bottom wells, positive K^+ and negative Cl^- gradients were generated. Both K^+ and Cl^- ions are used for volume changes in cell migration. The positive gradient for K^+ is supported as being a chemoattractant in view of the significantly increased migration, $p = 0.0144$, in MEM versus Dulbecco's PBS in the lower wells. None of the wells contained FBS for the above comparison. However, MEM in the lower wells was associated with significantly increased cell migration with 0.1 and 1% FBS also present, $p = 0.0136$ and $p = 0.000442$, respectively, compared to Dulbecco's PBS in the lower wells having the same FBS concentrations. Averages of rows for the Densitometry units indicated by bars are shown with 95% confidence limits (B, D, and E). Variability in staining of the background migration, as shown in the top rows of representative assays (A) and assay-to-assay variation for each cell line in Appendix A (Figures A2 and A3), are routine findings. Each circle of stained migrated cells shown is 3 mm in diameter.

3.3. KCN Genes Differentially Expressed in 70 Studies

3.3.1. General Features of Detected Differentially Expressed KCN Genes

The availability of K^+ for cancer cell survival and migration suggested by experimental studies just described led to consideration of the large KCN family of genes being altered in cancer cells. Published genomic landscapes, i.e. heat maps (46 studies), Venn diagrams, volcano plots, tables, etc. were found in 70 cancer studies including KCN (potassium channel) family members as one or more of 53 KCN genes that were differentially expressed genes (DEG) along with numerous co-expressed non-KCN DEG. Selection criteria for DEG (mostly $p < 0.05$ differences, chance of false discovery, etc.) were set by the authors who incidentally detected and reported the KCN DEG among groups of DEG Appendix B (Table B1, sample view, and the full list, AllE1E70DEG3239Total, is available after the References and Disclaimer in a table format). Parameters were applied in each study for a particular type of malignancy, without or with perturbations, such as tumor treatment, transcription factor, over-expression of an oncogene(s), or according to survival, disease progression, primary versus metastasis, recurrence, etc. The 53 KCN DEG are distributed across 17 chromosomes (1-3, 5-12, 17-21, and X). Although many of these KCN genes encode membrane pore subunits with K^+ selectivity, some provide modulatory/regulatory effects on pore function when present with other subunits that may also function independently as pores. Heterodimers among KCN family members are common. Members of 4 KCN subfamilies, Kv (voltage dependent, related, *KCNA*, *KCNQ*, *KCNH*, etc.), Kir (inwardly rectifying, *KCNJ*), K2P (tandem two pore domain , *KCNK)*, and KCa (calcium dependent, related, *KCNM*, *KCNN*, etc.) were found in 32(46%), 10(14%), 14(20%), and 29(41%), respectively, of the 70 studies.

3.3.2. Proton(H^+) Sensitivity of Detected KCN DEG

In keeping with the connection proposed for K^+ and H^+, the H^+-sensitivity of KCN DEG encoded proteins was relevant. At least 33 (62.3%) of the 53 KCN DEG encode gene products that are H^+-sensitive according to 135 publications listed in Appendix B (Table B2). Fifty-two (74.79%) of the 70 studies contained at least one KCN DEG identified as being H^+- sensitive. One, 2, 3, and 6 H^+-sensitive KCN DEG genes were found in 36, 14, 1, and 1 of the studies, respectively. H^+- sensitive genes in each of the 4 subfamilies, Kv, Kir, K2P, and KCa were found as DEG in 17 (24%), 9 (13%), 13 (19%), and 21(30%) of 70 studies, respectively. The most frequently detected DEG, *KCNN4* and *KCNMA1*, present in 9 and 6 studies, respectively, encode H^+-sensitive proteins (red H^+ above columns) and are also Ca^{2+}-sensitive (Figure 3A).

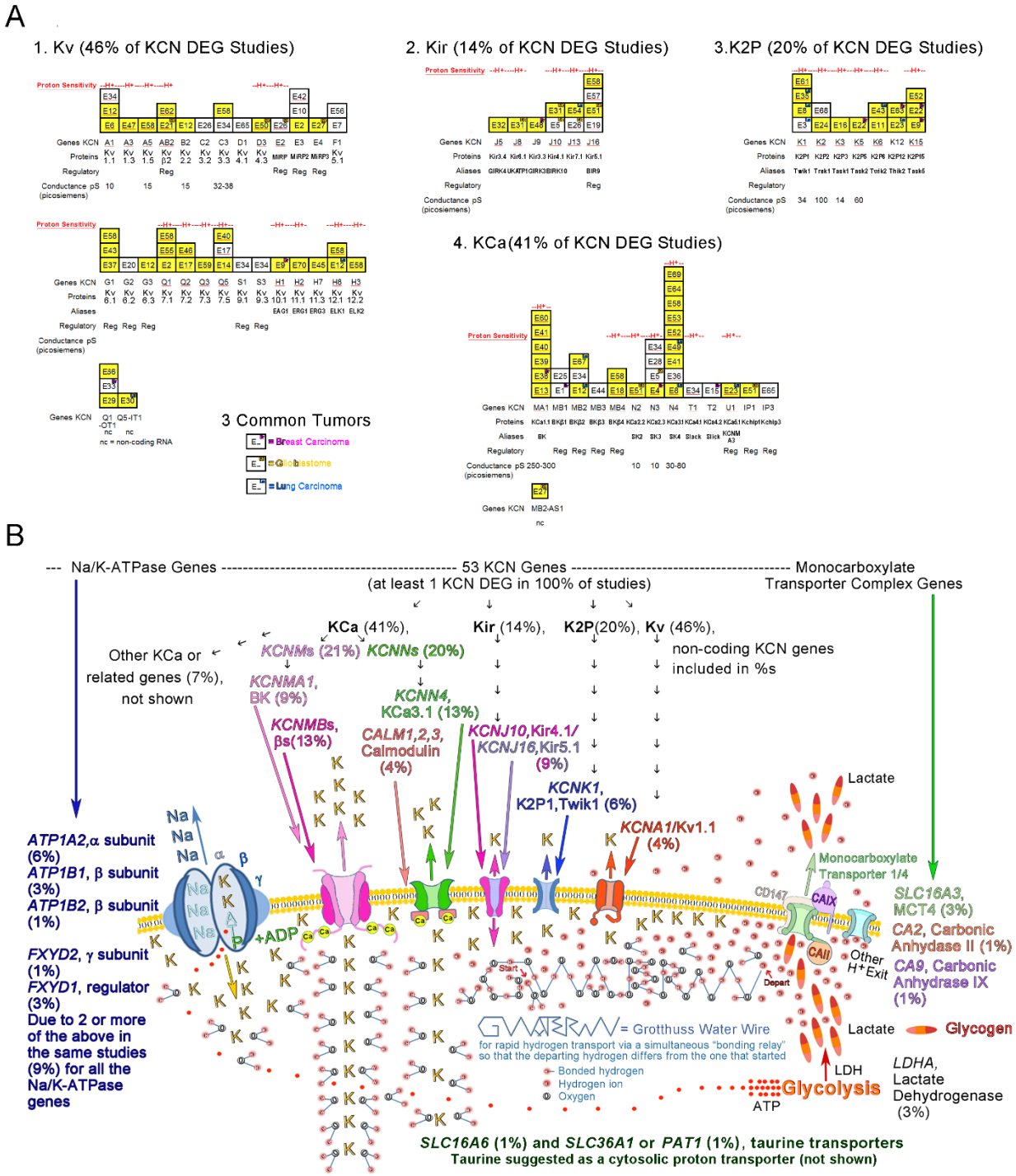

Figure 3. The KCN DEG and related non-KCN DEG detected in E1-E70 studies with relevant information are shown. (**A**) 53 KCN DEG of 4 KCN subfamilies detected are listed along the x-axes in the specific studies that are listed vertically in boxes above the specific KCN gene names, reflecting their frequency in 70 studies. The 3 most frequent types of tumors (breast, glioblastoma, and lung) are highlighted with color-coded superscripts, as listed under the first group of histograms. The 33 (62.26%) of KCN DEG that encode H^+-sensitive proteins are labeled with red H^+ above each column. Studies with KCNs detected

that encode H^+-sensitive proteins also have their names underlined in red within the boxes of the histograms. 52(74.29%) of the 70 studies contain at least one KCN encoding a H^+-sensitive protein. Yellow shading of the boxes labeled for specific studies indicates that these studies were included in 1 or more of 8 categories shown later (Figure 4A). The non-coding KCNs are in separate small histograms included with their appropriate KCN subfamily group. If only studies that included at least one protein-coding KCN DEG are considered, then 52(78.79%) of those 66 studies contained at least one KCN encoding a H^+-sensitive protein. Multiple KCN DEG were detected in 18 (27.27%) of 66 studies. (**B**) A stochastic view of K^+-related dynamics in cancer cells is presented based on collective incidences of both KCN and related non-KCN DEG identified in E1-E70. Images of the most frequent members of each of the 4 KCN subfamilies along with pertinent non-KCN membrane proteins and their complexes are consistent with published graphical representations [141-148]. There were relatively few studies in E1-E70 with differential expressions detected for genes encoding Na/K-ATPases (9% for 5 genes), the monocarboxylase transporter complex (5% for 3 genes), lactate dehydrogenases (3% for 1 gene), taurine transporters (2% for 2 genes), and 0% for related functional analogues not listed. Therefore, abnormal K^+ flux allowing K^+/H^+ exchange, if present in these same cancer studies with KCN DEG present, suggests KCN DEG for playing a role in the pH changes following rapid cytosolic H^+ transport (putatively Grotthuss type) to exit sites that include release of protons with lactate. Also, the lack of DEG for glycogen synthases assumes only normal (if any) intracellular storage of lactate as glycogen. Abnormal accumulations of K^+ at inner membrane surfaces may have occurred due to KCN DEG (in assorted combinations) to exchange with bound H^+, either due to genetic loss or down regulation of any of the numerous KCN membrane proteins mediating outward flux or a gain via KCNs mediating increased inward flux. The movement of K^+-$7H_2O$ (represented by 2 H_2O per K^+ shown in a "cross sectional" view) within the cells may bring water to outer cytoplasmic regions, possibly enhancing Grotthuss conditions near inner membranes in cancer cells. The putative K^+-related changes in cancer cells that at the same time maintain relatively normal expression levels of pertinent non-KCN genes, as seen in the majority of the 70 KCN DEG studies, would be consistent with the complex scenario shown (**B**). E1-E70 citations are listed in *Section 3.3.6. Categories Among Studies with E1-E70 Citations Per Category*.

3.3.3. Coding and Multiplicity of KCN DEG and Non-KCN DEG

Four of the 70 studies identified only non-coding KCN genes, *KCNQ1-OT1* (E29, E33, and E66) and *KCNQ5-IT1* (E30), as DEG. Study E27 identified *KCNMB2-AS1* as well as *KCNE4* as DEG. Disregarding the 4 studies with only non-coding KCNs detected as DEG, multiple (2 - 9) KCN DEG were found in 18 (27.3%) of 66 studies with protein-coding KCN DEG. Thirty-eight (71.70%) of the 53 KCN DEG were detected with other coding KCN DEG in at least one of the 66 studies. There were 102 instances of 53 KCN DEG in a total of 3,239 DEG instances (2,490 non-KCN DEG without repeats). The average numbers of KCN DEG and all DEG per study were 1.53 +/- 0.33 (95% CI) and 45.91+/- 7.92 (95% CI), respectively. The correlation coefficient for number of KCN DEG and size of all DEG (KCN and non-KCN) groups was 0.379. If only the studies that included at least one protein coding KCN DEG are considered, then 52 (78.79%) of the 66 studies detected at least one H^+-sensitive KCN DEG (Figure 3A).

3.3.4. Malignancies in E1-E70

The 3 most frequently found types of malignancies in the 70 studies were lung cancer, breast cancer, and glioblastoma with detected genes encoding H^+- sensitive products **bolded** in the following list. The lung cancer studies with their KCNs include: E3(***KCNK1***), E8(***KCNK1***, ***KCNN4***), E12(***KCNH8***, *KCNMB2*), E23(***KCNU1***), E30(*KCNQ5-IT1*), E35(***KCNK1***), E43(***KCNK6***), E49(***KCNN4***), 2), E54(***KCNJ13***), E63(*KCNK12*), and E67(*KCNMB2*). The breast cancer studies include: E1(*KCNMB1*), E4(***KCNN3***), E9(***KCNH1***, ***KCNK15***), E15(*KCNT2*), E22(***KCNK5***, ***KCNK15***), E33(*KCNQ1-OT1*), E38(***KCNMA1***), E48(*KCNJ9*), and E63(*KCNK12*). The glioblastoma studies include: E5(***KCNJ10***, ***KCNN3***), E21(***KCNAB2***), E26(***KCNE2***, ***KCNJ13***), E27(KCNE4, KCNMB2-AS1), E31(***KCNJ10***), E50(***KCND3***), E51(KCNIP1, ***KCNJ16***, ***KCNN2***). H^+-sensitive KCNs were found in 86%, 73%, and 44% of the 7 glioblastoma, 11 lung cancer, and 9 breast cancer studies, respectively. All three of the melanoma studies detected H^+-sensitive KCN DEG. Numerous types of malignancy listed in Appendix B, including NCI-60 cell lines (E16), detected H^+-sensitive KCN DEG, see Appendix B (Figure B1A). Common informative protein abbreviations in the KCN family are also listed (Figure B1B). E1-E70 citations for E1 – E70 are listed in *Section 3.3.6. Categories Among Studies with E1-E70 Citations Per Category*

3.3.5. Stochastic View of K^+-Related Dynamics in E1-E70

A percentage based stochastic view of K^+-related gene expression dynamics in cancer cells is presented based on collective incidences of both KCN and related non-KCN DEG identified by the authors of each paper. Images of the most frequent members of each of the 4 KCN subfamilies along with pertinent non-KCN membrane proteins and their complexes are consistent with published graphical representations [141-148]. In view of the relatively small number of 70 studies with differential expressions detected for genes shown in Figure 3B that encode Na/K-ATPase (9% for 5 genes), the monocarboxylase transporter complex (5% for 3 genes), lactate dehydrogenases (3% for 1 gene), taurine transporters (2% for 2 genes), and 0% for genes encoding functional analogue proteins not listed, the abnormal K^+ flux in these same cancers with KCN DEG can be considered for supplying K^+ for a K^+/H^+ exchange that initiates pH changes. Rapid cytosolic H^+ transport (putatively involving Grotthuss water wires) to exit sites for proton release with lactate is included to complete the pH reversal scenario. The pertinent lack of DEG in the E1-E70 studies for glycogen synthases, to mediate anomalous storage of lactate without extrusion, is included because glycogen storage of lactate occurs in humans, mice, bacteria, etc. [149-152]. Abnormal accumulations of K^+ at inner membrane surfaces are illustrated since they are proposed to promote K^+/ H^+ exchange that releases bound H^+. Accumulations of K^+ occur either due to genetic loss or down regulation of KCN membrane proteins mediating outward flux or increased inward flux due to a gain or loss in copy number and/or expression of the KCN genes found to be differentially expressed in E1-E70. The movement of K^+-7H_2O (indicated with 2 H_2O per K^+, as a “cross-sectional” view in Figure 3B within cells may bring water to outer cytoplasmic regions, possibly promoting Grotthuss conditions in cancer cells near inner membranes. These putative K^+-related changes in cells that maintain relatively normal expression levels of pertinent non-KCN genes as seen in the majority of the KCN DEG studies suggest the scenario shown (Figure 3B).

3.3.6. Categories Among Studies with E1-E70 Citations Per Category

Eight categories describe 50 of the 70 studies (Figure 4A). These were author-designated which also had relevant DEG in at least one of the E1-E70 studies. Some studies belonged in more than one category and 20 studies were in no category as designated last item in the list below.

1. Of the 18 studies in the <u>first category</u> of histone/chromatin/epigenetic (His/Chr/Epi or histone/DNA), 10 were in this category due to specific genes described by the authors of the studies, including: E2(*N6AMT1*, previously *KMT9*), E13(*MSH2*, *BET*), E32(*H3K27me3*, *EZH2*), E41(*HDAC8*), E46(*KDM2B*), E49(*KMT2D*), and E53(*H3K27*). Also, E27's and E29's authors focused on chromatin access and imprinting, respectively. Two imprinted genes, *KCNQOT1* and *PAX8*, were DEG in E29. Twenty-one imprinted DEG (*AXL*, *DLK1*, *GDAP1L1*, *GNG7*, *GRB10*, *IGF2*, *KCNQ1*, *KCNQOT1*, *LRRTM1*, *MEG3*, *NDN*, *NNAT*, *NTM*, *PAX8*, *PEG3*, *PEG10*, *PHLDA2*, *PLAGL1*, *RHOBTB3*, *RTL1*, and *TFPI2*) were detected among a total of 2560 DEG for a rate of 0.82% in E1 - E70. When repeats are included, there were 32 instances of imprinted genes among 3,242 instances of DEG in E1-E70 for a rate of 0.99%. Detection of 0.82% or 0.99% imprinted genes is expected from the genome (approximately 200, i.e. less than1% of all genes) according to Tucci and colleagues who also provided a list of human imprinted genes [153]. Therefore, the presence of imprinted genes was not used as an inclusion criterion for the His/Chr/Epi category. In addition to the 10 studies per author designations, 8 additional studies detected His/Chr/Epi related DEG as follows: E4(*DNMT3B*), E30(*KDMA-AS1*), E31(*H2A.X*, previously *H2AFX*), E37(*H2AC18*), E43(*H2AC18*, *H2BC5*, *H2BC12*), E45(*NUPR1*), E58(*DNMT3B*), and E66(*BDR4*, *H1-4*(previously *HIST1HIE*)). The entire His/Chr/Epi category includes the following studies with their citations: E2 [154], E4 [155], E13 [156], E27 [157], E29 [158], E30 [159], E31[160], E32 [161], E37 [162], E41 [163], E43 [164], E45 [165], E46 [166], E49 [167], E53 [168], E58 [169], E59 [170], and E66 [171] (Figure 4A, left side).

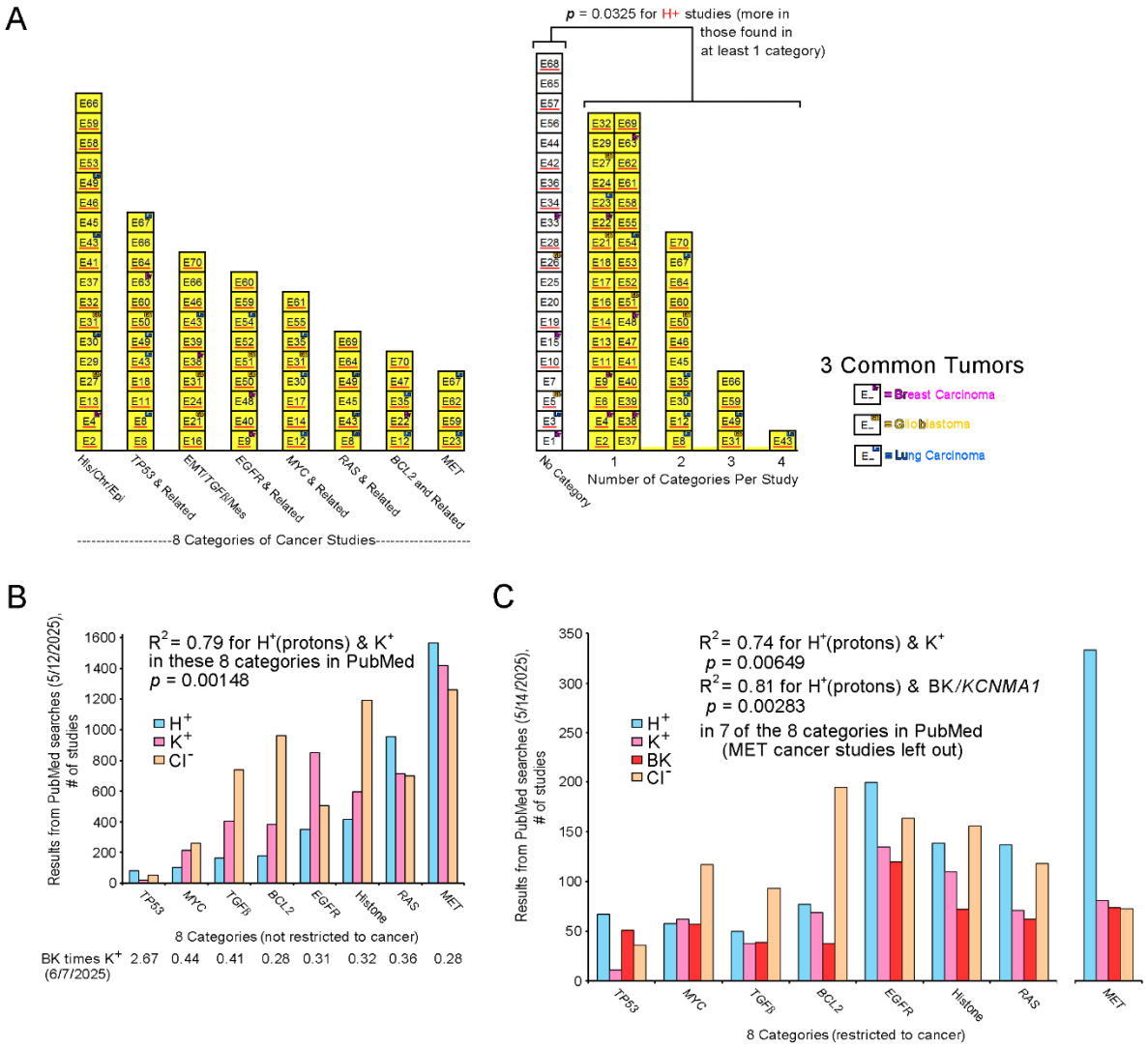

D

8 Categories (not restricted to cancer)

5/13/2025	*TP53*	*MYC*	*TGFbeta*	*BCL2*	*EGFR*	HISTONE	*RAS*	*MET*
TP53	X							
MYC	1709	X						
TGFbeta	408	1382	X					
BCL2	1573	3977	1315	X				
EGFR	2983	1695	1857	1754	X			
HISTONE	1090	2436	1602	1517	1142	X		
RAS	2202	3737	1840	1182	7337	1414	X	
MET	838	506	803	390	4861	609	1432	X

Figure 4. Oncogenes and DNA modifiers may play a role in cancer studies detecting KCN DEG encoding H^+-sensitive proteins. (**A**) The KCN DEG that encode H^+-sensitive proteins are highlighted with red underlining of the study names. Histograms of 8 categories (x-axis) of cancer studies among E1-E70 that contain KCN DEG are shown in the left histogram. The right histogram also includes 20 studies in "no category" (see text) in the first column. Comparison of the studies in “no category” versus those included in at least one of eight categories shown in the left histogram indicated a significant difference for the

number of studies detecting KCN DEG encoding H^+-sensitive proteins. With a Fisher's Exact test studies that detected one or more KCN DEG that encoded a H^+-sensitive protein showed a significant difference in the numbers of studies if the studies were in at least one of the eight categories versus no category, p = 0.0325. (**B – D)** The PubMed database (more than 38 million citations) was checked with word searches for the incidence of oncogene and histone publications related to H^+, K^+, BK (encoded by *KCNMA1*), and Cl^- (contrasting ion) to detect correlations related to findings in the 70 studies selected by detection of KCN DEG. (**B**) On May 12, 2025, searches for each category of "TP53", "MYC", "TGFbeta", "BCL2", "EGFR", "histone", "RAS", and "MET" were performed separately for "proton", "potassium", and "chloride". For all 8 categories, the total numbers of citations for "proton", "potassium", and "chloride" were 1565, 1418, and 1261, respectively, and the Pearson's product-moment correlations for "proton" with "potassium" and "proton" with "chloride" were R = 0.891 (p = 0.00148) and 0.599 (p = 0.0584), respectively. The Pearson's product moment correlation for "potassium" and "chloride" was 0.689 (p = 0.0295). R^2 for "proton" with "potassium" was 0.79. "BK" and "potassium" searches on 6/7/2025 revealed "BK" as a potential large component of the "potassium" citations, approximately one third for 7 of the categories. (**C**) When the same searches also included "cancer" as a third word, the numbers of citations for "proton", "potassium", "BK", and "chloride" on May 14, 2025, were 1061, 577, 513 (88.9% of "potassium" search results), and 952, respectively. However, when MET was left out for better "proton" correlations, the numbers of citations for "proton", "potassium", "BK", and "chloride" on May 14, 2025, were 728, 496, 439 (88.5% of "potassium" search results), and 879, respectively, and the Pearson's product-moment correlations for "proton" with "potassium" and "chloride" were R = 0.860 (p = 0.00649) and 0.462 (p = 0.148), respectively, across the 7 categories. Pearson's product-moment correlation for "proton" with "BK" was R = 0.901 (p = 0.00283) across the 7 categories. R^2 for "proton" with "BK" was 0.81. R^2 for "proton" with "potassium" was 0.74. The results for correlation between numbers of "Met" citations and those for the ions differed in results from the "cancer" searches in (C) compared to search results not restricted to "cancer" shown in (B). (**D**) The numbers of citations shared among the 8 categories of 7 oncogenes and histone are shown. E1-E70 citations are listed in *Section 3.3.6. Categories Among Studies with E1-E70 Citations Per Category*

---

2. In the <u>second category</u> there were 9 studies on *TP53* according to the authors' focus in E6, E8, E11, E49, E49, E60, E63, E64, and E67. Additionally, 3 studies found *TP53* and related genes as DEG as follows: E18(*MDM2*), E43(*TP53INP1A*), and E50(*TP53*). The 12 studies in this category are as follows: E6 [172], E8 [173], E11 [174], E18 [175], E43 [164], E49 [167], E50 [176], E60 [177], E63 [178], E64 [179], E66 [171], and E67 [180] (Figure 4A, left side).

3. In the <u>third category</u> there were 7 studies on Epithelial Mesenchymal Transition (EMT)/ *TGFb*/ Mesenchymal Tumor (EMT/*TGFb*/Mes) according to the authors' focus with specific genes, *CDH1*, *2*, *VIM*, *TGFb1*, *2*, *3*, in some of these studies as follows: E16(*CDH1*,*2*, *TGFb1*, *VIM*), E24(*TGFb1*), E31, E38, E39, E43(*CDH2*), and E46. Three additional studies also found some of these genes as follows: E21(*TGFb1*), E66(*VIM*), and E70(*CDH2*, *TGFb2*, *TGFb3*). The 10 studies this category are as follows: E16 [181], E21 [182], E24 [183], E31 [160], E38 [184], E39 [185], E43 [164], E46 [166], E66 [171], and E70 [186] (Figure 4A, left side).

4. In the fourth category there were 5 studies on *EGFR* and related genes according to the authors with corresponding DEG in two of their studies as listed, E9, E48, E50(*EGFR*, *ERBB2*), E51(*EGFR*), and E52. Additionally, 4 studies found related DEG as follows: E40(*NRG1*), E54(*NRG2*), E59(*NRG1*), and E60(*ERBB4*). The 9 studies in this category are as follows: E9 [187], E40 [188], E48 [189], E50 [176], E51 [190], E52 [191], E54 [192], E59 [170], and E60 [177] (Figure 4A, left side).

5. In the fifth category there were 5 studies on *MYC* according to the authors with *MYC* as a DEG in 2 of the studies as seen in the following list: E14(*MYC*), E30, E31, E55, and E61(*MYC*). Additionally, 3 studies had *MYC* or one of its related genes as seen here: E12(*MYCL*), E17(*MYCN*), and E35(*MYC*). The 8 studies this category are as follows: E12 [193], E14 [194], E17 [195], E30 [159], E31 [160], E35 [196], E55 [197], and E61 [198] (Figure 4A, left side).

6. The sixth category is comprised of 6 studies on *RAS* per the authors' interest, with *KRAS* found as a DEG in 2 studies as follows: E8, E43, E45, E49, E64(*KRAS*), and E69(*KRAS*). The 6 studies this category are as follows: E8 [173], E43 [164], E45 [165], E49 [167], E64 [179], E69 [199] (Figure 4A, left side).

7. In the seventh category the authors focused on *BCL2* in E47 but did not list it as a DEG. However, 4 other studies identified *BCL2* as a DEG and 1 also identified *BCL2L1* as well, as seen in the following list: E12(*BCL2*), E22(*BCL2*), E35(*BCL2*), and E70(*BCL2*, *BCL2L1*). The 5 studies in this category are as follows: E12 [193], E22 [200], E35 [196], E47 [201], E70 [186] (Figure 4A, left side).

8. In the eighth category the authors focused on *MET* in 1 study and found it as a DEG, E23(*MET*). Additionally, 3 studies also identified *MET* as a DEG, E59(*MET*), E62(*MET*), and E67(*MET*). The 4 studies in this category are as follows: E23 [202], E59 [170], E62 [203], E67 [180] (Figure 4A, left side). All studies in the 8 categories are shaded yellow in Figure 4.

9. No category. Twenty studies were not in any of the above 8 categories and are listed as follows: E1 [204], E3 [205], E5 [206], E7 [207], E10 [208], E15 [209], E19 [210], E20 [211], E25 [212], E26 [213], E28 [214], E33 [215], E34 [216], E36 [217], E42 [218], E44 [219], E56 [220], E57 [221], E65 [222], and E68 [223] (Figure 4A, right histogram, no yellow shading).

3.3.7. H^+-Sensitivity Significant in E1-E70 Studies Within 8 Categories

A histogram (Figure 4, right side) shows the studies collectively in the 8 categories versus those not in any category, with the studies that detected H^+-sensitive KCN DEG underlined with red. The difference for detection of H^+-sensitive KCN DEG was significant between the two groups, $p = 0.0325$, Fisher's Exact Test for count data. Eleven studies were in 2 categories (E8, E12, E30, E35, E45, E46, E50, E60, E64, E67, and E70). Four studies were in 3 categories (E31, E49, E59, and E66), and E43 was included in 4 categories. All 8 categories were among those that were shared in studies (Figure 4A**,**

right histogram, yellow shading). E1-E70 citations are listed in *Section 3.3.6. Categories Among Studies with E1-E70 Citations Per Category.*

3.3.8. PubMed Citations for "Proton", "Potassium", etc. in Categories

The PubMed database was checked with word searches for the incidence of 7 oncogenes and histone publications being related to those for H^+, K^+, BK (encoded by *KCNMA1*), and Cl^-(a potential contrasting ion), without and with "cancer", to compare with the 70 studies selected based on detection of KCN DEG. On May 12, 2025, searches for each category of TP53, MYC, TGFbeta, BCL2, EGFR, histone, RAS, and MET were performed separately for "proton", "potassium", and "chloride" and "cancer" was not included. For all 8 categories, the total numbers of citations for "proton", "potassium" and "chloride" were 1565, 1418, and 1261, respectively, and Pearson's product moment correlations for "proton" with "potassium" and "chloride" were R = 0.891 (p = 0.00148) and 0.599 (p = 0.0584), respectively. Pearson's product-moment correlation for "potassium" with "chloride" was 0.689 (p = 0.0295). R^2 for proton with potassium was 0.79. Later searches on 6/7/2025 for "BK" and "potassium" revealed "BK" citations were probably a large component of those for "potassium", possibly about one third in 7 categories (TP53 was much greater than one third) and are listed also below the x axis (Figure 4B). When the searches also included "cancer" as a third word, the numbers of citations for "proton", "potassium", "BK", and "chloride" on May 14, 2025, were 1061, 577, 513, and 952, respectively. However, when MET was left out, the numbers of citations for "proton", "potassium", "BK", and "chloride" on May 14, 2025, were 728, 496, 439, and 879, respectively, and Pearson's product-moment correlations for "proton" with "potassium" and "chloride" were improved, R = 0.860 (p = 0.00649) and 0.462 (p = 0.4623), respectively, using only 7 categories. Analysis prior to MET removal is not shown. R^2 for "proton" with "potassium" for 7 categories after MET removal was 0.74. Pearson's product-moment correlation across the 7 categories for "proton" with "BK" was R = 0.901 (p = 0.00283). R^2 for correlation of "proton" with "BK" across the 7 categories was 0.81. It is unknown why citations in the MET category no longer positively participated in the correlation seen in previous searches without "cancer" for "proton" and "potassium" but may have been due to the tendency for negative studies to remain unpublished. The answer could be important but is beyond the scope of this study. It also was noted that compared to searches without "cancer" shown in Figure 4B, the "BK" citations appeared to constitute an even larger proportion of "potassium" searches when "cancer" was included, while assuming that "potassium" in the searches included all or most of "BK" citations (Figure 4C). Numerous citations were shared pairwise in 2-word searches (not restricted to cancer) among the 8 categories of 7 oncogenes and histone with the numbers shown (Figure 4D). Thus, many studies involving the 8 categories describe them collectively. The E1-E70 studies provide a broad view of KCN genes among potassium studies. Citation searches of several KCN proteins other than BK did not produce sufficient numbers for comparisons.

3.3.9. Non-KCN DEG Repeats in E1-E70

The non-KCN DEG found repeatedly in up to 5-7 studies were often detected with *KCNN4* and some with *KCNMA1*. Among the non-KCN repeat DEG, *ITGA2/*Integrin Alpha-2 was detected most frequently (7 studies). Six of these also included H^+-sensitive KCN DEGs which are bolded as follows: **E8** (***KCNK1, -N4***)**,** E15, **E39** (***KCNMA1***), **E41**(***KCNMA1***, ***-N4***), **E49**(***KCNN4***), **E64**(***KCNN4***), and **E69**(***KCNN4***). *KCNN4* was the most frequently found DEG, 9 times total and in 5 of 7 studies with *ITGA2* as a DEG. The four studies of co-expressed *KCNN4*, *ITGA2*, and *PLAUR*, E8 [173], E41 [163], E49 [167], and E69 [199], included 2 lung cancers, 1 melanoma, and 1 pancreatic cancer, in the categories of *His/Chr/Epi*, *TP53*, and *RAS* as listed (Figure 5A**,** left Venn diagram). *HMGA2/*High Mobility Group AT-hook 2, *LIF/*Leukemia Inhibitory Factor, and *PLAUR/*Plasminogen Activator, Urokinase Receptor (UPAR) were identified as non-KCN DEG in 6 studies each that also often detected *KCNN4* as a DEG.

A

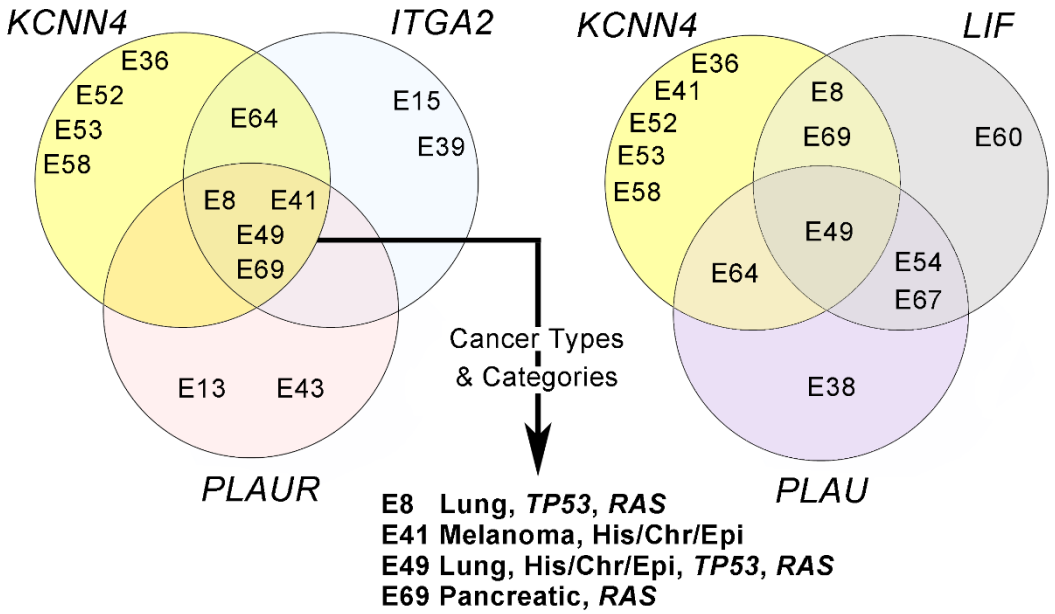

B

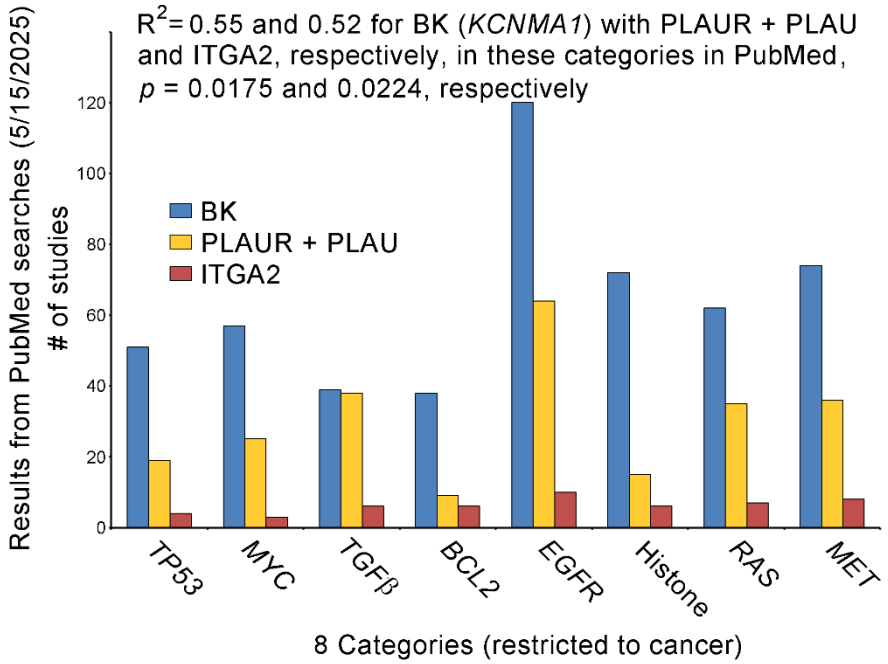

KCNMA1/BK
KCNN4/KCa3.1, IK, SK4, or Gardos channel
ITGA2/Integrin A2
LIF/Leukemia Inhibitory Factor
PLAU/Urokinase-Type Plasminogen Activator (uPA)
PLAUR/uPA Receptor

Figure 5. Repeat non-KCN DEG were found, often with *KCNN4* and some with *KCNMA1*. (A) Among the non-KCN repeat DEG, *ITGA2*/Integrin Alpha-2 was detected most frequently (7 studies). Six of these studies also included H^+-sensitive KCN DEGs which are bolded as follows: **E8** (***KCNK1, -N4***), E15, **E39** (***KCNMA1***), **E41**(***KCNMA1***, ***-N4***), **E49**(***KCNN4***), **E64**(***KCNN4***), and **E69**(***KCNN4***). *KCNN4* was the most frequently found DEG, 9 times total and in 5 of 7 studies for *ITGA2*. The four studies of co-expressed *KCNN4*, *ITGA2*, and *PLAUR*, E8 [173], E41[163], E49 [167], and E69 [199] , included 2 lung cancers, 1 melanoma, and 1 pancreatic cancer, in the categories of *His/Chr/Epi*, *TP53*, and *RAS* as listed (top left Venn diagram). One study detected *KCNN4*, *LIF*, and *PLAU* together as DEG (top right Venn diagram). One study, E41 [163], detected *KCNMA1*, *KCNN4, ITGA2*, and *PLAUR* together as DEG (not shown). (**B**) PubMed word searches for shared citations among "BK" (encoded by *KCNMA1)* and "PLAUR" + "PLAU" and "ITGA2" found correlations of $R^2 = 0.55$, $p = 0.0175$, and $R^2 = 0.52$, $p = 9.0224$, respectively, across the 8 categories of 7 oncogenes and histone.

Two studies detected *KCNN4*, *ITGA2*, and *PLAU* (found in 5 studies, ligand for PLAUR) together as DEG (not shown). *PLAUR* and *PLAU* were DEG together in only one study. Ten studies had either *PLAUR* and/or *PLAU* as DEG. Three studies detected *KCNN4*, *ITGA2*, and *LIF* together (not shown) and one study detected *KCNN4*, *LIF*, and *PLAU* together as DEG (Figure 5A, right Venn diagram). One study, E41 [163], detected *KCNMA1*, *KCNN4, ITGA2*, and *PLAUR* together as DEG (not shown).

Searches of PubMed for shared citations in cancer searches with "BK" with "PLAUR + PLAU" and then "ITGA2" in 3-word searches including "cancer" found significant Pearson's product-moment correlations of R = 0.742 ($p = 0.0175$) and 0.718 ($p = 0.0224$), respectively, and $R^2 = 0.55$ and 0.52, respectively, across the 8 categories of 7 oncogenes and "histone" when each was used as a third word (Figure 4B). Although none of the other potassium channels could be checked in this way, repeats in E1-E70 may have value for eventually identifying functionally relevant co-expressed non-KCN DEG's products to study experimentally with KCN gene products, especially *KCNN4* and *KCNMA1*.

Also, non-KCN DEG found in E1-E70 overlap with those in recent studies of genes encoding circulating proteins associated with risk for numerous types of cancer. The following genes found as DEG in 4 - 6 of the E1-E70 studies, that are shared with the two studies, are as follows with their frequency (X = times): *FGFR3* (5X), *GDF15* (4X), *IGFBP3* (5X), *IGFBP7* (4X), *KRT19* (4X), and *PLAUR* (6X) [224,225].

3.3.10. Non-KCN DEG Superfamilies in E1-E70

Nine superfamilies of non-KCN DEG were detected in E1-E70 with at least 15 occurrences. The instances of superfamily occurrences included as follows: 74X for SLC (Solute Carrier), 32X for COL (Collagen), 27X for ITG (Integrin), 22X for TMEM (Transmembrane), 21X for CD (Cluster of Differentiation), 19X for GPR (G-Protein coupled Receptor), 18X for SOX (Sry-related HMG bOX), 15X for SERPIN (SERine Proteinase INhibitors), and 15X for TNFRSF (Tumor Necrosis Factor Receptor Super Family) superfamily members. DEG repeated in at least 2 studies were present in all of the superfamilies listed.

The largest numbers of repeat non-KCN DEG occurrences were the 7X, 5X, and 4X DEG occurrences of *ITGA2* (previously mentioned), *SOX2*, and *SLC1A2/*Excitatory Amino Acid Transporter 2 (EAAT2), respectively, among the superfamilies. EAAT2 clears glutamate from the extracellular space at synapses [226-228]. *SLC16A3*, monocarboxylate transporter 4, was a DEG in 2 studies as shown (Figure 3B). Six Regulators of G protein Signaling (RGS) family members were also found as DEG in 7 studies. Eighteen (25.7%) of the 70 studies had either GPR or RGS family member DEG. Among the GPR DEG found, none are known as being H^+-sensitive as described in Appendix B (Text B1). Four carbonic anhydrase genes, *CA2*, *CA9*, *CA12*, and *CA14* were found among 5 studies. *CA2* and *CA9* are shown (Figure 3B). Genes encoding subunits of Na/K-ATPases, *ATP1A2*, *ATP1B1*, and *ATP1B2*, were DEG in 4, 2, and 1 of the E1-E70 studies, respectively (See Fig. 3B). Aquaporin family genes, *AQP1*, *AQP3* and *AQP4*, were collectively DEG in ten of the E1-E70 studies.

3.3.11. KCNs Encoding H^+-Sensitive Proteins in E1- E70 in Ten Cancer Reviews

Ten reviews describing KCN family members in malignancy were compared with detection of KCN members in E1-E70. The numbers of KCN genes described in reviews are listed as follows: 7 in a review of glioblastomas [229], 3 in a meeting report for a colloquium on cancer [230], 23 in a review listing 18 cancer types [231], 13 in a review that listed 10 cancer types [232], 9 in a review mentioning 17 cancer types [233], 21 in a review that listed 14 cancer types [234], 12 in a review mentioning at least 13 cancer types [235], 15 in a review that listed 7 cancer types [236], 13 in a review that listed 13 cancer types [237], and 13 in a review that mentioned 11 cancer types [238]. Twenty KCNs found in 35 (one half) of E1 - E70 studies overlap with those in the reviews and are listed as follows: *KCNA1*, *A3*, *A5*, *D1*, *H1*, *H2*, *H7*, *J5*, *J8*, *J10*, *K2*, *K3*, *K5*, *K15*, *MA1*, *N2*, *N3*, *N4*, *Q1*, and*T2*. The ten reviews combined with E1-E70 highlight KCN genes that encode H^+-sensitive proteins. At least one KCN gene in each of 29 studies (82.85% of 35 overlapping studies from E1 – E70) encodes a H^+-sensitive protein and these studies are listed as follows: E4, E5, E6, E8, E9, E12, E13, E16, E22, E24, E28, E31, E32, E34, E36, E38, E39, E40, E41, E47, E49, E52, E53, E58, E60, E64, E68, E69, and E70. The remaining overlapping studies included E15, E29, E33, E45, E65, and E66. Citations for E1-E70 are in *Section 3.3.6. Categories Among Studies with E1-E70 Citations Per Category*.

3.3.12. Long Introns (20,000 bp or longer) in E1-E70's KCN DEG

Many genes in the KCN family have long introns (at least 20,000 bp in length). Long introns can affect gene expression and may play a role in gene regulation. Also, they may be affected by genetic damage as cancer develops and evolves. Thirty-one (58.5%) of the 53 KCN DEG detected in E1-E70 contain long introns, some much greater than 20,000 bp. Seven KCN DEG (*KCNC2*, *D3*, *H1*, *H8*, *MA1*, *Q1*, and *T2*) each contain at least one intron that is 100,000 – 199,999 bp in length. Five KCN DEG (*KCNH7*, *IP1*, *Q3*, *MA1*, and *MB2*) each contain at least one 200,000 - 299,999 bp intron and *KCNB2* and *KCNQ5* each contain at least one intron that is 300,000 – 399,999 bp long. Fourteen of the KCN DEG in E1-E70 contain multiple long introns. *KCNMA1* and *KCNT2* each

contain seven long introns. *KCNN4* is among the KCN DEG that do not contain any long introns. Forty-one (58.6%) of the E1-E70 studies contained at least one KCN DEG that had at least one long intron. Nine studies had multiple (2 – 4) KCN DEG with long introns. However, *KCNA3*, *A5,* and *F1* in E1-E70 have only one exon and therefore do not contain any introns. Intron data from the Ensembl database, was obtained in 2023 and 2025, last accessed 6/22/2025, Ensembl browser 114 (May 2025 release). The contrast between the introns of *KCNMA1* and *KCNN4* is striking and raises the possibility of increased preservation of *KCNN4* as a smaller target when genetic damage occurs but this is unknown.

3.4. Study of Selected KCN DEG in REMBRANDT

3.4.1. Rationale and Preliminary REMBRANDT Survey

Based on glioblastoma cell adherence to dying cells, "palisading" around necrotic tumor regions, chemotaxis to serum and possibly a potassium gradient, and the tendency of glioblastoma cells to invade white matter tracts, the possibility of potassium acting as a chemoattractant in the CNS biological milieu led to a search for KCN DEG in the brain tumor database, REMBRANDT, concurrently while searching for KCN DEG in studies of various cancer types already described. REMBRANDT (as a part of the online Georgetown Database of Cancer (G-DOC) was queried. Among potassium channel related genes, KCN family members were selected because of their H^+- sensitive and modulatory/regulatory members, independence from energy requirements for many members, susceptibility to genomic damage due to the wide genomic distribution of the large KCN family (at least 90 members), potential to be downstream effectors of oncogenes, possible interactions with G-proteins, complex relationships with biological milieus, and additionally their major roles in glial and neuronal functions. Initial queries in the Online Mendelian Inheritance in Man (OMIM) database (https://omim.gov) in 2018-2019 and literature descriptions of KCN genes [239] yielded 41 KCN genes with neuronal as well as astrocytic expressions in the human brain to consider. All 41 genes were found in loci that corresponded to known regions of chromosomal losses, gains, or both in glioblastomas, published as Figure 3-76 in a book authored by Burger PC and Scheithauer BW [1]. These genes are distributed as follows: Chromosome (Ch) 1 (*KCNA2*, *A3*, *C4*, *N3*, *J9*, *J10*, *K2*, *K1*); Ch2 (*KCNJ3*, *J13*); Ch3(*KCNMB2*, *MB3*); Ch5 (*KCNN2*, *MB1*); Ch6 (*KCNK17*), Ch8 (*KCNQ3*); Ch9 (*KCNT1*); Ch10 (*KCNMA1, K18*), Ch11 (*KCNJ11*, *C1*, *A4*, *K4*, *J5*); Ch12 (*KCNA1*, *A5*, *A6*, *J8*, *MB4*); Ch14 (*KCNK10*), Ch17 (*KCNJ12*, *J16*, *J2*); Ch19 (*KCNN1*, *N4*, *C3*); Ch20 (*KCNB1*, *Q2*); Ch21 (*KCNJ15*, *J6*); and Ch22 (*KCNJ4*). The most numerous were in the KCNJ subfamily genes (*KCNJ2*,*3*,*4*,*5*,*6*,*8*,*9*,*10*,*11*,*12*,*13*,*15*, and*16*) encoding inwardly rectifying potassium channel forming proteins(Kir) and their modulators/regulators, Kir2.1, 3.1, 2.3, 3.4, 3.2, 6.1, 3.3, 4.1, 6.2, 2.2, 7.1, 4.2, and 5.1. Kir channels can be relatively occluded by Mg^{2+} or polyamines when cell membrane potentials are positive relative to the equilibrium potential of K^+ that allows only a small outward current. At membrane potentials negative to the equilibrium potential of K^+, Mg^{2+} and polyamines leave the channels by flowing into the cell so a large inward K^+ current can occur [240,241]. Kirs, including Kir4.1, may also extrude K^+. Kir 4.1 and 5.1 are present in both astrocytes and oligodendrocytes [39,242].

A preliminary survey of REMBRANDT for expression of 21 KCN family members,12 other potassium flow related genes, and 4 housekeeping genes (HKG) checked for differences in glioblastomas from patients, with and without a history of seizure medications. Seizures could be an indicator for abnormal levels of potassium [243-245]. With "unknowns for gene expression" included, there were 84 and 18 glioblastomas, with and without a history of anti-seizure medication, respectively. Compared to the absolute difference in the expression of HKG (*PPIA*, *RPLP0*, *YWHAZ*, and *B2M*) between the two groups, the single or average absolute median values of reporter probes for *KCNJ10*, *KCNK3*, *ATP1A1*, *KCNN3*, *KCNJ13*, *KCNMB2*, *SLC12A7*/KCC4, *KCNN2*, *KCNMB1*, *GJA1*, *KCND2*, *KCNK9*, *SLC1A2*/EAAT2, *KCNJ2*, and *KCNJ16* exceeded the average HKG difference (0.1131) of median values. Others, including *ATP1A2*, *KCNA2*, *KCNA3*, *KCNK1*, *KCNIP3*, *KCNMB3*, *SLC1A3*/EAAT1, *SLC12A2*/NKCC1, *KCNT1*, *KCNMA1*, *LRRC55*, *KCNA1*, *KCNMB4*, *GJB2*, *GJB6*, *SLC12A6*/KCC3, and *FXYD7*, did not exceed the average HKG difference in expression. The preliminary data (not further analyzed) suggested that the subset of glioblastomas in patients with seizures (according to medication history) had expressions of KCN family member genes that could be compared to the same genes in oligodendrogliomas (less invasive glial tumor) from patients who also had seizures. Abnormalities in potassium-related gene expressions, such as among the KCN family members, resulting in potassium flux related to worse malignant behavior could potentially underly differences in behavior between the related gliomas, oligodendrogliomas and glioblastomas.

3.4.2. Specificity in Gene Expressions Reflecting Cell of Origin

Checks were made for expected findings. Expression of *ATP1A2* (alpha subunit of Na/K-ATPase specific for glial cells) was higher in both types of glial tumors versus its neuronal specific counterpart (*ATP1A1*) in the patients on anti-seizure medications. The medians of two reporter probes available for each gene yielded significant differences, $p = 0.0345$ and 0.0278, respectively, for oligodendrogliomas and glioblastomas using 2-tailed, unpaired t-tests (Figure 6A). The specificity of expression for connexin genes in astrocytic cells, *GJA1*/Cx43, *GJB6*/Cx30, and *GJB2*/Cx26, was used to verify the expected cells of origin for the two types of glial tumors, oligodendrogliomas and glioblastomas [242,246,247], in REMBRANDT patients on anti-seizure drugs. The medians of single reporter probes for expression of astrocytic type connexins, collectively as a group, were significantly greater in the glioblastomas, $p = 0.0477$ (1-tailed, paired t test), (Figure 6B). Results using multiple reporters for oligodendrocyte type connexins were not available. More prominent vascularization of glioblastomas versus oligodendrogliomas was consistent with a trend for greater expression of *VEGFA*, $p = 0.166$, in the glioblastomas among the patients with known anti-seizure treatment (not shown).

REMBRANDT

(REpository for Molecular Brain Neoplasia DaTa)

A — Anti-seizure Rx

Gene	Oligo	GBM
ATP1A1	2.92049	2.91169
versus	5.08693	4.84342
ATP1A2	9.58621	9.49969
	9.90387	10.03376
p values	0.03449*	0.02776*

B — Anti-seizure Rx

Gene	Oligo	GBM
GJA1	3.79493	3.92367
GJB2	4.61600	4.93627
GJB6	6.89208	7.01980

p value for Oligo versus GBM = 0.04765*

C

Gene	Large Group Oligo	Large Group GBM	Anti-seizure Rx Oligo	Anti-seizure Rx GBM
KCNJ10	7.88072	6.94161	7.88221	6.82805
	3.35772	3.27711	3.31175	3.19652
KCNJ16	8.12864	6.81784	8.30402	7.30945
	7.41947	6.30007	7.59016	6.54826
KCNK3	5.25703	5.33609	5.09866	5.41457
	7.22861	7.62468	7.36709	7.52793
KCNK10	5.26409	5.21112	5.31340	5.01056
	11.18701	10.50502	11.33574	10.54029
	8.66476	8.52497	8.84111	8.53841
CA12	9.36679	9.25853	9.31132	9.29754
	8.39995	8.14632	8.43690	8.03071
	10.92476	10.72416	10.92042	10.68890
	6.29452	6.07502	6.00293	5.98906
	5.39249	5.50748	5.84638	5.23676
	7.07346	5.45519	7.74194	5.83069
TP53	11.58190	12.11004	11.43341	12.11586
	7.86090	7.95125	7.79580	8.06428

D — Anti-seizure Rx

Gene	Gene OMG difference	HKG	Oligo	GBM	HKG OMG difference
KCNJ10	1.05416	*PPIA*	6.90772	7.09117	- 0.18345
	0.11523		10.16633	9.76835	0.39798
KCNJ16	0.99457		9.45655	9.81833	- 0.36178
	1.04190		7.43305	6.78537	0.64768
KCNK3	- 0.31591		6.63263	6.71673	- 0.08410
	- 0.16084		6.64463	6.92428	- 0.27965
KCNK10	0.30284		8.79386	8.84473	- 0.05087
	0.79545		8.68471	8.74586	- 0.06115
	0.30270	*RPLP0*	9.77174	9.73344	0.03830
CA12	0.01378		9.26984	9.68827	- 0.41843
	0.40619		9.98964	9.80454	0.18510
	0.23152		9.82984	9.70374	0.12610
	0.01387		9.54447	9.22953	0.31494
	0.60962	*YWHAZ*	5.91707	4.53647	1.38060
	1.91125		5.59831	5.48575	0.11256
TP53	- 0.68245		7.86566	8.97262	- 1.10696
	- 0.26848		5.82757	6.57399	- 0.74642
		B2M	5.15497	5.61879	- 0.46382
			8.55786	8.41906	0.13880
			9.17194	8.68818	0.48376

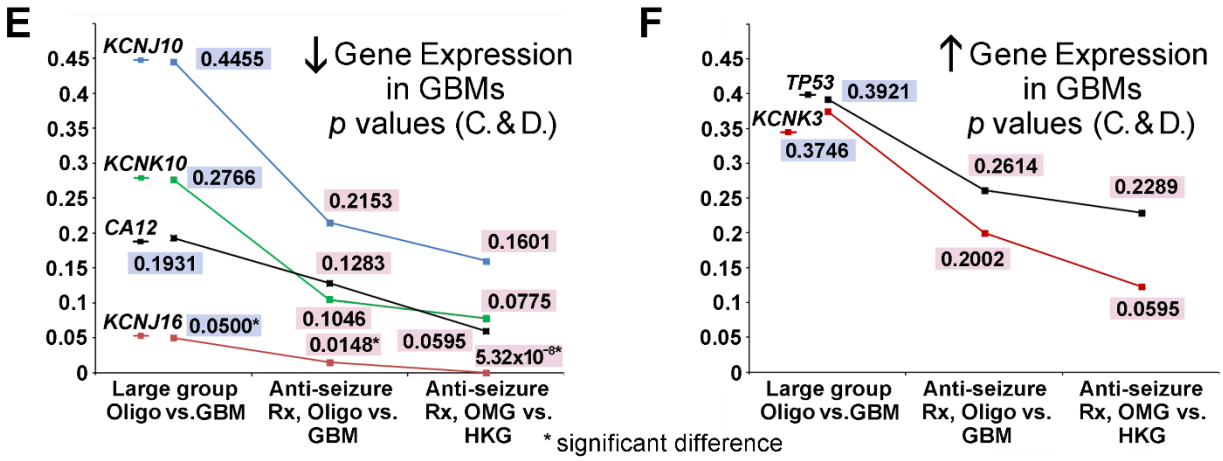

Figure 6. Results for oligodendrogliomas (Oligo) and glioblastomas (GBM) from REMBRANDT. (**A – D**) Median reporter probe values of microarray gene expression results from Oligo and GBM tumor tissue are shown in columns as indicated. Pink backgrounds (A – F) indicate results are from patients on anti-seizure medications (Anti-seizure Rx). Results with a blue background (C, E, F). are from Large Group patients (medication history not used for criteria). (**A**) The *p* values of t-tests are at the bottoms of columns for comparisons of *ATP1A1*/Na/K-ATPase subunit alpha 1, neural specific, versus *ATP1A2*/Na/K-ATPase subunit alpha 2, glial specific in Oligo and GBM with significant differences confirming glial origins. (**B**) Single median reporter probe values for astrocytic-specific (versus oligodendroglial) values for gap junction genes with higher levels of expression in GBM versus Oligo as expected. (**C**) Values listed for median

reporter probes for 4 KCN genes (See text) and 2 other genes, *CA12*/carbonic anhydrase 12 and *TP53*/p53. (**D**) An additional method to evaluate expression of genes shown (C)**,** calculated Oligo Minus GBM (OMG) differences of the median probe results for each gene of interest and the housekeeping genes (HKG). These differences were then compared to correct for variation in tissue handling, assay-to-assay variation within and between institutions, etc. (**E – F**) The *p* values are shown graphically for decreased and increased gene expressions in GBM, respectively. Significance improved dramatically for *KCNJ16* with this approach and trends became stronger for other genes. Oligo = oligodendroglioma, GBM = glioblastoma, Rx = medication, HKG = housekeeping genes. REMBRANDT (part of the Georgetown Database of Cancer (G-DOC).

3.4.3. KCN Gene Expressions in Patients on Seizure Medications

Limiting tumor comparisons to patients on anti-seizure medications improved detection between the two types of invasive glial tumors. Without using the history of seizure medications, a difference in expression of *KCNJ16*/Kir5.1 in glioblastomas (less expression), $p = 0.05$, of borderline significance, became significant in glioblastomas using the smaller group of patients on anti-seizure drugs, $p = 0.0148$. Trends also improved for differences in expressions of *KCNJ10*Kir4.1, *KCNK3*/TASK1, and *KCNK10*/TREK2, (all H^+-sensitive, Appendix B (Table B2) and [248,249]) with reporter probe data (Figure 6C) and *p* values (Figures 6E - F) shown along with other genes, *CA12*/carbonic anhydrase 12 and *TP53*/p53. *SLC16A1*/MCT1, *PTEN*, and other non-KCN genes (not shown), also showed some improvement in the difference between oligodendrogliomas and glioblastomas when comparisons were limited to patients on anti-seizure drugs. Median results of five *SLC16A1*/MCT1 probes indicating increased expression in glioblastomas, but without significance, had $p = 0.269$ and $p = 0.255$ in the smaller group with a history of anti-seizure medication.

3.4.4. Oligodendroglioma Minus Glioblastoma (OMG) Normalization

Housekeeping gene (HKG) normalization was used to correct for loss of genomic integrity, differences in tissue handling, assay to assay variation within and between institutions, etc. in the comparisons using the microarrays of two different type of tumors in REMBRANDT. It was used for comparisons in patients on anti-seizure medications. Oligodendroglioma Minus Glioblastoma (OMG) differences (increased or decreased) were calculated for each reporter probe's median expression. These OMG differences for each DEG were compared to the OMG differences for all 4 HKGs. Enhancement of the previously detected differences resulting in better *p* values as shown (Figures 6D-F). The OMG difference for *KCNJ16*, decreased in glioblastomas, became highly significant, $p = 5.532 \times 10^{-8}$. The trends for several other genes improved. The *t*-tests were calculated for unpaired samples with unequal variance in the OMG comparisons. The median probe data (Adobe Flash format) in Figures 6A-D is no longer available online in REMBRANDT (Georgetown website, see Materials and Methods, Subsection *2.3. Databases*).

3.5.1. KCN DEG Shared in E1-E70, REMBRANDT, and Glioblastoma Cell Lines [22]

Whole exome and RNA sequencing data of LN18, LN229, T98G, U87, U343, and U373 human glioblastoma cell lines, available as Open Access in Patil et al.'s Supplementary Materials [22], revealed data for many of the KCN DEG and genes of interest found in the E1-E70 and REMBRANDT studies. Also, 3 and 5 of these cell lines were also used for the cell settling and cell migration studies, respectively, described earlier. Their data availability is described in the **Data Availability Statement** that follows this article's text. They described their methodology in detail [22], with some information also included here. For each of the GBM cell lines, U87, T98G, LN229, LN18, U343, and U373, a 62 Mb region of the genome was targeted. Alignment was to human reference genome hg19. Their single nucleotide variant (SNV) was considered to be a potential Cancer Specific Mutation (CSM) if present in the COSMIC database (Reference 18 in [22]) and/or was present in GBM TCGA exome sequencing data (their references 8,9). Data for 4 cell lines, U87, T98G, LN229, and LN18, had an average concordance of 65.3% with the COSMIC database (their reference 18) and 74.74% with the Broad Institute's CCLE database (their reference 19). In addition to CSMs, Patil et al. reported small insertions and deletions (indels) in a size range of -49 to +29 bases. Differential gene expression data per Patil and colleagues was obtained via comparisons of their RNA-seq data from six GBM cell lines, U87, T98G, LN18, LN229, U343, and U373, with expression data of five normal brain tissue samples from TCGA, with a cut off value of a 2-fold change in absolute expressions. Their results for 2,214 genes compared with those that were also present in TCGA GBM tumor samples had a concordance of approximately 73%. Of the 2,214 genes in the Patil study,1,831 (82.7%) were down regulated. For the 1,621 genes similarly up or down regulated in both the TCGA and Patil et al. studies, 79.64% were down regulated.

Among the KCN genes identified by Patil and colleagues, 42 KCN genes had CSM and indels. The DNA changes identified in 18 of the 42 KCN genes occurred in at least 3 of their glioblastoma cell lines. The KCN family group, with the highest number of members (ten) with reported DNA changes, included *KCNJ1*, *2*, *3*, *5*, *6*, *10*, *12*, *13*, *14*, and*16*. Patil and colleagues identified 69 CSM among KCN family member genes, representing 4.33% of 1,594 CSM found in all the genes they sequenced. Also, the 68 indels (25 insertions and 43 deletions) that they found in KCN family members represented 1.75% of all 3,892 indels found in the 6 glioblastoma cell lines. For comparison with this study of KCN DEG in E1-E70 and genes of interest in REMBRANDT, shared KCN DEG with their sequencing results revealed DNA alterations including CSM, INS, and DEL. Twenty-three of the E1-E70 KCN DEG and 4 of the REMBRANDT study's KCN genes of interest based on expression had changes described in the genomes of 6 glioblastoma cell lines by Patil et al. Those detected in E1-E70 (glioblastomas (7) with 28 other cancer types) are marked with light green squares on the right side of lists, and genes of interest (significant difference or trends) found in REMBRANDT are bolded (*KCNJ10*, *KCNJ16*, *KCNK3*, and *KCNK10*), (Figure 7A). Patil et al. found that all 51 KCN family members with gene expressions detected in the six glioblastoma cell lines were down regulated versus normal with the 51 expressed KCN family member genes representing 1.48% of all 3428 genes found to be differentially expressed in the cell lines. Average gene expression levels of RNA determined by Patil et al. are listed in descending order of abundance, including 27 and 4 of the E1-E70 and REMBRANDT KCN genes, respectively, along with names of encoded proteins (Figure 7B). *KCNJ16*, which was

significantly down regulated in REMBRANDT's glioblastomas, when compared to oligodendrogliomas, was ranked among the lowest detectable expressing genes in the 6 glioblastoma cell lines studied by Patil et al. Only four of the 51 KCN genes with expression values ranging from <0.001 to 803.719 (modeled counts) had lower expression than detected for *KCNJ16* (Figure 7B). The log2 fold RNA changes from normal calculated using their Supplementary Table S6 [22], are shown for the 51 KCNs with detectable RNA in the glioblastoma cell lines. The 27 genes (52.94%) with encoded H^+- sensitive proteins and the 24 KCN genes with DNA changes are highlighted on the graph (Figure 7C). Of the 53 KCNs in E1-E70 there are 38 (71.70%) also described by Patil et al. in their glioblastoma cell lines, either with the DNA changes shown and/or with RNA expressions detected. Of the seven GBM studies in E1-E70, six (85.71%) each shared 1 - 3 KCN DEG with those described by Patil et al. The specific glioblastoma studies in E1-E70 with these KCN DEG are E5, E21, E26, E27, E31, and E51. Only one, E50, of the E1-E70 glioblastoma studies did not detect a KCN DEG corresponding to those with RNA expression detected by Patil et al. [22]. There is a large overlap of KCNs encoding proteins with H^+-sensitivity in E1-E70, REMBRANDT, and those described by Patil et al. (Figure 7C). References for H^+-sensitivities are cited in Appendix B, Table B2, and earlier in Section *3.4.3. KCN Gene Expressions in Patients on Seizure Medications,* for the encoded proteins of *KCNA1*, *KCNA3*, *KCNA5*, *KCNAB2*, *KCNH1*, *KCNH3*, *KCNJ10*, *KCNJ16*, *KCNK1*, *KCNK3*, *KCNMB4*, *KCNN3*, *KCNQ1*, *KCNQ2*, *KCNQ3*, *KCNQ5*, and *KCNT1*. References for H^+-sensitivity of the proteins encoded by additional KCN genes shown (Figure 7C) are as follows: *KCNA2*/Kv1.2 [250], *KCNA4/*Kv1.4 [251,252], *KCNC4*/Kv3.4 [253], *KCNH4*/ELK1 [254], *KCNJ3*/GIRK1 [255,256], *KCNJ11*/Kir6.2,IKATP [257,258], *KCNJ12*/Kir2.2,HIRK1 [259] (variant), *KCNK9*/K2P9,TASK3 [260,261], and *KCNK17*/K2P17.1,TALK2,TASK4 [262].

A

Gene	Ch	5'UTR	Protein coding	Introns	3'UTR	# Cell Lines
■ *KCNA1*	12				DEL	1
■ *KCNA3*	1				INS,CSM	3
KCNA6	12				INS(2)	5
KCNA7	19		DEL			1
KCNAB1	3				DEL(5)	6
KCNB1	20				CSM	1
KCNC1	11				CSM	1
■ *KCNC3*	19				INS	2
KCNC4	1		CSM		CSM	2
■ *KCND1*	X	CSM	CSM			2
KCND2	7	CSM				1
KCNE1	21				INS	4
■ *KCNE4*	2				INS	3
■ *KCNG3*	2		CSM		CSM	2
KCNG4	16	CSM				1
■ *KCNH1*	1		CSM		DEL(2),CSM(2)	5
■ *KCNH8*	3		CSM		CSM	2
■ *KCNIP3*	2				CSM	1
KCNIP4	4			INS(2),DEL(5), CSM	INS(3), DEL(3)	6
KCNJ1	11				INS	1
KCNJ2	17				INS,DEL	3
KCNJ3	2				INS,CSM	5
■ *KCNJ5*	11	CSM(4)			INS,DEL	5
KCNJ6	21				CSM(2)	1
■ ***KCNJ10***	1				DEL,CSM	2
KCNJ12	17		DEL,CSM(23, 10 silent)		INS,DEL(3)	6
■ *KCNJ13*	2	DEL				1
KCNJ14	19				INS,CSM	2
■ ***KCNJ16***	17			DEL	INS(2),DEL	4
■ *KCNK2*	1		CSM		INS(3),DEL, CSM	6
■ ***KCNK3***	2				CSM	1
KCNK10	14			CSM	INS,DEL(4), CSM(2)	6
KCNK16	6		CSM			1
■ *KCNMA1*	10				DEL,CSM	3
■ *KCNMB1*	5				DEL	1
■ *KCNMB3*	3	INS,DEL	DEL			4
KCNN1	19		CSM			1
■ *KCNN2*	5		INS			4
■ *KCNN3*	1		CSM(5,2silent)			1
■ *KCNQ1*	11		CSM(2,1silent)	DEL(6) CSM(2)		6
■ *KCNS1*	20				DEL	1
■ *KCNT2*	1		CSM		CSM	2

■ = DEG in E1 - E70 & REMBRANDT DEG are bolded

UTR = Untranslated Region, DEL = Deletion, INS = Insertion, CSM = Cancer Specific Mutation (Single Allele Substitution)

B

	Gene	Ave. RNA	Protein Name
■	1. *KCNAB2*	803.719	Kvβ2
	2. *KCNC4*	351.847	Kv3.4
■	3. *KCNMB4*	217.130	BKβ4
■	4. *KCNIP3*	191.967	KChIP3
	5. *KCNB1*	155.982	Kv2.1
■	6. *KCNN3*	129.440	KCa2.3, SK3
■	7. ***KCNJ10***	94.083	Kir4.1
■	8. *KCNF1*	74.733	Kv5.1
	9. *KCNIP4*	72.195	KChIP4
■	10. *KCNK1*	60.489	K2P1,TWIK1
■	11. *KCNC3*	60.440	Kv3.3
■	12. ***KCNK3***	54.020	K2P3,TASK1
■	13. *KCNQ5*	51.475	Kv7.5
	14. *KCNIP2*	47.120	KChIP2
■	15. *KCNH3*	46.225	Kv12.2,ELK2
■	16. *KCNA1*	45.318	Kv1.1
	17. *KCNAB1*	36.674	Kvβ1
	18. *KCNJ6*	36.411	Kir3.2,GIRK2
	19. *KCNJ4*	35.865	Kir2.3,HIRK2
	20. *KCNK9*	26.810	K2P9.1,TASK3
■	21. *KCNQ3*	22.001	Kv7.3
	22. *KCNJ12*	21.544	Kir2.2,HIRK1
	23. *KCNA2*	19.745	Kv1.2
■	24. *KCNT2*	17.533	KCa4.2,SLICK
	25. *KCND2*	16.774	Kv4.2
	26. ***KCNK10***	13.840	K2P10.1,TREK2
■	27. *KCNQ1*	13.662	Kv7.1
	28. *KCNN1*	11.494	KCa2.1, SK1
	29. *KCNJ11*	11.242	Kir6.2,IKATP
■	30. *KCNIP1*	10.936	KChIP1
■	31. *KCNS1*	6.771	Kv9.1
■	32. *KCNT1*	6.494	KCa4.1,SLACK
	33. *KCNJ3*	6.335	Kir3.1,GIRK1
	34. *KCNH4*	5.574	Kv12.3,ELK1
■	35. *KCNJ9*	5.470	Kir3.3,GIRK3
	36. *KCNC1*	5.398	Kv3.1,NGK2
	37. *KCNK12*	5.346	K2P12.1,THIK2
	38. *KCNS2*	3.877	Kv9.2
	39. *KCNA4*	3.813	Kv1.4
■	40. *KCNH1*	3.485	Kv10.1,Eag1
	41. *KCNV1*	2.739	Kv8.1,
■	42. *KCNG2*	2.675	Kv6.2
	43. *KCNK13*	0.965	K2P13.1,THIK1
■	44. *KCNA5*	0.947	Kv1.5
■	45. *KCNA3*	0.833	Kv1.3
■	46. *KCNB2*	0.833	Kv2.2
■	47. ***KCNJ16***	0.833	Kir5.1
	48. *KCNA6*	0.584	Kv1.6
■	49. *KCNQ2*	0.432	Kv7.2
■	50. *KCNC2*	< 0.001	Kv3.2
	51. *KCNK17*	< 0.001	K2P17.1,TALK2

C

KCN Genes with Detected RNA in 6 Glioblastoma Cell Lines (ave. in B. above, LN18,LN229,T98G,U87,U343,U373)

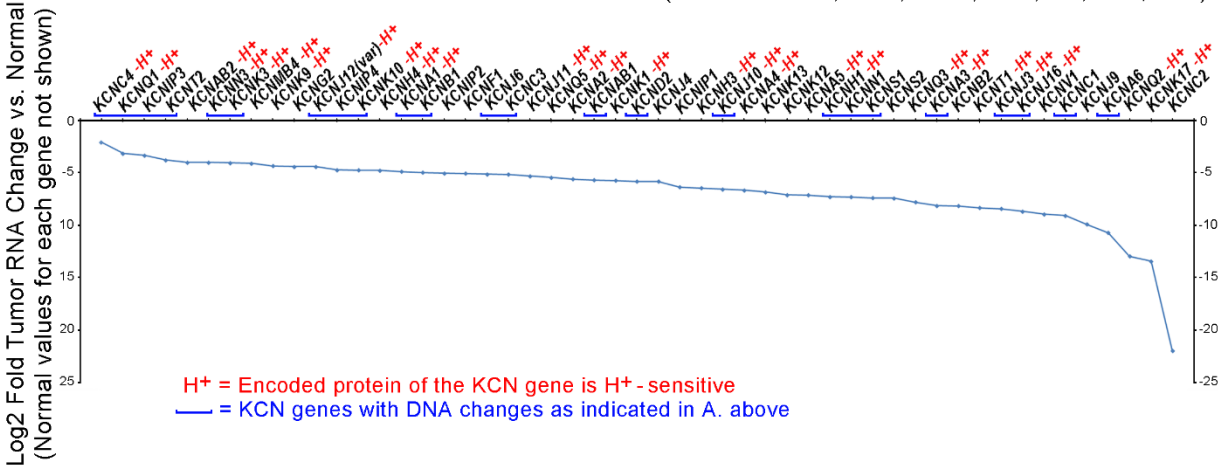

Figure 7. Many KCN DEG detected in E1-E70 studies (Figures 3 - 5). and in REMBRANDT (Figure 6). were included in whole genome and expression studies of 6 glioblastoma cells lines by Patil et al. [22]. They reported on LN18, LN229, T98G, U87, U343, and U373 cell lines. For comparisons, the shared KCN DEG detected in E1-E70 (29 cancers including 7 glioblastomas) are marked with light green squares and the KCN DEG found in REMBRANDT are bolded (**A** and **B)**. (**A**) Sequencing results revealed DNA alterations including cancer specific mutations (CSM), insertions (INS), and deletions (DEL). Twenty-three KCN DEG (of 53 in E1-E70, See Figures 3 and 4) and those with potential significance in REMBRANDT (3 with trends and 1 significant KCN DEG, See Figure 6C - F), were detected with changes in the genomes of 6 cell lines (usually > 1) by Patil et al. Several shared KCN DEG were genetically altered in all 6 cell lines. (**B**) Average gene expression levels of RNA determined by Patil et al. are listed in descending order of abundance, including 27 and 4 of the E1-E70 KCN DEG and REMBRANDT's KCN DEG and genes of interest, respectively, along with names of their encoded proteins. (**C**) Log2 fold RNA changes in the combined tumor cell lines versus normal (see text) are shown graphically. KCNs encoding H^+-sensitive proteins are highlighted as red (H^+) and the KCNs found to have DNA changes in (A) are highlighted with underlining blue brackets (␣). Of the 51 KCNs with detectable RNA in the glioblastoma cell lines, 27 (52.94%) encoded proteins that are H^+- sensitive. Of the 53 KCNs in E1-E70 there are 38 (71.70%) also described by Patil et al. in glioblastoma cell lines, either with altered DNA and/or RNA expression values. Of the seven GBM studies in E1-E70, six (85.71%) shared 1 - 3 KCN DEG with those described by Patil et al. [22]. See the text and Appendix B (Figure B1A) for specific glioblastoma studies in E1-E70 and the references for each study are given in Section *3.3.6. Categories Among Studies with E1-E70 Citations Per Category.*

4. Discussion

4.1. Input of Functional U87 Studies

The decision to stochastically investigate potassium in cancer was based on earlier FBS cell migration assays and then observing cytology of glioblastoma cell in settling assays. After fluid was wicked away as cells settled on glass slides, not only was expected cell death and cytoplasmic vacuolization seen, but also small groups of cancer cells clustered around single dying cells. Although malignant cells from body fluid specimens sometimes ingest whole cells, the tight cell adherence of robustly viable cells to dying settled cells that were formerly in cell suspension was a surprise. Uncentrifuged cancer cells from clinical body fluid specimens viewed microscopically, after gentle filtration and dissolution of filters [263,264], do not have this appearance, at least routinely. However, the morphology of the settled, viable cells clustered around single necrotic cells did resemble characteristic rimming of deeply staining glioblastoma cells ("pseudopalisades") around necrotic foci in glioblastoma tumor tissue as described in the Introduction, Section *1.1. General*. Also, basophilic staining in tumor cells of tumors with central necrosis with more alkaline cytoplasmic pH detected in necrotic areas has been established experimentally in cervical cancer cells [265]. Clues, as mentioned earlier, to form a hypothesis for the glioblastoma cells in settling assays and their rimming around necrosis in tissue included (*i*) the viability of cancer cells rimming single dying cells seemed protected from the negative effect of fluid removal, (*ii*) relatively darker staining of some viable clustered tumor cells possibly reflected a pH change in them, and (*iii*) when

ATP is depleted, cells open their cation channels to release K^+ (major cation) before rupturing [266-268]. Potassium efflux has been seen in cancer cells [269].

A chemotactic role for potassium was supported in view of cell migration assays, previously performed for planning the use of FBS to optimize glioblastoma cell lines migrating to HGF. Results could not rule out an unidentified serum constituent acting as a chemoattractant. Multiple cell lines migrated to FBS alone with dose responses. Also, U87 cells migrated significantly (p = 0.0144) with a positive gradient present of K^+ generated by MEM (5.3 mM K^+ in a milieu of amino acids, vitamins, etc.) versus 4.5 mM K^+ in "Migration" media, in the absence of FBS and HGF, and was improved in the presence of FBS (Figure 2E). Support for potassium as the chemoattractant possibly inciting their reversal of pH is also considered.

4.2. Mechanistic Proposal for a New Route to pH Reversal

The KCN family members, many pH sensitive, cooperate to control potassium levels at cell membranes in a putatively H^+-sensitive manner. A new hypothesis is that K^+, as a monovalent exchange cation for H^+, frees bound protons from inner cell membranes for rapid cytoplasmic transfers to proton extruders, and instigates pH reversal in cancer if the control of potassium flux is deregulated. Whether rapid delivery of H^+ to exit sites occurs via the Grotthuss mechanism during pH reversal is also a new consideration that could explain how freed protons become available for rapid cytoplasmic proton transfers to cell exit sites during pH reversal in at least some malignancies. Although the Grotthuss mechanism of rapid proton transfer via "water wires" has been described for proteins and the tight junction of the blood brain barrier [270-272], cytoplasmic Grotthuss type proton transfer in cancer cells has not been recognized. As migrating tumor cells flatten and squeeze into small spaces such as between a nerve fiber and its surrounding nerve sheath or along and then through dense basement membranes, bone, cartilage, etc. there should be microaqueous intracellular regions of tumor cells generated temporarily. The cell settling assays removed fluid to create a microaqueous condition for all cells with simultaneous exposure to K^+ from single dying cells within some clusters of cells. These centralized dying cells could also have become "sinks" for protons released from the surrounding viable tumor cells.

Putatively, entry of K^+ across membranes into the viable cells in settling assays provided replacement ions for H^+ bound to fixed inner membrane anions (and possibly to H^+ bound to cytosolic proteins) that permitted newly freed H^+ (rapidly formed H_3O^+) to diffuse through the cytoplasm, possibly via cytosolic Grotthuss water wires formed under microaqueous conditions to serve as a "root system" for supplying protons to extruders. In tissue, viable microaqueous malignant cells may use a potassium flux, K^+/H^+ exchange, proton transfer in water, and then cell exit of protons as a response to stress or oncogenes to acidify the microenvironment with activation of proteases, etc. for cell migration. Simultaneously a higher cytosolic pH is provided to activate alkaline-sensitive intracellular proteins promoting cell survival. An alkaline pHi leads to maximal tumor cell proliferation coupled with increased glycolysis and adaptation to hypoxia *in silico* [273] and is associated with increased flux of glycolytic enzymes, migration, and invasion experimentally [274]. Also, when pHi increases, H^+ diffusion increases [275], possibly enhancing pH reversal for survival of single, migrating cancer cells.

4.3. Further Consideration of KCN Genes in Cancer, Including Key Negative Findings

Simultaneous studies of multiple KCN genes of interest in REMBRANDT and those in KCN cancer reviews, including those with H^+-sensitivity, supported the ongoing stochastic investigation of KCN family members as DEG in unbiased cancer studies. The relatively large number of studies allowed investigation of H^+-related associations with the expression of the KCN gene family's numerous members differentially expressed in malignancy. KCNs in E1-E70 studies overlapped with KCN genes of interest in REMBRANDT (*KCNJ16*, *KCNJ10*, *KCNK3*, and *KCNK10*, all 4 encoding H^+-sensitive proteins), and with 20 KCN genes covered in ten reviews. At least one KCN DEG in each of 29 studies (82.85% of the 35 studies from E1-E70 overlapping with the KCNs in ten reviews) encodes a H^+-sensitive protein. Potassium ions may redistribute in cancer cells to exchange with H^+ in pH reversal via differential expression in the KCN family members that encode H^+-sensitive proteins, possibly related to oncogenes, genetic damage, etc.

The KCN family offers the possibility of a large variety and range of dynamic distributions of K^+ via its numerous members, networking, biological milieus, modulation by oncogenes, histone/DNA modifiers, etc. Also, potassium is supplied by blood pulsing through the vascular system, although locally haphazard in cancer, and by the firing of action potentials along axons in nerve fibers and white matter tracts. The formation of synapses between tumor cells and neurons provide K^+ as well as other synaptic substances [276]. These sources may be increased or decreased in cancer. Activation of proteases by extracellular acidosis that degrade connective tissues provide increased access to neural and vascular K^+ during migration and metastasis. Multiple proton extruders have been proposed for glycolytic/plurimetabolic type glioblastoma cells [277]. Also, the microaqueous surface conditions in cell settling assays and during tissue invasion *in vivo* suggest a lower probability of CO_2 dissolving in surrounding extracellular fluid to form carbonic acid that dissociates to hydrogen and bicarbonate ions for cell uptake. The possibility of having taurine function significantly as a carrier of cytoplasmic H^+ seems less likely since the only taurine transporters found as DEG in E1 – E70, *SLC16A6* and *SLC36A1* (or *PAT1*, former name), were present in low numbers (Figure 3B). No non-KCN DEG were found for carnitine transporters. Adaptations took place in the cell settling assays and in some invasive scenarios without extracellular fluid being available. Also, the aquaporin genes, *AQP1* and *AQP4* genes, whose products mediate water flux, were only found in 3 of the E1-E70 studies. *AQP3*, found in 4 studies, encodes aquaglyceroporin that mediates glycerol, uncharged solutes, and water flux [278].

In the E1 - E70 studies important negatives include non-KCN DEG representing proton extruders, carbonic anhydrases, etc. with some mentioned in the Results and earlier in this section of the Discussion. Importantly, only a few studies found *ATP1A2* encoding Na/K-ATPase and related genes (as a group < 10%) to be differentially expressed in E1-E70. Its role as an important negative is supported by a report that digoxin, an inhibitor of Na^+/K^+ ATPase, an active inward K^+ transporter, has been found to reduce the size of circulating tumor cell clusters in women with metastatic breast cancer, -2.2 cells per cluster [279]. Others are also shown (Figure 3B). Some negatives (lacking significant differential expression) were described in the REMBRANDT analysis.

In support of finding *KCNK* genes as DEG in 20% of E1-E70, with *KCNK1*/K2P1 being most frequent, this is consistent with the loss of *KCNK1* being associated with breast cancer cell survival when necrosis was induced [118]. Also, the ten reviews of KCN genes found in cancer as described in the RESULTS, Section 3.*3.3.11. KCNs Encoding H^+-Sensitive Proteins in E1- E70 in Ten Cancer Reviews*, included overlap with 4 members of the K2P (*KCNK* genes) and 4 members of the KCa (*KCNM* and *KCNN* gene groups) subfamilies and others. In E1-E70, *KCNN4* and *KCNMA1*, were the most frequently detected KCN DEG, 9 and 6 studies, respectively.

4.4. E1-E70 Studies Related to 7 Oncogenes and Histone/DNA Modulation

Among the E1-E70 studies, 50 were in 8 categories of histone/DNA modulator involvement and/or having relationships to one or more of 7 oncogenes (*TP53*, *TGFβ*, *EGFR*, *MYC*, *RAS*, *BCL2*, and *MET*). Sixteen studies were in more than one category. Migration of 7 of the 8 glioblastoma cell lines responded to HGF, the ligand of *MET*'s encoded Met [280,281] as shown (Figure 2). Others have proposed a role of multiple oncogenes, including *EGFR*, *RAS* (*KRAS* and H*RAS*), *MYC*, and *TGFβ*, that overlap with the oncogenes in E1-E70 studies, and histone/DNA modifiers to interact on paths to malignancy in a context driven manner [282]. Lactate can activate *TGFβ* [283-286]. Also, "upregulation of oncogenic pathways" has been described in clinically evident precancerous lesions of 12 different types of malignancies in studies reviewed recently [287].

The collective influence of multiple oncogenes on downstream potassium channels may promote K^+ flux at inner membranes of tumor cells, possibly with refilling needed if outflow via large flow K^+ channels is anomalously high. Oncogenes could be involved upstream in promoting K^+/H^+ exchange leading to pH reversal. The 50 KCN studies related to 7 oncogenes and/or histone/DNA modulation were significantly (p = 0.0325) more likely to have at least one or more KCN DEG encoding a H^+-sensitive protein than the other 20 KCN studies in “no category”.

Retrieval of citation data from PubMed revealed a significant correlation in the numbers of studies of H^+ with K^+ across all 8 categories of 7 oncogenes and histone in 2-word searches without restriction to cancer. However, the category for MET had to be removed to achieve a comparable correlation of H^+ with K^+, when searches were restricted to “cancer” using 3-word searches (Figure 4C). Although explanations require definitive studies, this may reflect under-reporting of negative studies. The PubMed citations reveal that citations for BK (*KCNMA1* encoded) probably constitute a large proportion (approximately one third) of studies involving K^+ and H^+ across the categories of 7 oncogenes and “histone” not restricted to cancer and the BK citations may represent most of the studies when restricted to “cancer” (Figure 4B-C). Findings in this study are consistent with at least some H^+-sensitive KCN DEG in addition to *KCNMA1*/BK being influenced by six oncogenes (those listed previously but not MET) and histone modulation related to K^+ flux (possibly via activation of ACLY, see *Section 1.3. Metabolic Need for Proton Extrusion in Cancer*). Oncogenes and histone modulation through KCN genes/proteins may play a role in H^+ dynamics.

4.5. Non-KCN DEG in Multiple E1-E70 Studies

In E1-E70, the most frequent non-KCN DEG found was *ITGA2* in 7 studies, and *HMGA2*, *LIF*, and *PLAUR* were each found in 6 studies with *ITGA2*, *LIF*, and *PLAUR* shown in Venn diagrams (Figure 5A). Also, to support the relevance of cancer gene expression studies with unbiased detection of KCN DEG, six non-KCN DEG, i.e. *FGFR3*, *GDF15*, *IGFBP3*, *IGFBP7*, *KRT19*, and *PLAUR*, each included in at least 4 of the E1-E70 studies, were also identified by others as encoding circulating proteins associated with a risk of cancer [224,225]. *PLAUR*, found in 6 of E1-E70 studies, was also co-expressed with the most frequent KCN genes that are also H^+-sensitive, *KCNN4* and *KCNMA1* in 4 and 2 studies, respectively. *KCNN4*, *PLAUR*, and *PLAU* were detected together as DEG (Figure 5A) in E49 [167], a study associated with 3 categories, RAS, TP53, and His/Chr/Epi. BK (encoded by *KCNMA1*) citations in PubMed correlated with those for PLAUR + PLAU and ITGA2 (Figure 5B).

4.6. Specific Roles for Redistribution of K^+ in Cancer

Studies on intracellular pH-regulating systems, potassium channel inhibitors have been used with interesting results, including "slower recovery from CO_2 acidification" in early frog skeletal muscle experiments [288]. Potassium channels have been recognized as playing important roles in cancer, including volume changes [289,290] but without also considering K^+ for exchange with H^+ on fixed anions to then incite cytoplasmic proton transfers to cell exit sites. The intermediate step of rapid cytoplasmic proton transfer is plausible. Volume changes in cancer cells, problems in their blood supply, stiff tissues constraining migrating cells, etc. that lead to microaqueous conditions in the cytoplasm may help generate Grotthuss conditions that build a putative water-wire type root system to supply proton extruders.

Removal of K^+ from cell interiors may occur via flux of unsolvated K^+ through KCN channels after it has lost its aggregated water. Large outward (*KCNMA1*/BK), intermediate outward (*KCNN4*/IK), bidirectional (*KCNJ10-KCNJ16*/Kir4.1-Kir5.1 dimers or homomeric versions), etc. may alter cytosolic flows to bring centrally located intracellular water via K^+-$7H_2O$ (loosely aggregated) to the cell periphery where water wires form to provide rapid proton transfers. Alternatively, simultaneous changes in Cl^- channels (CLCN detected only once as a DEG in E1-E70 was *CLCN7*) and aquaporins (only a few DEG in E1-E70, see earlier Discussion) could help redistribute intracellular water but stochastically their participation as major players seemed unlikely in E1-E70 based on DEG detected. Na^+ binds water tightly so it is probably not responsible for water redistribution (See Introduction *1.4. Complexity of K^+ Flux,* 4th paragraph for related information on Na^+). Redistributed water regionally within cells may promote appropriate Grotthuss conditions, especially during cell migration but is not established as doing so.

K^+ released outside the cells through high volume calcium gated K^+ channels, etc. could be recycled via refilling through KCN channels (if available) or by Na/K-ATPase that brings K^+ in across cell membranes that could also displace fixed H^+ ions. Accumulated K^+ near the high flow outward channels prior to its release may displace fixed H^+ ions. The intermediate and large conductance K^+ channels encoded by, *KCNN4* and *KCNMA1*, respectively, found 9 and 6 times, respectively, and other KCNNs (*KCNN2*, *3*) and the KCNMBs (*KCNMB1*, *2*, *3*, *4* whose products regulate *KCNMA1*/BK) were found as DEG

in 5 and 8 studies, respectively, (only a few in the same studies) in E1-E70. Kir4.1 and Kir5.1 encoded by *KCNJ10* and *KCNJ16*, respectively, were found in 2 and 4 studies, respectively, in E1-E70 studies. Also, *KCNJ16* was detected as a DEG (less expression in glioblastomas versus oligodendrogliomas) in REMBRANDT, and with less expression in the 6 glioblastoma cell lines versus normal when studied by Patil, et al. [22]. Also, *KCNMB2* and *KCNJ16* are genes predicted to be negatively affected on chromosomes 3 and 17, respectively, in U87 glioblastoma cells, Supplemental Table 3 in Clark et al. [139]. Additionally, redistribution of K^+ away from mitochondria within the cells' interior may affect mitochondrial K^+-dependent enzymes to influence malignant behavior. The alkaline pH of cancer cell cytoplasm in pH reversal activates ACLY which can lead to histone changes to possibly help explain the correlation of 50 studies in E1-E70 with KCN DEG that encode H^+-sensitive proteins with 8 categories of histone/DNA modulators and 7 oncogenes (Figure 4A).

The E1-E70 study results only revealed gene expressions that crossed thresholds set by the authors of each study for significance (mostly $p < 0.05$) independently of any KCN consideration. Lower gene expression levels may be collectively biologically relevant in a network of KCN encoded proteins mediating potassium flux. Co-expression of non-KCN DEG (Figure 5) may become relevant as a signature of K^+ dynamics if they occur in additional studies.

SUMMARY

Migration and settling assays provided data to support and focus further experimental investigation of potassium flux in cancer cells. Although the reversed pH of cancer cells, generated via acid export by multiple extruders, is well established and of potential therapeutic value, the initiating events potentially involving potassium in providing intracellular protons to proton extruders could yield additional therapeutic targets. The multiple tumor models and range of study approaches used by many authors produced stochastic evidence for the large KCN potassium channel family playing a role in at least a subset of malignancies, with H^+-sensitive members as potential downstream effectors of oncogenes. Although any future therapeutic suggestions regarding alterations of potassium channels carries concern regarding effects on the heart [291], the role for potassium channels as mediators of K^+ flux that promotes K^+/H^+ exchange for proton transfer and subsequent efflux needs further exploration in cancer. The stochastic view of cancers based on unbiased studies detecting KCN genes incidentally in genomic landscapes suggests that encoded H^+-sensitive KCN proteins may be downstream effectors of one or more drivers in cancer. Oncogenes may promote adaptation to adverse events and genetic damage to cells, including KCN genes, to optimize cell fitness for survival, possibly as a spectrum of ongoing changes that include the extreme outcome of becoming dedifferentiated, single migrating cells, via pH reversal. Also, cancer specific structural alterations of surface proteins encoded by genetically flawed KCN genes may add to the repertoire of targets for immune attack in personalized medical treatments. Author curated, published gene landscapes in complex cancer studies are useful for stochastically identifying candidates in the large KCN gene family that encode downstream effectors of oncogenes that may initiate pH reversal. They also offer cancer

antigens to consider. Also, tumor models are identified in this manner where significant changes in KCN gene expression have been seen in malignancy.

Funding: The cell settling and cell migration research was funded by the Walter L. Copeland Fund for Cranial Research, The Pittsburgh Foundation, Pittsburgh, PA, D2003-0305 and D2006-0379; The Nick Eric Wichman Foundation, Ellicott City, MD, No Number; The Beez Foundation, Somerset, NJ., No Number; and the American Heart Association, Ohio Valley Affiliate, AHA 9960398V.

Data Availability Statement: Data generated in this study will be available upon request from the corresponding author. Please note that data from REMBRANDT per Adobe Flash (not available after 12/31/2020) can be seen in Figure 6 except for a few instances described which can also be made available on request. KCN gene data obtained from the published manuscript by Patil, V. et al. (22) follows the terms of their statement "an open access article distributed under the terms of the Creative Commons Attribution License, which permits unrestricted use, distribution, and reproduction in any medium, provided the original author and source are credited". 34%, 31%, 13%, and 6% of the papers used in the E1-E70 study were found in Cancer Research, Cancer Cell, Nature Communications, and Journal of Molecular Diagnostics, respectively. Others are from 11 journals, 1 paper each. Papers for E1 – E70 are cited in Section *3.3.6. Categories Among Studies with E1-E70 Citations Per Category*.

Acknowledgements: Ian F. Pollack, MD, University of Pittsburgh, Children's Hospital of Pittsburgh, provided laboratory space, supplies, technicians, and glioblastoma cell lines, George K. Michalopoulos, MD, PhD, Department of Pathology, University of Pittsburgh, provided information on hepatocyte growth factor and MET. The Departments of Pathology and Neurological Surgery, University of Pittsburgh, provided institutional support for cell settling and migration experimental work. The 1301 authors of 70 papers (E1-E70) are thanked for outstanding contributions to the medical science literature used for gathering stochastic information on the KCN gene family while at Kent State, Kent, OH. I thank the Brain Health Research Institute of Kent State University, Kent, Ohio, as a current member, for technical advice and ongoing academic research activities.

Author Contributions: The author performed the cell settling and migration assays, and the immunoblot at a previous institution, The University of Pittsburgh, Pittsburgh, PA. The author performed analysis of REMBRANDT, collection and analysis of 70 studies detecting KCN DEG, etc. and all other aspects of the study (text, figures, etc.) while associated with Kent State University, Kent, OH. Consultation for statistical advice and the use of EndNote was obtained and appreciated but the offered acknowledgement for the advice was not desired.

Conflicts of Interest: The author declares no conflicts of interest. The funders had no role in the design of the study; in the collection, analyses, or interpretation of data; in the writing of the manuscript; or in the decision to publish the results.

Abbreviations

The following abbreviations are used in this manuscript.

ACLY	ATP Citrate Lyase
Arg1	Arginase 1
AS	Anti-seizure

BK	Big K (encoded by *KCNMA1)*
BSA	Bovine serum albumin
CD	Cluster Differentiation
CLCN	Chloride Channels gene family, *CLCN1,2,3*, etc.
COL	Collagen
CSM	Cancer Specific Mutation
Cx	Connexin
DEG	Differentially expressed gene(s)
E	Expression
EAAT	Excitatory Amino Acid Transporter
EAG1	Ether-A-Go-Go-K^+ Channel Protein 1
ELK1,2	EAG Like K^+ Channel Proteins 1,2
EMT	Epithelial Mesenchymal Transition
ERG1,3	EAG Related Gene K^+ Channel Proteins 1,3
FBS	Fetal bovine serum
GABA	Gamma-aminobutyric acid
GBM	Glioblastoma
G-DOC	Georgetown Database of Cancer
Girk3,4	G protein-activated Inward Rectifier K^+Channel Proteins, 3,4
GPR	G-protein Coupled Receptor
G-proteins	Guanosine-triphosphate-binding proteins
GWATERW	Grotthuss water wire
HGF	Hepatocyte growth factor
His/Chr/Epi	Histone/Chromatin/Epigenetic
HKG	House-keeping gene
IK	Intermediate K (encoded by *KCNN4*)
Indels	Insertions and Deletions
ITAG2	Integrin 2
ITG	Integrin
K2P	Tandem 2 pore domain KCN subfamily proteins
Kca	Calcium stimulated KCN subfamily proteins
Kchip1,3	Kv channel interacting proteins 1,3
KCNA	Subgroup of KCN genes, *KCNA1,2,3,etc.*
KCNAB	Subgroup of KCN genes, *KCNAB1,2,3*
KCNB	Subgroup of KCN genes, *KCNB1,2*
KCNC	Subgroup of KCN genes, *KCNC1,2,3,etc.*
KCND	Subgroup of KCN genes, *KCND1,2,3*
KCNE	Subgroup of KCN genes, *KCNE1,2,3, etc.*
KCNG	Subgroup of KCN genes, *KCNG1,2,3,etc.*
KCNH	Subgroup of KCN genes, *KCNH1,2,3, etc.*
KCNIP	Subgroup of KCN genes, *KCNIP1,2,3, etc.*
KCNJ	Subgroup of KCN genes, *KCNJ1,2,3, etc.*
KCNK	Subgroup of KCN genes, *KCNK1,2,3, etc.*

KCNM	Subgroup of KCN genes, *KCNM,A1,B1,B2, etc.*
KCNN	Subgroup of KCN genes, *KCNN1,2,3, etc.*
KCNQ	Subgroup of KCN genes, *KCNQ1,2,3, etc.*
KCNS	Subgroup of KCN genes, *KCNS1,2,3, etc.*
KCNT	Subgroup of KCN genes, *KCNT1,2*
Kir	Inwardly directing KCN subfamily proteins
Kv	Voltage dependent KCN subfamily proteins
LDH	Lactate dehydrogenase
LIF	Leukemia Inhibitory Factor
MCT	Monocarboxylate transporter
MEM	Minimal Essential Media
Mes	Mesenchymal
MiRP	MinK (minimal K^+channel protein related peptide)
Na/K ATPase	Sodium/potassium ATPase
NOX	NADPH oxidases
Oligo	Oligodendroglioma
OMG	Oligodendroglioma Minus Glioblastoma
OMIM	Online Mendelian Inheritance in Man
PBS	Phosphate buffered saline
pHe	Extracellular pH
pHi	Intracellular pH
PIP2	Phosphatidyl inositol 4,5 bisphosphate
R	Pearson product-moment correlation
REMBRANDT	Repository of Molecular Brain Neoplasia Data
RGS	Regulator of G protein signaling
ROS	Reactive oxygen species
RRID	Research Resource Identifier
SERPIN	Serine proteinase inhibitors
SNV	Single Nucleotide Variant
SK	Small K (encoded by some *KCNN* genes)
Slack	Sequence like a calcium -activated K^+ channel protein
SLC	Solute Carrier
Slick	Sequence like intermediate Con-ductance K^+ channel protein
SOX	Sry-related HMG BOX
TasK1,2,5	Twik-related Acid Sensitive K^+ channel proteins 1,2,5
Thik2	Tandem pore domain Halothane Inhibited K^+ channel protein 2
TMEM	Transmembrane
TNFRSF	Tumor Necrosis Factor Receptor Super Family
Trek1	Twik-Related K^+ channel protein 1
TwiK1,2	Tandem pore domain in Weak Inward Rectifying K^+

	Channel proteins 1,2
uPA	Urokinase-Type Plasminogen Activator

Appendix A

Figure A1.

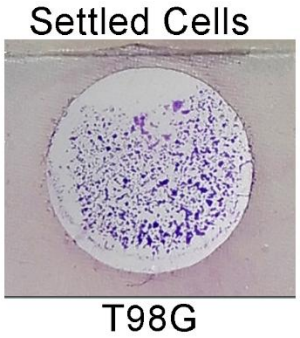

Figure A1. Macroscopic view of settled T98G glioblastoma cells on a Neuro Probe microscopic slide. One of 8 round 7 mm diameter areas that had been the bottom of a settling chamber well. Some cell clumping is noted. Diff Quik stain.

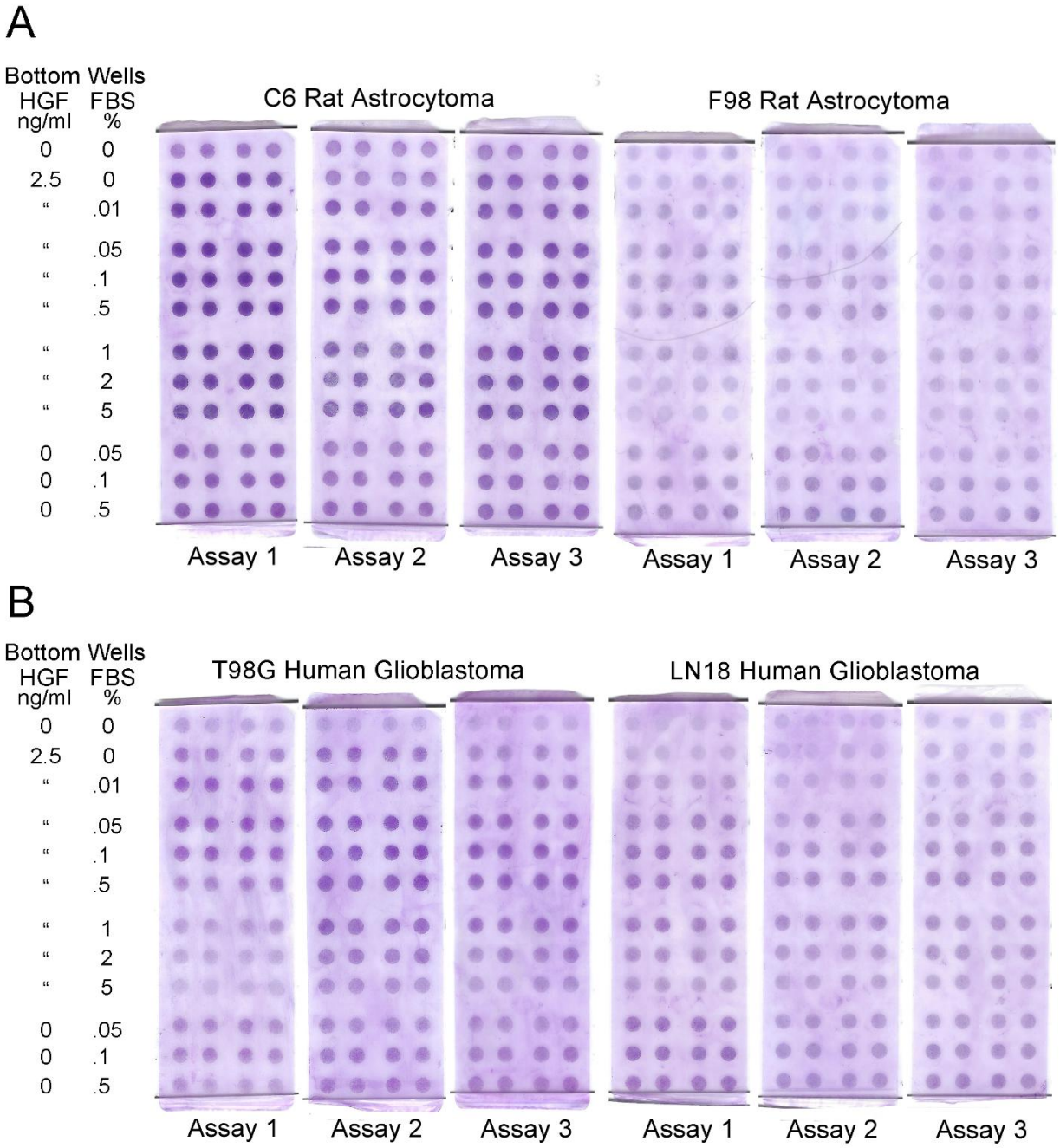

Figure A2. All three migration assays for each cell line (C6, F98, T98G, and LN18) in studies of HGF and FBS chemoattraction. One assay per cell line is shown in Figure 2A. Portions of assays that were digitized and analyzed are shown in Figure 2B. Text in Section 3.2. *Cell Migration with HGF and Serum Chemoattraction* and the Figure 2 legend provide additional information. Each circle of stained migrated cells is 3 mm in diameter.

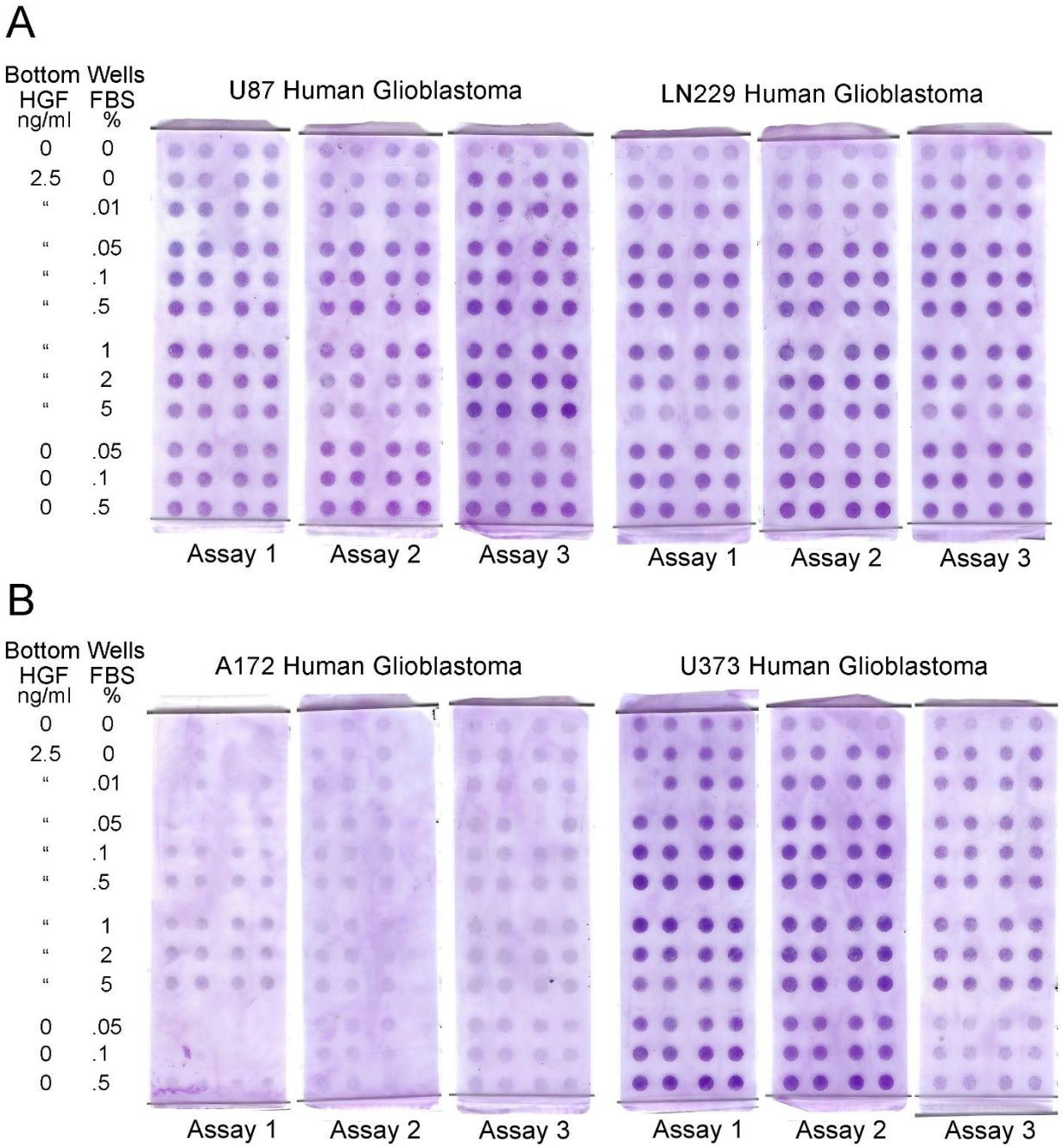

Figure A3. All three migration assays for each cell line (U87, LN229, F98, A172, and U373) in studies of HGF and FBS chemoattraction. One assay per cell line is shown in Figure 2A. Portions of assays that were digitized and analyzed are shown in Figure 2B. Text in Section 3.2. *Cell Migration with HGF and Serum Chemoattraction* and the Figure 2 legend provide additional information. Each circle of stained migrated cells is 3 mm in diameter.

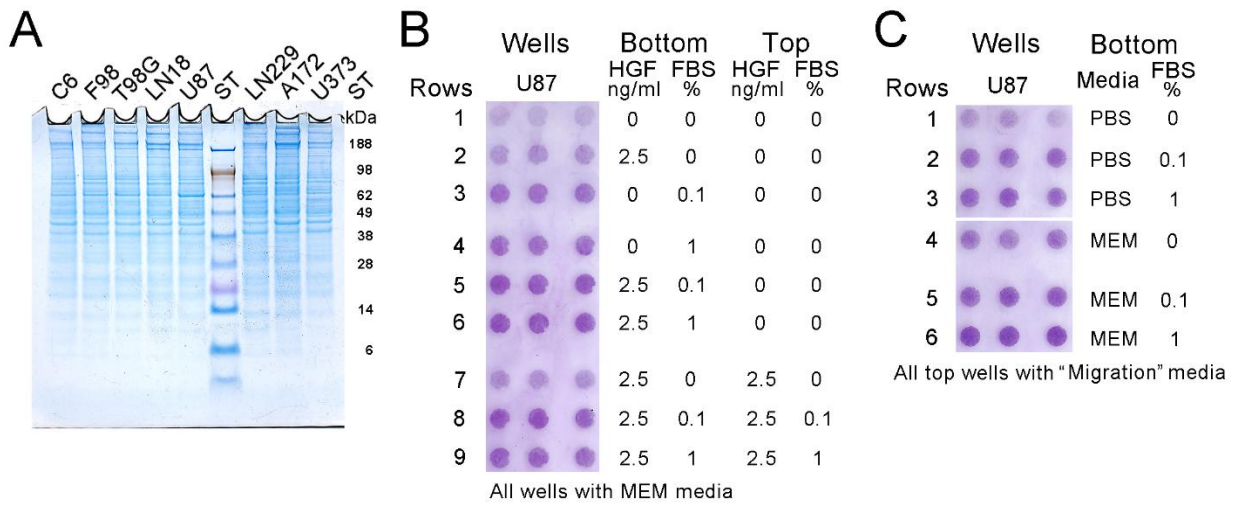

Figure A4. Additional images for Figure 2. (A) Gel image for the immunoblot in Figure 2C showing equal loading of protein in each lane for all 8 cell lines. (B) Scanned image of the U87 migration assay shown in Figure 2D. Chemoattraction of HGF and 2 concentrations of FBS and chemokinesis of HGF, with and without 2 concentrations of FBS, were analyzed in U87 cells. (C) Scanned image of the U87 migration assay shown in Figure 2E. Dulbecco's PBS and MEM were tested as media in the lower wells for migration without and with 2 concentrations of FBS present. The image of the filter removed (white horizontal line) an unrelated portion of the assay that tested a different batch of FBS for suitability in future migration assays. Text in Section 3.2. *Cell Migration with HGF and Serum Chemoattraction* and the Figure 2 legend provide additional information. Each circle of stained, migrated cells is 3 mm in diameter.

Appendix B

Table B1. A sample of alphabetized differentially expressed genes (DEG) in E1-E70 studies. See AllE1E70DEG3239Total for the entire list of DEG in a table format after the References and Disclaimer.

DEG Name	Study Number
A2M	E21
AAK1	E65
AATK	E54
AB113AP	E1
ABCA1	E50
ABCA12	E54
ABCB10	E48
ABCB1A	E69
ABCC3	E70
ABCD1	E31
See full list…	See full list…

Table B2. KCN genes in E1-E70 studies that encode H^+-sensitive proteins.

KCN Gene	Protein	Reference
KCNA1	Kv1.1	[292]
KCNA3	Kv1.3	[293,294]
KCNA5	Kv1.5	[295-301]
KCNAB2	Kvbeta2	[302,303]
KCND3	Kv4.3	[304-306]
KCNE2	MiRP1	[85,307-311]
KCNE3	MiRP2, R83H variant	[253]
KCNH1	Kv10.1, EAG1	[254,312]
KCNH2	Kv11.1, HERG1	[254,313-325]
KCNH3	Kv12.2, ELK2	[254]
KCNH8	Kv12.1, ELK3	[254,326]
KCNJ5	Kir3.4, GIRK4	[255,256,327]
KCNJ8	Kir6.1, KATP-1	[327-333]
KCNJ10	Kir4.1, BIRK10	[334-336]
KCNJ10/KCNJ16	Kir4.1/Kir5.1heterodimer	[72,326,337-343]
KCNJ13	Kir7.1	[72,327,344]
KCNK1	K2P1, TWIK1	[343,345-350]
KCNK2	K2P2, TREK1	[343,348,351-357]
KCNK3	K2P3, TASK1	[343,346,348,355,358-361]
KCNK5	K2P5, TASK2	[237,343,346,348,362-369]
KCNK6	K2P6, TWIK2	[346,370,371]
KCNK15	K2P15, TASK5	[372]
KCNMA1	KCa1.1, BK, Slo1, maxiK	[96,373-388]
KCNMB4	BKbeta4	[389-393]
KCNN2	KCa2.2, SK2	[394]
KCNN3	KCa2.3, SK3	[394]
KCNN4	KCa3.1, SK4, Gardos	[394-397]
KCNQ1	Kv7.1, KvLQT1	[85,237,307-309,311,399-405]
KCNQ2	Kv7.2	[402(described data),406,407]
KCNQ3	Kv7.3	[406]
KCNQ5	Kv7.5	[408]
KCNT1	KCa4.1, Slo2.2, KNa1.1	[409-412]
KCNU1	KCa5.1, Slo3, KCNMA3	[389,412-418]

A

	Types of Malignancy with KCNs Among Differentially Expressed Genes (DEG)	# of Studies	Specific studies with H^+-sensitive KCN DEG underlined
1	Adrenocortical carcinoma/?precursor	2	E32 (J5), E68 (K2)
2	Acute myelogenous leukemia	2	E11 (K6), E59 (Q3)
3	Bladder carcinoma	1	E7
4	Breast carcinoma (See E_)	9	E1, E4 (N3), E9 (H1, K15), E15, E22 (K5, K15), E33, E38 (MA1), E48, E63
5	Chordoma	1	E24 (K2)
6	Chronic lymphocytic leukemia	1	E37
7	Colorectal carcinoma	4	E2 (Q1), E36 (N4), E61 (K1), E63
8	Cutaneous squamous carcinoma	1	E44
9	Ependymoma	1	E57 (J16)
10	Ewing sarcoma	1	E10 (E3)
11	Gastric carcinoma	2	E13 (MA1), E45
12	Glioblastoma (See E_)	7	E5 (J10, N3), E21 (AB2), E26 (E2, J13), E27, E31 (J8, J10), E50 (D3), E51 (J16, N2)
13	Liposarcoma	1	E18 (MB4)
14	Liver carcinoma	2	E20, E64 (N4)
15	Lung carcinoma (See E_)	11	E3 (K1), E8 (K1, N4), E12 (A1, H8), E23 (U1), E30, E35 (K1), E43 (K6), E49 (N4), E54 (J13), E63, E67
16	Lymphoma	2	E47 (A3), E53 (N4)
17	Malignant peripheral nerve sheath tumor	1	E70 (H2)
18	Medulloblastoma	2	E6 (A1), E55 (Q1)
19	Melanoma	3	E14 (Q5), E39 (MA1), E41 (MA1, N4)
20	Multiple myeloma	1	E28 (N3)
21	Neuroblastoma	3	E17 (Q2, Q5), E56, E66
22	Ovarian carcinoma	4	E25, E34 (A1, N3, T1), E58 (A5, H3, H8, J16, MB4, N4, Q1), E60 (MA1)
23	Pancreatic ductal carcinoma	2	E42 (E3), E69 (N4)
24	Pituitary neuroendocrine tumor	1	E65
25	Prostate carcinoma	3	E40 (MA1, Q5), E52 (K15, N4), E62 (AB2)
26	Renal carcinoma	3	E19 (J16), E29, E63
27	Synovial sarcoma	1	E46 (Q2)
28	Thyroid carcinoma	1	E19 (J16)
29	Uterine endometrial carcinoma	1	E63

B

KCN Family	Common informative protein abbreviations
KCNH	EAG1 - Ether-A-Go-Go-K^+ channel protein 1
	ELK1,2 - EAG Like K^+ channel proteins 1,2
	ERG1,3 - EAG Related Gene K^+ channel proteins 1,3
KCNJ	Girk3,4 - G protein-activated Inward Rectifier K^+ channel proteins 3,4
KCNIP	Kchip1,3 - Kv channel interacting proteins 1,3
KCNE	MiRP - MinK(minimal K^+ channel protein (also ISK)) related peptide
	MiRP2,3 - MiRP2,3
KCNT	Slack - Sequence Like A Calcium-activated K^+ channel protein (also K channel, Na activated, subfamily member 1)
	Slick - Squence Like Intermediate Conductance K^+ channel protein (also Sodium and chloride activated ATP sensitive K^+ channel protein)
KCNK	Twik 1,2 - Tandem pore domains in Weak Inward Rectifying K^+ channel proteins 1,2
	Task 1,2,5 - Twik-related Acid Sensitive K^+ channel proteins 1,2,5
	Thik2 - Tandem pore domain Halothane Inhibited K^+ channel protein 2
	Trek1 - Twik-Related K^+ channel protein 1
KCNJ	UKATP1 - ATP sensitive inward rectifier K^+ channel protein 8

Figure B1. Types of malignancies studied in E1-E70 and informative protein abbreviations for proteins in the KCN family are listed. **(A)** Specific studies are listed for each type of 29 malignancies with their detected KCN DEG. Red underlining indicates the KCN DEG that encode H^+-sensitive proteins. Boxes that correspond with studies of brain, breast, and lung malignancies are color coded, yellow, pink, and blue, respectively. These graphics are also used in the histograms shown in Figures 3 and 4. (**B**) Some of the common protein abbreviations for KCN family members in Figure 3 indicating functional information not explained in the text are included.

Text B1. Potential Interactions of KCN Proteins with H^+-Sensitive G Protein-Coupled Receptors.

Multiple KCN proteins have interactions with four G protein-coupled receptors encoded by *GPR4*, *65*, *68*, and *151* that are among 6 reported to be H^+-sensitive [419-425]. H^+-sensitive proteins encoded by GPR genes are found in many types of tumors [423,424,426,427]. Functional complementation between proteins encoded by *GPR4* and *KCNK5*/TASK2 [427,428,429] and related expression profiles of proteins encoded

by *GPR31*, G*PR151*, *KCNK3*/TASK1, and *KCNK9*/TASK3 have been found in tumors [425]. STRING interactions (Gene Cards, 10/17/2024) of proteins encoded by *GPR4*, *65*, *68*, and*151* as a group included proteins encoded by 9 KCNs, *KCNJ8*, *K1, K2, K4, K5*, *K10*, *K16*, *K17*, and *K18*. Among these, 8 of the 70 studies (E3, 8, 22, 24, 31,35, 61, 68) detected *KCNJ8*, *K1, K2, K5* as DEG. Also, although *GPR39*'s encoded protein is not reported to be H^+-sensitive, it interacts with the four H^+-sensitive proteins encoded by *GPR4*, *65*, *68*, and *132*. *GPR39* is a DEG found in 2 of the 70 studies, E14 [194] and E60 [177], that also detected *KCNQ5* and *KCNMA1*, respectively. The ligand of the protein encoded by *GPR39* is encoded by *GPNMB* [430] and *GPNMB* was a DEG in 3 studies, E26 [213], E29 [158], and E49 [167]. *GPR35*'s protein (also not H^+-sensitive) interacts with *GPR4*'s encoded H^+-sensitive receptor protein. *GPR35* is a DEG in two studies that found *KCNG2* and *KCNE3*, in E20 [211] and E42 [218], respectively. The ligand for *GPR35*'s receptor protein is kynurenic acid [431]. *GPR84*'s protein (also not H^+-sensitive) interacts with *GPR65*'s encoded H^+-sensitive receptor protein. *GPR84* is a DEG from two studies that found *KCNK6* in E11 [174] and *KCNK12* and *KCNU1* in E23 [202]. The ligands for *GPR84*'s receptor protein are medium-chain fatty acids [432]. Thirteen of the14 studies (out of 70) with potential indirect GPR protein sensitivity to H^+ also detected KCN DEG that encode H^+-sensitive proteins. Potentially, KCN DEG encoded proteins in 13 (18.6%) of the E1-E70 studies have indirect involvement with H^+-sensitive G-protein-coupled receptor proteins via STRING interactions (Gene Cards, 10/17/2024) or as described above according to the cited literature. They may function collaboratively with GPR encoded H^+-sensitive proteins in tumors.

References

1. Burger PC, Scheithauer BW. Tumors of the Neuroglia and Choroid Plexus. Tumors of the Central Nervous System. Washington, D.C.: American Registry of Pathology; 2007. p 55-77.
2. Ge L, Hoa NT, Wilson Z, Arismendi-Morillo G, Kong XT, Tajhya RB*, et al.* Big Potassium (BK) ion channels in biology, disease and possible targets for cancer immunotherapy. Int Immunopharmacol **2014**;22:427-43
3. Freshney RI. Defined media and supplements. Table 8.6. Constituents of serum. In: Capes-Davis A, Gregory C, Przyborski S, editors. Culture of Animal Cells. Hoboken, New Jersey: John Wiley & Sons, Inc.; 2016. p 141.
4. Kros JM. Grading of gliomas: the road from eminence to evidence. J Neuropathol Exp Neurol **2011**;70:101-9
5. Puchalski RB, Shah N, Miller J, Dalley R, Nomura SR, Yoon JG*, et al.* An anatomic transcriptional atlas of human glioblastoma. Science **2018**;360:660-3
6. Brat DJ, Castellano-Sanchez AA, Hunter SB, Pecot M, Cohen C, Hammond EH*, et al.* Pseudopalisades in glioblastoma are hypoxic, express extracellular matrix proteases, and are formed by an actively migrating cell population. Cancer Res **2004**;64:920-7
7. Rong Y, Durden DL, Van Meir EG, Brat DJ. 'Pseudopalisading' necrosis in glioblastoma: a familiar morphologic feature that links vascular pathology, hypoxia, and angiogenesis. J Neuropathol Exp Neurol **2006**;65:529-39
8. Chesler M, Kraig RP. Intracellular pH of astrocytes increases rapidly with cortical stimulation. Am J Physiol **1987**;253:R666-70
9. Chesler M, Kraig RP. Intracellular pH transients of mammalian astrocytes. J Neurosci **1989**;9:2011-9
10. Brookes N. Intracellular pH as a regulatory signal in astrocyte metabolism. Glia **1997**;21:64-73
11. Theparambil SM, Weber T, Schmalzle J, Ruminot I, Deitmer JW. Proton Fall or Bicarbonate Rise: Glycolytic Rate in Mouse Astrocytes Is Paved By Intracellular Alkalinization. J Biol Chem **2016**;291:19108-17

12. Vaupel P, Kallinowski F, Okunieff P. Blood flow, oxygen and nutrient supply, and metabolic microenvironment of human tumors: a review. Cancer Res **1989**;49:6449-65
13. Boron WF. Regulation of intracellular pH. Adv Physiol Educ **2004**;28:160-79
14. Andersen AP, Moreira JM, Pedersen SF. Interactions of ion transporters and channels with cancer cell metabolism and the tumour microenvironment. Philos Trans R Soc Lond B Biol Sci **2014**;369:20130098
15. Spugnini EP, Sonveaux P, Stock C, Perez-Sayans M, De Milito A, Avnet S*, et al.* Proton channels and exchangers in cancer. Biochim Biophys Acta **2015**;1848:2715-26
16. Swietach P, Vaughan-Jones RD, Harris AL, Hulikova A. The chemistry, physiology and pathology of pH in cancer. Philos Trans R Soc Lond B Biol Sci **2014**;369:20130099
17. Swietach P, Boedtkjer E, Pedersen SF. How protons pave the way to aggressive cancers. Nat Rev Cancer **2023**;23:825-41
18. McIntyre A, Hulikova A, Ledaki I, Snell C, Singleton D, Steers G*, et al.* Disrupting Hypoxia-Induced Bicarbonate Transport Acidifies Tumor Cells and Suppresses Tumor Growth. Cancer Res **2016**;76:3744-55
19. White KA, Grillo-Hill BK, Barber DL. Cancer cell behaviors mediated by dysregulated pH dynamics at a glance. J Cell Sci **2017**;130:663-9
20. Bhuvaneshwar K, Belouali A, Singh V, Johnson RM, Song L, Alaoui A*, et al.* G-DOC Plus - an integrative bioinformatics platform for precision medicine. BMC Bioinformatics **2016**;17:193
21. Madhavan S, Gusev Y, Harris M, Tanenbaum DM, Gauba R, Bhuvaneshwar K*, et al.* G-DOC: a systems medicine platform for personalized oncology. Neoplasia **2011**;13:771-83
22. Patil V, Pal J, Somasundaram K. Elucidating the cancer-specific genetic alteration spectrum of glioblastoma derived cell lines from whole exome and RNA sequencing. Oncotarget **2015**;6:43452-71
23. Deplazes E, Poger D, Cornell B, Cranfield CG. The effect of H(3)O(+) on the membrane morphology and hydrogen bonding of a phospholipid bilayer. Biophys Rev **2018**;10:1371-6
24. Eigen M, De Maeyer L. Self-dissociation and protonic charge transport in water and ice. Proc R Soc (Lond) A **1958**;247 A.:505-33
25. Johnson DE, Casey JR. Cytosolic H+ microdomain developed around AE1 during AE1-mediated Cl-/HCO3- exchange. J Physiol **2011**;589:1551-69
26. Vaughan-Jones RD, Peercy BE, Keener JP, Spitzer KW. Intrinsic H(+) ion mobility in the rabbit ventricular myocyte. J Physiol **2002**;541:139-58
27. Xie F, Tikhonov DS, Schnell M. Electric nuclear quadrupole coupling reveals dissociation of HCl with a few water molecules. Science **2024**;384:1435-40
28. Grotthuss CJT. Memoire sur la decomposition de l'eau et des corps qu'elle tient en dissolution a l'aide de l'electricite galvanique. Ann Chim **1806**;58:54-74
29. Adelroth P. Preface: Special issue on proton transfer in biological systems. Biochem Biophys Acta **2006**;1757:867-70
30. Cukierman S. Et tu, Grotthuss! and other unfinished stories. Biochim Biophys Acta **2006**;1757:876-85
31. Gutman M, Nachliel E, Friedman R. The mechanism of proton transfer between adjacent sites on the molecular surface. Biochim Biophys Acta **2006**;1757:931-41
32. Mulkidjanian AY, Heberle J, Cherepanov DA. Protons @ interfaces: implications for biological energy conversion. Biochim Biophys Acta **2006**;1757:913-30
33. Ben-Amotz D. Electric buzz in a glass of pure water. Science **2022**;376:800-1
34. Kariev AM, Green ME. Water, Protons, and the Gating of Voltage-Gated Potassium Channels. Membranes (Basel) **2024**;14

35. Horowitz SB, Paine PL. Reference phase analysis of free and bound intracellular solutes. II. Isothermal and isotopic studies of cytoplasmic sodium, potassium, and water. Biophys J **1979**;25:45-62
36. Schornack PA, Gillies RJ. Contributions of cell metabolism and H+ diffusion to the acidic pH of tumors. Neoplasia **2003**;5:135-45
37. Schwab A, Wojnowski L, Gabriel K, Oberleithner H. Oscillating activity of a Ca(2+)-sensitive K+ channel. A prerequisite for migration of transformed Madin-Darby canine kidney focus cells. J Clin Invest **1994**;93:1631-6
38. Schwab A, Nechyporuk-Zloy V, Fabian A, Stock C. Cells move when ions and water flow. Pflugers Arch **2007**;453:421-32
39. Horio Y. Potassium channels of glial cells: distribution and function. Jpn J Pharmacol **2001**;87:1-6
40. Sontheimer H. An unexpected role for ion channels in brain tumor metastasis. Exp Biol Med (Maywood) **2008**;233:779-91
41. Schwab A, Stock C. Ion channels and transporters in tumour cell migration and invasion. Philos Trans R Soc Lond B Biol Sci **2014**;369:20130102
42. Catacuzzeno L, Sforna L, Esposito V, Limatola C, Franciolini F. Ion Channels in Glioma Malignancy. Rev Physiol Biochem Pharmacol **2021**;181:223-67
43. Beckner ME, Chen X, An J, Day BW, Pollack IF. Proteomic characterization of harvested pseudopodia with differential gel electrophoresis and specific antibodies. Lab Invest **2005**;85:316-27
44. Tjaderhane L, Larjava H, Sorsa T, Uitto VJ, Larmas M, Salo T. The activation and function of host matrix metalloproteinases in dentin matrix breakdown in caries lesions. J Dent Res **1998**;77:1622-9
45. Fasciglione GF, Marini S, D'Alessio S, Politi V, Coletta M. pH- and temperature-dependence of functional modulation in metalloproteinases. A comparison between neutrophil collagenase and gelatinases A and B. Biophys J **2000**;79:2138-49
46. Kato Y, Lambert CA, Colige AC, Mineur P, Noel A, Frankenne F*, et al.* Acidic extracellular pH induces matrix metalloproteinase-9 expression in mouse metastatic melanoma cells through the phospholipase D-mitogen-activated protein kinase signaling. J Biol Chem **2005**;280:10938-44
47. Gatenby RA, Gawlinski ET, Gmitro AF, Kaylor B, Gillies RJ. Acid-mediated tumor invasion: a multidisciplinary study. Cancer Res **2006**;66:5216-23
48. Gioia M, Fasciglione GF, Monaco S, Iundusi R, Sbardella D, Marini S*, et al.* pH dependence of the enzymatic processing of collagen I by MMP-1 (fibroblast collagenase), MMP-2 (gelatinase A), and MMP-14 ectodomain. J Biol Inorg Chem **2010**;15:1219-32
49. Pillai SR, Damaghi M, Marunaka Y, Spugnini EP, Fais S, Gillies RJ. Causes, consequences, and therapy of tumors acidosis. Cancer Metastasis Rev **2019**;38:205-22
50. Rohani N, Hao L, Alexis MS, Joughin BA, Krismer K, Moufarrej MN*, et al.* Acidification of Tumor at Stromal Boundaries Drives Transcriptome Alterations Associated with Aggressive Phenotypes. Cancer Res **2019**;79:1952-66
51. Sun H, Zhou Y, Skaro MF, Wu Y, Qu Z, Mao F*, et al.* Metabolic Reprogramming in Cancer Is Induced to Increase Proton Production. Cancer Res **2020**;80:1143-55
52. Buhl M, Hutson T, Missio A, Walton JC. Sulfur and Phosphorus Oxyacid Radicals. J Phys Chem A **2022**;126:760-71
53. Walton JC. Radical-Enhanced Acidity: Why Bicarbonate, Carboxyl, Hydroperoxyl, and Related Radicals Are So Acidic. J Phys Chem A **2017**;121:7761-7
54. Walton JC. Microhydration and the Enhanced Acidity of Free Radicals. Molecules **2018**;23
55. Segal MS, Beem E. Effect of pH, ionic charge, and osmolality on cytochrome c-mediated caspase-3 activity. Am J Physiol Cell Physiol **2001**;281:C1196-204

56. Duffy HS, Ashton AW, O'Donnell P, Coombs W, Taffet SM, Delmar M*, et al.* Regulation of connexin43 protein complexes by intracellular acidification. Circ Res **2004**;94:215-22
57. Hirst-Jensen BJ, Sahoo P, Kieken F, Delmar M, Sorgen PL. Characterization of the pH-dependent interaction between the gap junction protein connexin43 carboxyl terminus and cytoplasmic loop domains. J Biol Chem **2007**;282:5801-13
58. Palacios-Prado N, Briggs SW, Skeberdis VA, Pranevicius M, Bennett MV, Bukauskas FF. pH-dependent modulation of voltage gating in connexin45 homotypic and connexin45/connexin43 heterotypic gap junctions. Proc Natl Acad Sci U S A **2010**;107:9897-902
59. Monterisi S, Michl J, Hulikova A, Koth J, Bridges EM, Hill AE*, et al.* Solute exchange through gap junctions lessens the adverse effects of inactivating mutations in metabolite-handling genes. Elife **2022**;11
60. Ranganathan NS, Srere PA, Linn TC. Comparison of phospho- and dephospho-ATP citrate lyase. Arch Biochem Biophys **1980**;204:52-8
61. Wu T, Jun S, Choi EJ, Sun J, Yang EB, Lee HS*, et al.* 53BP1-ACLY-SLBP-coordinated activation of replication-dependent histone biogenesis maintains genomic integrity. Nucleic Acids Res **2022**;50:1465-83
62. Beckner ME, Fellows-Mayle W, Zhang Z, Agostino NR, Kant JA, Day BW*, et al.* Identification of ATP citrate lyase as a positive regulator of glycolytic function in glioblastomas. Int J Cancer **2010**;126:2282-95
63. Wellen KE, Hatzivassiliou G, Sachdeva UM, Bui TV, Cross JR, Thompson CB. ATP-citrate lyase links cellular metabolism to histone acetylation. Science **2009**;324:1076-80
64. Lazaropoulos MP, Gibb AA, Chapski DJ, Nair AA, Reiter AN, Roy R*, et al.* Nuclear ATP-citrate lyase regulates chromatin-dependent activation and maintenance of the myofibroblast gene program. Nat Cardiovasc Res **2024**;3:869-82
65. Scott JG, Basanta D, Chinnaiyan P, Canoll P, Swanson KR, Anderson AR. Production of 2-hydroxyglutarate by isocitrate dehydrogenase 1-mutated gliomas: an evolutionary alternative to the Warburg shift? Neuro Oncol **2011**;13:1262-4
66. Girault A, Brochiero E. Evidence of K+ channel function in epithelial cell migration, proliferation, and repair. Am J Physiol Cell Physiol **2014**;306:C307-19
67. Boyle Y, Johns TG, Fletcher EV. Potassium Ion Channels in Malignant Central Nervous System Cancers. Cancers (Basel) **2022**;14
68. Cohen NA, Sha Q, Makhina EN, Lopatin AN, Linder ME, Snyder SH*, et al.* Inhibition of an inward rectifier potassium channel (Kir2.3) by G-protein betagamma subunits. J Biol Chem **1996**;271:32301-5
69. Ruppersberg JP. Intracellular regulation of inward rectifier K+ channels. Pflugers Arch **2000**;441:1-11
70. Niemeyer MI, Stutzin A, Sepulveda FV. A voltage-independent K+ conductance activated by cell swelling in Ehrlich cells is modulated by a G-protein-mediated process. Biochim Biophys Acta **2002**;1562:1-5
71. Bedard K, Krause KH. The NOX family of ROS-generating NADPH oxidases: physiology and pathophysiology. Physiol Rev **2007**;87:245-313
72. Hibino H, Inanobe A, Furutani K, Murakami S, Findlay I, Kurachi Y. Inwardly rectifying potassium channels: their structure, function, and physiological roles. Physiol Rev **2010**;90:291-366
73. Sahoo N, Hoshi T, Heinemann SH. Oxidative modulation of voltage-gated potassium channels. Antioxid Redox Signal **2014**;21:933-52
74. Rivera-Aponte DE, Mendez-Gonzalez MP, Rivera-Pagan AF, Kucheryavykh YV, Kucheryavykh LY, Skatchkov SN*, et al.* Hyperglycemia reduces functional expression of astrocytic Kir4.1 channels and glial glutamate uptake. Neuroscience **2015**;310:216-23

75. Wang J, Li Y, Jiang C. MiR-133b contributes to arsenic-induced apoptosis in U251 glioma cells by targeting the hERG channel. J Mol Neurosci **2015**;55:985-94
76. Pegg AE. Functions of Polyamines in Mammals. J Biol Chem **2016**;291:14904-12
77. Cabanos C, Wang M, Han X, Hansen SB. A Soluble Fluorescent Binding Assay Reveals PIP(2) Antagonism of TREK-1 Channels. Cell Rep **2017**;20:1287-94
78. Li D, Xia L, Chen M, Lin C, Wu H, Zhang Y*, et al.* miR-133b, a particular member of myomiRs, coming into playing its unique pathological role in human cancer. Oncotarget **2017**;8:50193-208
79. Verkhratsky A, Nedergaard M. Physiology of Astroglia. Physiol Rev **2018**;98:239-389
80. Bukiya AN, Dopico AM. Regulation of BK Channel Activity by Cholesterol and Its Derivatives. Adv Exp Med Biol **2019**;1115:53-75
81. Burton MJ, Cresser-Brown J, Thomas M, Portolano N, Basran J, Freeman SL*, et al.* Discovery of a heme-binding domain in a neuronal voltage-gated potassium channel. J Biol Chem **2020**;295:13277-86
82. Dudem S, Boon PX, Mullins N, McClafferty H, Shipston MJ, Wilkinson RDA*, et al.* Oxidation modulates LINGO2-induced inactivation of large conductance, Ca(2+)-activated potassium channels. J Biol Chem **2023**;299:102975
83. Dudem S, Large RJ, Kulkarni S, McClafferty H, Tikhonova IG, Sergeant GP*, et al.* LINGO1 is a regulatory subunit of large conductance, Ca(2+)-activated potassium channels. Proc Natl Acad Sci U S A **2020**;117:2194-200
84. Rotko D, Kunz WS, Szewczyk A, Kulawiak B. Signaling pathways targeting mitochondrial potassium channels. Int J Biochem Cell Biol **2020**;125:105792
85. Abbott GW. Control of Biophysical and Pharmacological Properties of Potassium Channels by Ancillary Subunits. Handb Exp Pharmacol **2021**;267:445-80
86. Abbott GW. Kv Channel Ancillary Subunits: Where Do We Go from Here? Physiology (Bethesda) **2022**;37:0
87. North KC, Zhang M, Singh AK, Zaytseva D, Slayden AV, Bukiya AN*, et al.* Cholesterol Inhibition of Slo1 Channels Is Calcium-Dependent and Can Be Mediated by Either High-Affinity Calcium-Sensing Site in the Slo1 Cytosolic Tail. Mol Pharmacol **2022**;101:132-43
88. Kim SS, Bae Y, Kwon O, Kwon SH, Seo JB, Hwang EM*, et al.* beta-COP Regulates TWIK1/TREK1 Heterodimeric Channel-Mediated Passive Conductance in Astrocytes. Cells **2022**;11
89. Pardo LA. Voltage-Gated Potassium Channels Beyond the Action Potential. Bioelectricity **2022**;4:117-25
90. Vaithianathan T, Schneider EH, Bukiya AN, Dopico AM. Cholesterol and PIP(2) Modulation of BK(Ca) Channels. Adv Exp Med Biol **2023**;1422:217-43
91. Huang X, He Y, Dubuc AM, Hashizume R, Zhang W, Reimand J*, et al.* EAG2 potassium channel with evolutionarily conserved function as a brain tumor target. Nat Neurosci **2015**;18:1236-46
92. Santos R, Ursu O, Gaulton A, Bento AP, Donadi RS, Bologa CG*, et al.* A comprehensive map of molecular drug targets. Nat Rev Drug Discov **2017**;16:19-34
93. Hutchings CJ, Colussi P, Clark TG. Ion channels as therapeutic antibody targets. MAbs **2019**;11:265-96
94. Weise-Cross L, Resta TC, Jernigan NL. Redox Regulation of Ion Channels and Receptors in Pulmonary Hypertension. Antioxid Redox Signal **2019**;31:898-915
95. Wang Y, Qi H, Liu Y, Duan C, Liu X, Xia T*, et al.* The double-edged roles of ROS in cancer prevention and therapy. Theranostics **2021**;11:4839-57
96. Park JK, Kim YC, Sim JH, Choi MY, Choi W, Hwang KK*, et al.* Regulation of membrane excitability by intracellular pH (pHi) changers through Ca2+-activated K+ current (BK channel) in single smooth muscle cells from rabbit basilar artery. Pflugers Arch **2007**;454:307-19

97. Lewandowska J, Kalenik B, Wrzosek A, Szewczyk A. Redox Regulation of Mitochondrial Potassium Channels Activity. Antioxidants (Basel) **2024**;13
98. Lee YM, Kim BJ, Chun YS, So I, Choi H, Kim MS*, et al.* NOX4 as an oxygen sensor to regulate TASK-1 activity. Cell Signal **2006**;18:499-507
99. Michl J, White B, Monterisi S, Bodmer WF, Swietach P. Phenotypic screen of sixty-eight colorectal cancer cell lines identifies CEACAM6 and CEACAM5 as markers of acid resistance. Proc Natl Acad Sci U S A **2024**;121:e2319055121
100. Selivanov VA, Zeak JA, Roca J, Cascante M, Trucco M, Votyakova TV. The role of external and matrix pH in mitochondrial reactive oxygen species generation. J Biol Chem **2008**;283:29292-300
101. Barar J, Omidi Y. Dysregulated pH in Tumor Microenvironment Checkmates Cancer Therapy. Bioimpacts **2013**;3:149-62
102. Damaghi M, Wojtkowiak JW, Gillies RJ. pH sensing and regulation in cancer. Front Physiol **2013**;4:370
103. Vrbka L, Vondrasek J, Jagoda-Cwiklik B, Vacha R, Jungwirth P. Quantification and rationalization of the higher affinity of sodium over potassium to protein surfaces. Proc Natl Acad Sci U S A **2006**;103:15440-4
104. Tansel B. Significance of thermodynamic and physical characteristics on permeation of ions during membrane separation: Hydrated radius, hydration free energy and viscous effects. Separation and Purification Technology **2012**;86:119-26
105. Danchin A, Nikel PI. Why Nature Chose Potassium. J Mol Evol **2019**;87:271-88
106. Kopec W, Kopfer DA, Vickery ON, Bondarenko AS, Jansen TLC, de Groot BL*, et al.* Direct knock-on of desolvated ions governs strict ion selectivity in K(+) channels. Nat Chem **2018**;10:813-20
107. Jing Z, Rackers JA, Pratt LR, Liu C, Rempe SB, Ren P. Thermodynamics of ion binding and occupancy in potassium channels. Chem Sci **2021**;12:8920-30
108. Lam CK, de Groot BL. Ion Conduction Mechanisms in Potassium Channels Revealed by Permeation Cycles. J Chem Theory Comput **2023**;19:2574-89
109. Collins KD. Charge density-dependent strength of hydration and biological structure. Biophys J **1997**;72:65-76
110. Nagy IZ, Lustyik G, Nagy VZ, Zarandi B, Bertoni-Freddari C. Intracellular Na+:K+ ratios in human cancer cells as revealed by energy dispersive x-ray microanalysis. J Cell Biol **1981**;90:769-77
111. Leslie TK, James AD, Zaccagna F, Grist JT, Deen S, Kennerley A*, et al.* Sodium homeostasis in the tumour microenvironment. Biochim Biophys Acta Rev Cancer **2019**;1872:188304
112. Allu AS, Tiriveedhi V. Cancer Salt Nostalgia. Cells **2021**;10
113. Bortner CD, Hughes FM, Jr., Cidlowski JA. A primary role for K+ and Na+ efflux in the activation of apoptosis. J Biol Chem **1997**;272:32436-42
114. Pietrzak M, Meyerhoff ME. Determination of potassium in red blood cells using unmeasured volumes of whole blood and combined sodium/potassium-selective membrane electrode measurements. Anal Chem **2009**;81:5961-5
115. Martinez-Valverde T, Vidal-Jorge M, Montoya N, Sanchez-Guerrero A, Manrique S, Munar F*, et al.* Brain microdialysis as a tool to explore the ionic profile of the brain extracellular space in neurocritical patients: a methodological approach and feasibility study. J Neurotrauma **2015**;32:7-16
116. Eil R, Vodnala SK, Clever D, Klebanoff CA, Sukumar M, Pan JH*, et al.* Ionic immune suppression within the tumour microenvironment limits T cell effector function. Nature **2016**;537:539-43
117. Lehmann HP, Henry JB. Appendix 4, Table A4-4. Whole Blood, Serum, and Plasma Chemistry. In: Henry JB, editor. Clinical Diagnosis and Management by Laboratory Methods. Philadelphia: W.B. Saunders; 1996. p 1450-4.

118. Ghosh S, Yang R, Duraki D, Zhu J, Kim JE, Jabeen M*, et al.* Plasma Membrane Channel TRPM4 Mediates Immunogenic Therapy-Induced Necrosis. Cancer Res **2023**;83:3115-30
119. Oliver D, Baukrowitz T, Fakler B. Polyamines as gating molecules of inward-rectifier K+ channels. Eur J Biochem **2000**;267:5824-9
120. Hopp L, Lasker N, Bamforth R, Aviv A. Characterization of Na(+)-K+ homeostasis of cultured human skin fibroblasts in the presence and absence of fetal bovine serum. J Cell Physiol **1992**;151:427-32
121. Abdullah NA, Hirata M, Matsumoto K, Aizawa H, Inoue R, Hamano S*, et al.* Contraction and depolarization induced by fetal bovine serum in airway smooth muscle. Am J Physiol **1994**;266:L528-35
122. Marton LJ, Heby O, Levin VA, Lubich WP, Crafts DC, Wilson CB. The relationship of polyamines in cerebrospinal fluid to the presence of central nervous system tumors. Cancer Res **1976**;36:973-7
123. Miska J, Rashidi A, Lee-Chang C, Gao P, Lopez-Rosas A, Zhang P*, et al.* Polyamines drive myeloid cell survival by buffering intracellular pH to promote immunosuppression in glioblastoma. Sci Adv **2021**;7
124. Monsorno K, Buckinx A, Paolicelli RC. Microglial metabolic flexibility: emerging roles for lactate. Trends Endocrinol Metab **2022**;33:186-95
125. Augustynek B, Kudin AP, Bednarczyk P, Szewczyk A, Kunz WS. Hemin inhibits the large conductance potassium channel in brain mitochondria: a putative novel mechanism of neurodegeneration. Exp Neurol **2014**;257:70-5
126. Bailey CS, Moldenhauer HJ, Park SM, Keros S, Meredith AL. KCNMA1-linked channelopathy. J Gen Physiol **2019**;151:1173-89
127. Zhao Y, Wang D, Xu T, Liu P, Cao Y, Wang Y*, et al.* Bladder cancer cells re-educate TAMs through lactate shuttling in the microfluidic cancer microenvironment. Oncotarget **2015**;6:39196-210
128. Zhang L, Li S. Lactic acid promotes macrophage polarization through MCT-HIF1alpha signaling in gastric cancer. Exp Cell Res **2020**;388:111846
129. Zhou HC, Xin-Yan Y, Yu WW, Liang XQ, Du XY, Liu ZC*, et al.* Lactic acid in macrophage polarization: The significant role in inflammation and cancer. Int Rev Immunol **2022**;41:4-18
130. Liebig C, Ayala G, Wilks JA, Berger DH, Albo D. Perineural invasion in cancer: a review of the literature. Cancer **2009**;115:3379-91
131. Bakst RL, Wong RJ. Mechanisms of Perineural Invasion. J Neurol Surg B Skull Base **2016**;77:96-106
132. Narayan P, Flynn J, Zhang Z, Gillespie EF, Mueller B, Xu AJ*, et al.* Perineural invasion as a risk factor for locoregional recurrence of invasive breast cancer. Sci Rep **2021**;11:12781
133. Hosoya K, Wakahara M, Ikeda K, Umekita Y. Perineural Invasion Predicts Unfavorable Prognosis in Patients With Invasive Breast Cancer. Cancer Diagn Progn **2023**;3:208-14
134. Beckner ME, Fellows-Mayle W, Agostino NR, Gobbel GT, Pollack IF. Tumor markers in pseudopodia for invasive migration. In: Swenson LI, editor. Progress in Tumor Marker Research. New York: Nova Science Publishers, Inc.; 2007. p 43-66.
135. Beckner ME, Gobbel GT, Abounader R, Burovic F, Agostino NR, Laterra J*, et al.* Glycolytic glioma cells with active glycogen synthase are sensitive to PTEN and inhibitors of PI3K and gluconeogenesis. Lab Invest **2005**;85:1457-70
136. Beckner ME, Zhang Z, Agostino NR, Day BW, Pollack IF. Albumin marks pseudopodia of astrocytoma cells responding to hepatocyte growth factor or serum. Lab Invest **2006**;86:1103-14
137. Silverman JF, Frable WJ. The use of the diff-quik stain in the immediate interpretation of fine-needle aspiration biopsies. Diagn Cytopathol **1990**;6:366-9
138. Eagle H. Amino acid metabolism in mammalian cell cultures. Science **1959**;130:432-7

139. Clark MJ, Homer N, O'Connor BD, Chen Z, Eskin A, Lee H*, et al.* U87MG decoded: the genomic sequence of a cytogenetically aberrant human cancer cell line. PLoS Genet **2010**;6:e1000832
140. Clark MJ, Homer N, O'Connor BD, Chen Z, Eskin A, Lee H*, et al.* Correction: U87MG Decoded: The Genomic Sequence of a Cytogenetically Aberrant Human Cancer Cell Line. PLoS Genet **2018**;14:e1007392
141. Becker HM. Carbonic anhydrase IX and acid transport in cancer. Br J Cancer **2020**;122:157-67
142. Noor SI, Jamali S, Ames S, Langer S, Deitmer JW, Becker HM. A surface proton antenna in carbonic anhydrase II supports lactate transport in cancer cells. Elife **2018**;7
143. Cheng J, Wen J, Wang N, Wang C, Xu Q, Yang Y. Ion Channels and Vascular Diseases. Arterioscler Thromb Vasc Biol **2019**;39:e146-e56
144. Crepalde MA, Faria-Campos AC, Campos SV. Modeling and analysis of cell membrane systems with probabilistic model checking. BMC Genomics **2011**;12 Suppl 4:S14
145. Sajic JL, Langthaler S, Baumgartner C. Creating a novel mathematical model of the Kv10.1 ion channel and controlling channel activity with nanoelectromechanical systems. Applied Sciences **2022**;12
146. Sun X, Lee HC, Lu T. Sorbs2 Deficiency and Vascular BK Channelopathy in Diabetes. Circ Res **2024**;134:858-71
147. Wulff H, Castle NA. Therapeutic potential of KCa3.1 blockers: an overview of recent advances, and promising trends. Expert Reviews Clinical Pharmacology **2010**;3:385-96
148. Zaika OL, Mamenko M, Palygin O, Boukelmoune N, Staruschenko A, Pochynyuk O. Direct inhibition of basolateral Kir4.1/5.1 and Kir4.1 channels in the cortical collecting duct by dopamine. Am J Physiol Renal Physiol **2013**;305:F1277-87
149. Fournier PA, Fairchild TJ, Ferreira LD, Brau L. Post-exercise muscle glycogen repletion in the extreme: effect of food absence and active recovery. J Sports Sci Med **2004**;3:139-46
150. Bangsbo J, Gollnick PD, Graham TE, Saltin B. Substrates for muscle glycogen synthesis in recovery from intense exercise in man. J Physiol **1991**;434:423-40
151. Talmadge RJ, Scheide JI, Silverman H. Glycogen synthesis from lactate in a chronically active muscle. J Appl Physiol (1985) **1989**;66:2231-8
152. Hydrean C, Ghosh A, Nallin M, Ghosh BK. Interrelationship of carbohydrate metabolism and alkaline phosphatase synthesis in Bacillus licheniformis 749/c. J Biol Chem **1977**;252:6806-12
153. Tucci V, Isles AR, Kelsey G, Ferguson-Smith AC, Erice Imprinting G. Genomic Imprinting and Physiological Processes in Mammals. Cell **2019**;176:952-65
154. Berlin C, Cottard F, Willmann D, Urban S, Tirier SM, Marx L*, et al.* KMT9 Controls Stemness and Growth of Colorectal Cancer. Cancer Res **2022**;82:210-20
155. Contreras-Espinosa L, Alcaraz N, De La Rosa-Velazquez IA, Diaz-Chavez J, Cabrera-Galeana P, Rebollar-Vega R*, et al.* Transcriptome Analysis Identifies GATA3-AS1 as a Long Noncoding RNA Associated with Resistance to Neoadjuvant Chemotherapy in Locally Advanced Breast Cancer Patients. J Mol Diagn **2021**;23:1306-23
156. Nargund AM, Xu C, Mandoli A, Okabe A, Chen GB, Huang KK*, et al.* Chromatin Rewiring by Mismatch Repair Protein MSH2 Alters Cell Adhesion Pathways and Sensitivity to BET Inhibition in Gastric Cancer. Cancer Res **2022**;82:2538-51
157. Pine AR, Cirigliano SM, Singhania R, Nicholson J, da Silva B, Leslie CS*, et al.* Microenvironment-Driven Dynamic Chromatin Changes in Glioblastoma Recapitulate Early Neural Development at Single-Cell Resolution. Cancer Res **2023**;83:1581-95
158. Yu Z, Lv Y, Su C, Lu W, Zhang R, Li J*, et al.* Integrative Single-Cell Analysis Reveals Transcriptional and Epigenetic Regulatory Features of Clear Cell Renal Cell Carcinoma. Cancer Res **2023**;83:700-19

159. Zhu Q, Zhang C, Qu T, Lu X, He X, Li W*, et al.* MNX1-AS1 Promotes Phase Separation of IGF2BP1 to Drive c-Myc-Mediated Cell-Cycle Progression and Proliferation in Lung Cancer. Cancer Res **2022**;82:4340-58
160. Guetta-Terrier C, Karambizi D, Akosman B, Zepecki JP, Chen JS, Kamle S*, et al.* Chi3l1 Is a Modulator of Glioma Stem Cell States and a Therapeutic Target in Glioblastoma. Cancer Res **2023**;83:1984-99
161. Mohan DR, Borges KS, Finco I, LaPensee CR, Rege J, Solon AL*, et al.* beta-Catenin-Driven Differentiation Is a Tissue-Specific Epigenetic Vulnerability in Adrenal Cancer. Cancer Res **2023**;83:2123-41
162. Abruzzo LV, Barron LL, Anderson K, Newman RJ, Wierda WG, O'Brien S*, et al.* Identification and validation of biomarkers of IgV(H) mutation status in chronic lymphocytic leukemia using microfluidics quantitative real-time polymerase chain reaction technology. J Mol Diagn **2007**;9:546-55
163. Emmons MF, Bennett RL, Riva A, Gupta K, Carvalho L, Zhang C*, et al.* HDAC8-mediated inhibition of EP300 drives a transcriptional state that increases melanoma brain metastasis. Nat Commun **2023**;14:7759
164. Newman AC, Kemp AJ, Drabsch Y, Behrends C, Wilkinson S. Autophagy acts through TRAF3 and RELB to regulate gene expression via antagonism of SMAD proteins. Nat Commun **2017**;8:1537
165. Min J, Vega PN, Engevik AC, Williams JA, Yang Q, Patterson LM*, et al.* Heterogeneity and dynamics of active Kras-induced dysplastic lineages from mouse corpus stomach. Nat Commun **2019**;10:5549
166. Banito A, Li X, Laporte AN, Roe JS, Sanchez-Vega F, Huang CH*, et al.* The SS18-SSX Oncoprotein Hijacks KDM2B-PRC1.1 to Drive Synovial Sarcoma. Cancer Cell **2018**;33:527-41 e8
167. Pan Y, Han H, Hu H, Wang H, Song Y, Hao Y*, et al.* KMT2D deficiency drives lung squamous cell carcinoma and hypersensitivity to RTK-RAS inhibition. Cancer Cell **2023**;41:88-105 e8
168. Chapuy B, McKeown MR, Lin CY, Monti S, Roemer MG, Qi J*, et al.* Discovery and characterization of super-enhancer-associated dependencies in diffuse large B cell lymphoma. Cancer Cell **2013**;24:777-90
169. Beddows I, Fan H, Heinze K, Johnson BK, Leonova A, Senz J*, et al.* Cell State of Origin Impacts Development of Distinct Endometriosis-Related Ovarian Carcinoma Histotypes. Cancer Res **2024**;84:26-38
170. Shih AH, Jiang Y, Meydan C, Shank K, Pandey S, Barreyro L*, et al.* Mutational cooperativity linked to combinatorial epigenetic gain of function in acute myeloid leukemia. Cancer Cell **2015**;27:502-15
171. Veschi V, Liu Z, Voss TC, Ozbun L, Gryder B, Yan C*, et al.* Epigenetic siRNA and Chemical Screens Identify SETD8 Inhibition as a Therapeutic Strategy for p53 Activation in High-Risk Neuroblastoma. Cancer Cell **2017**;31:50-63
172. da Silva LS, Mancano BM, de Paula FE, Dos Reis MB, de Almeida GC, Matsushita M*, et al.* Expression of GNAS, TP53, and PTEN Improves the Patient Prognostication in Sonic Hedgehog (SHH) Medulloblastoma Subgroup. J Mol Diagn **2020**;22:957-66
173. East P, Kelly GP, Biswas D, Marani M, Hancock DC, Creasy T*, et al.* RAS oncogenic activity predicts response to chemotherapy and outcome in lung adenocarcinoma. Nat Commun **2022**;13:5632
174. Ishizawa J, Nakamaru K, Seki T, Tazaki K, Kojima K, Chachad D*, et al.* Predictive Gene Signatures Determine Tumor Sensitivity to MDM2 Inhibition. Cancer Res **2018**;78:2721-31
175. Wang XQ, Wang XQ, Hsu A, Goytain A, Ng TLT, Nielsen TO. A Rapid and Cost-Effective Gene Expression Assay for the Diagnosis of Well-Differentiated and Dedifferentiated Liposarcomas. J Mol Diagn **2021**;23:274-84

176. Wang LB, Karpova A, Gritsenko MA, Kyle JE, Cao S, Li Y*, et al.* Proteogenomic and metabolomic characterization of human glioblastoma. Cancer Cell **2021**;39:509-28 e20
177. Soragni A, Janzen DM, Johnson LM, Lindgren AG, Thai-Quynh Nguyen A, Tiourin E*, et al.* A Designed Inhibitor of p53 Aggregation Rescues p53 Tumor Suppression in Ovarian Carcinomas. Cancer Cell **2016**;29:90-103
178. Mello SS, Valente LJ, Raj N, Seoane JA, Flowers BM, McClendon J*, et al.* A p53 Super-tumor Suppressor Reveals a Tumor Suppressive p53-Ptpn14-Yap Axis in Pancreatic Cancer. Cancer Cell **2017**;32:460-73 e6
179. Dong L, Lu D, Chen R, Lin Y, Zhu H, Zhang Z*, et al.* Proteogenomic characterization identifies clinically relevant subgroups of intrahepatic cholangiocarcinoma. Cancer Cell **2022**;40:70-87 e15
180. Zhang H, Christensen CL, Dries R, Oser MG, Deng J, Diskin B*, et al.* CDK7 Inhibition Potentiates Genome Instability Triggering Anti-tumor Immunity in Small Cell Lung Cancer. Cancer Cell **2020**;37:37-54 e9
181. Schwab A, Siddiqui A, Vazakidou ME, Napoli F, Bottcher M, Menchicchi B*, et al.* Polyol Pathway Links Glucose Metabolism to the Aggressiveness of Cancer Cells. Cancer Res **2018**;78:1604-18
182. Zhang Y, Cruickshanks N, Yuan F, Wang B, Pahuski M, Wulfkuhle J*, et al.* Targetable T-type Calcium Channels Drive Glioblastoma. Cancer Res **2017**;77:3479-90
183. Halvorsen SC, Benita Y, Hopton M, Hoppe B, Gunnlaugsson HO, Korgaonkar P*, et al.* Transcriptional Profiling Supports the Notochordal Origin of Chordoma and Its Dependence on a TGFB1-TBXT Network. Am J Pathol **2023**;193:532-47
184. Sahu SK, Tiwari N, Pataskar A, Zhuang Y, Borisova M, Diken M*, et al.* FBXO32 promotes microenvironment underlying epithelial-mesenchymal transition via CtBP1 during tumour metastasis and brain development. Nat Commun **2017**;8:1523
185. Verfaillie A, Imrichova H, Atak ZK, Dewaele M, Rambow F, Hulselmans G*, et al.* Decoding the regulatory landscape of melanoma reveals TEADS as regulators of the invasive cell state. Nat Commun **2015**;6:6683
186. Wu LMN, Deng Y, Wang J, Zhao C, Wang J, Rao R*, et al.* Programming of Schwann Cells by Lats1/2-TAZ/YAP Signaling Drives Malignant Peripheral Nerve Sheath Tumorigenesis. Cancer Cell **2018**;33:292-308 e7
187. Haider S, McIntyre A, van Stiphout RG, Winchester LM, Wigfield S, Harris AL*, et al.* Genomic alterations underlie a pan-cancer metabolic shift associated with tumour hypoxia. Genome Biol **2016**;17:140
188. Zhang D, Park D, Zhong Y, Lu Y, Rycaj K, Gong S*, et al.* Stem cell and neurogenic gene-expression profiles link prostate basal cells to aggressive prostate cancer. Nat Commun **2016**;7:10798
189. Ni Y, Schmidt KR, Werner BA, Koenig JK, Guldner IH, Schnepp PM*, et al.* Death effector domain-containing protein induces vulnerability to cell cycle inhibition in triple-negative breast cancer. Nat Commun **2019**;10:2860
190. Wang Z, Sun D, Chen YJ, Xie X, Shi Y, Tabar V*, et al.* Cell Lineage-Based Stratification for Glioblastoma. Cancer Cell **2020**;38:366-79 e8
191. Zhang Z, Karthaus WR, Lee YS, Gao VR, Wu C, Russo JW*, et al.* Tumor Microenvironment-Derived NRG1 Promotes Antiandrogen Resistance in Prostate Cancer. Cancer Cell **2020**;38:279-96 e9
192. Cheung WK, Zhao M, Liu Z, Stevens LE, Cao PD, Fang JE*, et al.* Control of alveolar differentiation by the lineage transcription factors GATA6 and HOPX inhibits lung adenocarcinoma metastasis. Cancer Cell **2013**;23:725-38
193. Kelenis DP, Rodarte KE, Kollipara RK, Pozo K, Choudhuri SP, Spainhower KB*, et al.* Inhibition of Karyopherin beta1-Mediated Nuclear Import Disrupts Oncogenic Lineage-Defining Transcription Factor Activity in Small Cell Lung Cancer. Cancer Res **2022**;82:3058-73

194. Pozniak J, Nsengimana J, Laye JP, O'Shea SJ, Diaz JMS, Droop AP*, et al.* Genetic and Environmental Determinants of Immune Response to Cutaneous Melanoma. Cancer Res **2019**;79:2684-96
195. Van de Velde LA, Allen EK, Crawford JC, Wilson TL, Guy CS, Russier M*, et al.* Neuroblastoma Formation Requires Unconventional CD4 T Cells and Arginase-1-Dependent Myeloid Cells. Cancer Res **2021**;81:5047-59
196. Cai L, DeBerardinis RJ, Xie Y, Minna JD, Xiao G. A Comparative Study of Neuroendocrine Heterogeneity in Small Cell Lung Cancer and Neuroblastoma. Mol Cancer Res **2023**;21:795-807
197. Kawauchi D, Robinson G, Uziel T, Gibson P, Rehg J, Gao C*, et al.* A mouse model of the most aggressive subgroup of human medulloblastoma. Cancer Cell **2012**;21:168-80
198. Topham C, Tighe A, Ly P, Bennett A, Sloss O, Nelson L*, et al.* MYC Is a Major Determinant of Mitotic Cell Fate. Cancer Cell **2015**;28:129-40
199. Alam A, Levanduski E, Denz P, Villavicencio HS, Bhatta M, Alhorebi L*, et al.* Fungal mycobiome drives IL-33 secretion and type 2 immunity in pancreatic cancer. Cancer Cell **2022**;40:153-67 e11
200. Altwegg KA, Viswanadhapalli S, Mann M, Chakravarty D, Krishnan S, Liu Z*, et al.* A First-in-Class Inhibitor of ER Coregulator PELP1 Targets ER+ Breast Cancer. Cancer Res **2022**;82:3830-44
201. Guieze R, Liu VM, Rosebrock D, Jourdain AA, Hernandez-Sanchez M, Martinez Zurita A*, et al.* Mitochondrial Reprogramming Underlies Resistance to BCL-2 Inhibition in Lymphoid Malignancies. Cancer Cell **2019**;36:369-84 e13
202. Roh W, Geffen Y, Cha H, Miller M, Anand S, Kim J*, et al.* High-Resolution Profiling of Lung Adenocarcinoma Identifies Expression Subtypes with Specific Biomarkers and Clinically Relevant Vulnerabilities. Cancer Res **2022**;82:3917-31
203. Vidal SJ, Rodriguez-Bravo V, Quinn SA, Rodriguez-Barrueco R, Lujambio A, Williams E*, et al.* A targetable GATA2-IGF2 axis confers aggressiveness in lethal prostate cancer. Cancer Cell **2015**;27:223-39
204. Alothman SJ, Kang K, Liu X, Krawczyk E, Azhar RI, Hu R*, et al.* Characterization of transcriptome diversity and in vitro behavior of primary human high-risk breast cells. Sci Rep **2022**;12:6159
205. Chen R, Khatri P, Mazur PK, Polin M, Zheng Y, Vaka D*, et al.* A meta-analysis of lung cancer gene expression identifies PTK7 as a survival gene in lung adenocarcinoma. Cancer Res **2014**;74:2892-902
206. Darmanis S, Sloan SA, Croote D, Mignardi M, Chernikova S, Samghababi P*, et al.* Single-Cell RNA-Seq Analysis of Infiltrating Neoplastic Cells at the Migrating Front of Human Glioblastoma. Cell Rep **2017**;21:1399-410
207. de Jong JJ, Narayan VM, Cronican AA, Gupta S, van Leenders GJLH, Boormans JL*, et al.* Gene expression profiling of muscle-invasive bladder cancer with secondary variant histology. Am J Clin Pathol **2021**;156:895-905
208. Harlow ML, Maloney N, Roland J, Guillen Navarro MJ, Easton MK, Kitchen-Goosen SM*, et al.* Lurbinectedin Inactivates the Ewing Sarcoma Oncoprotein EWS-FLI1 by Redistributing It within the Nucleus. Cancer Res **2016**;76:6657-68
209. Scheidmann MC, Castro-Giner F, Strittmatter K, Krol I, Paasinen-Sohns A, Scherrer R*, et al.* An In Vivo CRISPR Screen Identifies Stepwise Genetic Dependencies of Metastatic Progression. Cancer Res **2022**;82:681-94
210. Xu Q, Chen J, Ni S, Tan C, Xu M, Dong L*, et al.* Pan-cancer transcriptome analysis reveals a gene expression signature for the identification of tumor tissue origin. Mod Pathol **2016**;29:546-56
211. Zhang S, Zhou YF, Cao J, Burley SK, Wang HY, Zheng XFS. mTORC1 Promotes ARID1A Degradation and Oncogenic Chromatin Remodeling in Hepatocellular Carcinoma. Cancer Res **2021**;81:5652-65

212. Khlebus E, Vuttaradhi VK, Welte T, Khurana N, Celestino J, Beird HC*, et al.* Comparative Tumor Microenvironment Analysis of Primary and Recurrent Ovarian Granulosa Cell Tumors. Mol Cancer Res **2023**;21:483-94
213. Mirzaei R, D'Mello C, Liu M, Nikolic A, Kumar M, Visser F*, et al.* Single-Cell Spatial Analysis Identifies Regulators of Brain Tumor-Initiating Cells. Cancer Res **2023**;83:1725-41
214. Yao L, Wang JT, Jayasinghe RG, O'Neal J, Tsai CF, Rettig MP*, et al.* Single-Cell Discovery and Multiomic Characterization of Therapeutic Targets in Multiple Myeloma. Cancer Res **2023**;83:1214-33
215. Roda N, Cossa A, Hillje R, Tirelli A, Ruscitto F, Cheloni S*, et al.* A Rare Subset of Primary Tumor Cells with Concomitant Hyperactivation of Extracellular Matrix Remodeling and dsRNA-IFN1 Signaling Metastasizes in Breast Cancer. Cancer Res **2023**;83:2155-70
216. Restaino AC, Walz A, Vermeer SJ, Barr J, Kovacs A, Fettig RR*, et al.* Functional neuronal circuits promote disease progression in cancer. Sci Adv **2023**;9:eade4443
217. Song Y, Deng Z, Sun H, Zhao Y, Zhao R, Cheng J*, et al.* Predicting tumor repopulation through the gene panel derived from radiation resistant colorectal cancer cells. J Transl Med **2023**;21:390
218. Zhou X, An J, Kurilov R, Brors B, Hu K, Peccerella T*, et al.* Persister cell phenotypes contribute to poor patient outcomes after neoadjuvant chemotherapy in PDAC. Nat Cancer **2023**;4:1362-81
219. Inman GJ, Wang J, Nagano A, Alexandrov LB, Purdie KJ, Taylor RG*, et al.* The genomic landscape of cutaneous SCC reveals drivers and a novel azathioprine associated mutational signature. Nat Commun **2018**;9:3667
220. Pandey GK, Mitra S, Subhash S, Hertwig F, Kanduri M, Mishra K*, et al.* The risk-associated long noncoding RNA NBAT-1 controls neuroblastoma progression by regulating cell proliferation and neuronal differentiation. Cancer Cell **2014**;26:722-37
221. Witt H, Mack SC, Ryzhova M, Bender S, Sill M, Isserlin R*, et al.* Delineation of two clinically and molecularly distinct subgroups of posterior fossa ependymoma. Cancer Cell **2011**;20:143-57
222. Neou M, Villa C, Armignacco R, Jouinot A, Raffin-Sanson ML, Septier A*, et al.* Pangenomic Classification of Pituitary Neuroendocrine Tumors. Cancer Cell **2020**;37:123-34 e5
223. Fukumoto T, Umakoshi H, Iwahashi N, Ogasawara T, Yokomoto-Umakoshi M, Kaneko H*, et al.* Steroids-producing nodules: a two-layered adrenocortical nodular structure as a precursor lesion of cortisol-producing adenoma. EBioMedicine **2024**;103:105087
224. Papier K, Atkins JR, Tong TYN, Gaitskell K, Desai T, Ogamba CF*, et al.* Identifying proteomic risk factors for cancer using prospective and exome analyses of 1463 circulating proteins and risk of 19 cancers in the UK Biobank. Nat Commun **2024**;15:4010
225. Smith-Byrne K, Hedman A, Dimitriou M, Desai T, Sokolov AV, Schioth HB*, et al.* Identifying therapeutic targets for cancer among 2074 circulating proteins and risk of nine cancers. Nat Commun **2024**;15:3621
226. Suchak SK, Baloyianni NV, Perkinton MS, Williams RJ, Meldrum BS, Rattray M. The 'glial' glutamate transporter, EAAT2 (Glt-1) accounts for high affinity glutamate uptake into adult rodent nerve endings. J Neurochem **2003**;84:522-32
227. Al Awabdh S, Gupta-Agarwal S, Sheehan DF, Muir J, Norkett R, Twelvetrees AE*, et al.* Neuronal activity mediated regulation of glutamate transporter GLT-1 surface diffusion in rat astrocytes in dissociated and slice cultures. Glia **2016**;64:1252-64
228. Mai D, Chen R, Wang J, Zheng J, Zhang X, Qu S. Critical amino acids in the TM2 of EAAT2 are essential for membrane-bound localization, substrate binding, transporter function and anion currents. J Cell Mol Med **2021**;25:2530-48
229. Molenaar RJ. Ion channels in glioblastoma. ISRN Neurol **2011**;2011:590249
230. Pedersen SF, Stock C. Ion channels and transporters in cancer: pathophysiology, regulation, and clinical potential. Cancer Res **2013**;73:1658-61

231. Huang X, Jan LY. Targeting potassium channels in cancer. J Cell Biol **2014**;206:151-62
232. Pardo LA, Stuhmer W. The roles of K(+) channels in cancer. Nat Rev Cancer **2014**;14:39-48
233. Comes N, Serrano-Albarras A, Capera J, Serrano-Novillo C, Condom E, Ramon YCS*, et al.* Involvement of potassium channels in the progression of cancer to a more malignant phenotype. Biochim Biophys Acta **2015**;1848:2477-92
234. Prevarskaya N, Skryma R, Shuba Y. Ion Channels in Cancer: Are Cancer Hallmarks Oncochannelopathies? Physiol Rev **2018**;98:559-621
235. Iorio J, Petroni G, Duranti C, Lastraioli E. Potassium and Sodium Channels and the Warburg Effect: Biophysical Regulation of Cancer Metabolism. Bioelectricity **2019**;1:188-200
236. Girault A, Ahidouch A, Ouadid-Ahidouch H. Roles for Ca(2+) and K(+) channels in cancer cells exposed to the hypoxic tumour microenvironment. Biochim Biophys Acta Mol Cell Res **2020**;1867:118644
237. Petho Z, Najder K, Carvalho T, McMorrow R, Todesca LM, Rugi M*, et al.* pH-Channeling in Cancer: How pH-Dependence of Cation Channels Shapes Cancer Pathophysiology. Cancers (Basel) **2020**;12
238. Ganser K, Klumpp L, Bischof H, Lukowski R, Eckert F, Huber SM. Potassium Channels in Cancer. Handb Exp Pharmacol **2021**;267:253-75
239. Verkhratsky A, Parpura V. Physiology of Astroglia: Channels, Receptors, Transporters, Ion Signaling, and Gliotransmission. Verkhratsky A, Parpura V, editors. store.morganclaypool.com: Morgan & Claypool Publishers; 2015.
240. Lopatin AN, Makhina EN, Nichols CG. The mechanism of inward rectification of potassium channels: "long-pore plugging" by cytoplasmic polyamines. J Gen Physiol **1995**;106:923-55
241. Taura J, Kircher DM, Gameiro-Ros I, Slesinger PA. Comparison of K(+) Channel Families. Handb Exp Pharmacol **2021**;267:1-49
242. Beckner ME. A roadmap for potassium buffering/dispersion via the glial network of the CNS. Neurochem Int **2020**;136:104727
243. Schroder W, Hinterkeuser S, Seifert G, Schramm J, Jabs R, Wilkin GP*, et al.* Functional and molecular properties of human astrocytes in acute hippocampal slices obtained from patients with temporal lobe epilepsy. Epilepsia **2000**;41 Suppl 6:S181-4
244. Larson VA, Mironova Y, Vanderpool KG, Waisman A, Rash JE, Agarwal A*, et al.* Oligodendrocytes control potassium accumulation in white matter and seizure susceptibility. Elife **2018**;7
245. Song S, Luo L, Sun B, Sun D. Roles of glial ion transporters in brain diseases. Glia **2020**;68:472-94
246. Aronica E, Gorter JA, Jansen GH, Leenstra S, Yankaya B, Troost D. Expression of connexin 43 and connexin 32 gap-junction proteins in epilepsy-associated brain tumors and in the perilesional epileptic cortex. Acta Neuropathol **2001**;101:449-59
247. Caltabiano R, Torrisi A, Condorelli D, Albanese V, Lanzafame S. High levels of connexin 43 mRNA in high grade astrocytomas. Study of 32 cases with in situ hybridization. Acta Histochem **2010**;112:529-35
248. McClenaghan C, Schewe M, Aryal P, Carpenter EP, Baukrowitz T, Tucker SJ. Polymodal activation of the TREK-2 K2P channel produces structurally distinct open states. J Gen Physiol **2016**;147:497-505
249. Woo J, Jun YK, Zhang YH, Nam JH, Shin DH, Kim SJ. Identification of critical amino acids in the proximal C-terminal of TREK-2 K(+) channel for activation by acidic pH(i) and ATP-dependent inhibition. Pflugers Arch **2018**;470:327-37
250. Lee J, Kang M, Kim S, Chang I. Structural and molecular insight into the pH-induced low-permeability of the voltage-gated potassium channel Kv1.2 through dewetting of the water cavity. PLoS Comput Biol **2020**;16:e1007405

251. Claydon TW, Boyett MR, Sivaprasadarao A, Ishii K, Owen JM, O'Beirne HA*, et al.* Inhibition of the K+ channel kv1.4 by acidosis: protonation of an extracellular histidine slows the recovery from N-type inactivation. J Physiol **2000**;526 Pt 2:253-64
252. Li X, Bett GC, Jiang X, Bondarenko VE, Morales MJ, Rasmusson RL. Regulation of N- and C-type inactivation of Kv1.4 by pHo and K+: evidence for transmembrane communication. Am J Physiol Heart Circ Physiol **2003**;284:H71-80
253. Abbott GW, Butler MH, Goldstein SA. Phosphorylation and protonation of neighboring MiRP2 sites: function and pathophysiology of MiRP2-Kv3.4 potassium channels in periodic paralysis. FASEB J **2006**;20:293-301
254. Kazmierczak M, Zhang X, Chen B, Mulkey DK, Shi Y, Wagner PG*, et al.* External pH modulates EAG superfamily K+ channels through EAG-specific acidic residues in the voltage sensor. J Gen Physiol **2013**;141:721-35
255. Mao J, Li L, McManus M, Wu J, Cui N, Jiang C. Molecular determinants for activation of G-protein-coupled inward rectifier K+ (GIRK) channels by extracellular acidosis. J Biol Chem **2002**;277:46166-71
256. Mao J, Wu J, Chen F, Wang X, Jiang C. Inhibition of G-protein-coupled inward rectifying K+ channels by intracellular acidosis. J Biol Chem **2003**;278:7091-8
257. Wu J, Xu H, Yang Z, Wang Y, Mao J, Jiang C. Protons activate homomeric Kir6.2 channels by selective suppression of the long and intermediate closures. J Membr Biol **2002**;190:105-16
258. Cui N, Wu J, Xu H, Wang R, Rojas A, Piao H*, et al.* A threonine residue (Thr71) at the intracellular end of the M1 helix plays a critical role in the gating of Kir6.2 channels by intracellular ATP and protons. J Membr Biol **2003**;192:111-22
259. Maksaev G, Brundl-Jirout M, Stary-Weinzinger A, Zangerl-Plessl EM, Lee SJ, Nichols CG. Subunit gating resulting from individual protonation events in Kir2 channels. Nat Commun **2023**;14:4538
260. Meuth SG, Kleinschnitz C, Broicher T, Austinat M, Braeuninger S, Bittner S*, et al.* The neuroprotective impact of the leak potassium channel TASK1 on stroke development in mice. Neurobiol Dis **2009**;33:1-11
261. Buckler KJ. TASK channels in arterial chemoreceptors and their role in oxygen and acid sensing. Pflugers Arch **2015**;467:1013-25
262. Decher N, Maier M, Dittrich W, Gassenhuber J, Bruggemann A, Busch AE*, et al.* Characterization of TASK-4, a novel member of the pH-sensitive, two-pore domain potassium channel family. FEBS Lett **2001**;492:84-9
263. Bales CE, Durfee GR. Part I: Cytologic Techniques. In: Koss LG, editor. Diagnostic Cytology and Its Histopathologic Bases. Philadelphia: J.B. Lippincott Company; 1992. p 1484-6.
264. Folstad L, Look M, Pallavicini M. A polycarbonate filter technique for collection of sorted cells. Cytometry **1982**;3:64-5
265. Druzhkova I, Lukina M, Dudenkova V, Ignatova N, Snopova L, Gavrina A*, et al.* Tracing of intracellular pH in cancer cells in response to Taxol treatment. Cell Cycle **2021**;20:1540-51
266. Lemasters JJ. Molecular mechanisms of cell death. In: Coleman WB, Tsongalis GJ, editors. Molecular Pathology, The Molecular Basis of Disease. Burlington, MA: Academic Press; 2009. p 3-24.
267. Lemasters JJ. Molecular Mechanisms of Cell Death. In: Coleman WB, Tsongalis GJ, editors. Molecular Pathology, The Molecular Basis of Human Disease. Cambridge, MA: Academic Press; 2018. p 1-24.
268. Green DR. Nonapoptotic cell death pathways. Cell Death, Apoptosis and Other Means to an End. Cold Spring Harbor, NY: Cold Spring Harbor Laboratory Press; 2018. p 135.

269. Gow IF, Thomson J, Davidson J, Shennan DB. The effect of a hyposmotic shock and purinergic agonists on K+(Rb+) efflux from cultured human breast cancer cells. Biochim Biophys Acta **2005**;1712:52-61
270. Nakada T. The Molecular Mechanisms of Neural Flow Coupling: A New Concept. J Neuroimaging **2015**;25:861-5
271. Li C, Voth GA. A quantitative paradigm for water-assisted proton transport through proteins and other confined spaces. Proc Natl Acad Sci U S A **2021**;118
272. Drew D, Boudker O. Ion and lipid orchestration of secondary active transport. Nature **2024**;626:963-74
273. Persi E, Duran-Frigola M, Damaghi M, Roush WR, Aloy P, Cleveland JL*, et al.* Systems analysis of intracellular pH vulnerabilities for cancer therapy. Nat Commun **2018**;9:2997
274. Russell S, Xu L, Kam Y, Abrahams D, Ordway B, Lopez AS*, et al.* Proton export upregulates aerobic glycolysis. BMC Biol **2022**;20:163
275. Swietach P, Spitzer KW, Vaughan-Jones RD. pH-Dependence of extrinsic and intrinsic H(+)-ion mobility in the rat ventricular myocyte, investigated using flash photolysis of a caged-H(+) compound. Biophys J **2007**;92:641-53
276. Barron T, Yalcin B, Su M, Byun YG, Gavish A, Shamardani K*, et al.* GABAergic neuron-to-glioma synapses in diffuse midline gliomas. Nature **2025**;639:1060-8
277. Garofano L, Migliozzi S, Oh YT, D'Angelo F, Najac RD, Ko A*, et al.* Pathway-based classification of glioblastoma uncovers a mitochondrial subtype with therapeutic vulnerabilities. Nat Cancer **2021**;2:141-56
278. Xia J, Wang H, Li S, Wu Q, Sun L, Huang H*, et al.* Ion channels or aquaporins as novel molecular targets in gastric cancer. Mol Cancer **2017**;16:54
279. Kurzeder C, Nguyen-Strauli BD, Krol I, Ring A, Castro-Giner F, Nuesch M*, et al.* Digoxin for reduction of circulating tumor cell cluster size in metastatic breast cancer: a proof-of-concept trial. Nat Med **2025**;31
280. Moriyama T, Kataoka H, Seguchi K, Tsubouchi H, Koono M. Effects of hepatocyte growth factor (HGF) on human glioma cells in vitro: HGF acts as a motility factor in glioma cells. Int J Cancer **1996**;66:678-85
281. Yamamoto S, Wakimoto H, Aoyagi M, Hirakawa K, Hamada H. Modulation of motility and proliferation of glioma cells by hepatocyte growth factor. Jpn J Cancer Res **1997**;88:564-77
282. Yuan S, Almagro J, Fuchs E. Beyond genetics: driving cancer with the tumour microenvironment behind the wheel. Nat Rev Cancer **2024**;24:274-86
283. Baumann F, Leukel P, Doerfelt A, Beier CP, Dettmer K, Oefner PJ*, et al.* Lactate promotes glioma migration by TGF-beta2-dependent regulation of matrix metalloproteinase-2. Neuro Oncol **2009**;11:368-80
284. Hirschhaeuser F, Sattler UG, Mueller-Klieser W. Lactate: a metabolic key player in cancer. Cancer Res **2011**;71:6921-5
285. Seliger C, Leukel P, Moeckel S, Jachnik B, Lottaz C, Kreutz M*, et al.* Lactate-modulated induction of THBS-1 activates transforming growth factor (TGF)-beta2 and migration of glioma cells in vitro. PLoS One **2013**;8:e78935
286. Ward C, Meehan J, Gray ME, Murray AF, Argyle DJ, Kunkler IH*, et al.* The impact of tumour pH on cancer progression: strategies for clinical intervention. Explor Target Antitumor Ther **2020**;1:71-100
287. Zhou R, Tang X, Wang Y. Emerging strategies to investigate the biology of early cancer. Nat Rev Cancer **2024**;24:850-66
288. Putnam RW, Roos A, Wilding TJ. Properties of the intracellular pH-regulating systems of frog skeletal muscle. J Physiol **1986**;381:205-19

289. Fraser SP, Pardo LA. Ion channels: functional expression and therapeutic potential in cancer. Colloquium on Ion Channels and Cancer. EMBO Rep **2008**;9:512-5
290. Lang F, Stournaras C. Ion channels in cancer: future perspectives and clinical potential. Philos Trans R Soc Lond B Biol Sci **2014**;369:20130108
291. Martina M. Ion channel screening: advances in technologies and analysis. Front Pharmacol **2012**;3:86
292. Bretschneider F, Wrisch A, Lehmann-Horn F, Grissmer S. External tetraethylammonium as a molecular caliper for sensing the shape of the outer vestibule of potassium channels. Biophys J **1999**;76:2351-60
293. Somodi S, Hajdu P, Gaspar R, Panyi G, Varga Z. Effects of changes in extracellular pH and potassium concentration on Kv1.3 inactivation. Eur Biophys J **2008**;37:1145-56
294. Somodi S, Varga Z, Hajdu P, Starkus JG, Levy DI, Gaspar R*, et al.* pH-dependent modulation of Kv1.3 inactivation: role of His399. Am J Physiol Cell Physiol **2004**;287:C1067-76
295. Steidl JV, Yool AJ. Differential sensitivity of voltage-gated potassium channels Kv1.5 and Kv1.2 to acidic pH and molecular identification of pH sensor. Mol Pharmacol **1999**;55:812-20
296. Jager H, Grissmer S. Regulation of a mammalian Shaker-related potassium channel, hKv1.5, by extracellular potassium and pH. FEBS Lett **2001**;488:45-50
297. Kehl SJ, Eduljee C, Kwan DC, Zhang S, Fedida D. Molecular determinants of the inhibition of human Kv1.5 potassium currents by external protons and Zn(2+). J Physiol **2002**;541:9-24
298. Trapani JG, Korn SJ. Effect of external pH on activation of the Kv1.5 potassium channel. Biophys J **2003**;84:195-204
299. Zhang S, Kurata HT, Kehl SJ, Fedida D. Rapid induction of P/C-type inactivation is the mechanism for acid-induced K+ current inhibition. J Gen Physiol **2003**;121:215-25
300. Fedida D, Zhang S, Kwan DC, Eduljee C, Kehl SJ. Synergistic inhibition of the maximum conductance of Kv1.5 channels by extracellular K+ reduction and acidification. Cell Biochem Biophys **2005**;43:231-42
301. Wang S, Ding WG, Bai JY, Toyoda F, Wei MJ, Matsuura H. Regulation of human cardiac Kv1.5 channels by extracellular acidification. Pflugers Arch **2016**;468:1885-94
302. Tipparaju SM, Barski OA, Srivastava S, Bhatnagar A. Catalytic mechanism and substrate specificity of the beta-subunit of the voltage-gated potassium channel. Biochemistry **2008**;47:8840-54
303. Raph SM, Bhatnagar A, Nystoriak MA. Biochemical and physiological properties of K(+) channel-associated AKR6A (Kvbeta) proteins. Chem Biol Interact **2019**;305:21-7
304. Singarayar S, Bursill J, Wyse K, Bauskin A, Wu W, Vandenberg J*, et al.* Extracellular acidosis modulates drug block of Kv4.3 currents by flecainide and quinidine. J Cardiovasc Electrophysiol **2003**;14:641-50
305. Singarayar S, Singleton C, Tie H, Wyse K, Bursill J, Bauskin A*, et al.* Effects of components of ischemia on the Kv4.3 current stably expressed in Chinese hamster ovary cells. J Mol Cell Cardiol **2002**;34:197-207
306. Saegusa N, Garg V, Spitzer KW. Modulation of ventricular transient outward K(+) current by acidosis and its effects on excitation-contraction coupling. Am J Physiol Heart Circ Physiol **2013**;304:H1680-96
307. Heitzmann D, Grahammer F, von Hahn T, Schmitt-Graff A, Romeo E, Nitschke R*, et al.* Heteromeric KCNE2/KCNQ1 potassium channels in the luminal membrane of gastric parietal cells. J Physiol **2004**;561:547-57
308. Heitzmann D, Koren V, Wagner M, Sterner C, Reichold M, Tegtmeier I*, et al.* KCNE beta subunits determine pH sensitivity of KCNQ1 potassium channels. Cell Physiol Biochem **2007**;19:21-32

309. Heitzmann D, Warth R. No potassium, no acid: K+ channels and gastric acid secretion. Physiology (Bethesda) **2007**;22:335-41
310. Abbott GW, Roepke TK. KCNE2 and gastric cancer: bench to bedside. Oncotarget **2016**;7:17286-7
311. Engevik AC, Kaji I, Goldenring JR. The Physiology of the Gastric Parietal Cell. Physiol Rev **2020**;100:573-602
312. Terlau H, Ludwig J, Steffan R, Pongs O, Stuhmer W, Heinemann SH. Extracellular Mg2+ regulates activation of rat eag potassium channel. Pflugers Arch **1996**;432:301-12
313. Anumonwo JM, Horta J, Delmar M, Taffet SM, Jalife J. Proton and zinc effects on HERG currents. Biophys J **1999**;77:282-98
314. Berube J, Chahine M, Daleau P. Modulation of HERG potassium channel properties by external pH. Pflugers Arch **1999**;438:419-22
315. Jiang M, Dun W, Tseng GN. Mechanism for the effects of extracellular acidification on HERG-channel function. Am J Physiol **1999**;277:H1283-92
316. Jo SH, Youm JB, Kim I, Lee CO, Earm YE, Ho WK. Blockade of HERG channels expressed in Xenopus oocytes by external H+. Pflugers Arch **1999**;438:23-9
317. Terai T, Furukawa T, Katayama Y, Hiraoka M. Effects of external acidosis on HERG current expressed in Xenopus oocytes. J Mol Cell Cardiol **2000**;32:11-21
318. Vereecke J, Carmeliet E. The effect of external pH on the delayed rectifying K+ current in cardiac ventricular myocytes. Pflugers Arch **2000**;439:739-51
319. Zhou Q, Bett GC. Regulation of the voltage-insensitive step of HERG activation by extracellular pH. Am J Physiol Heart Circ Physiol **2010**;298:H1710-8
320. Van Slyke AC, Cheng YM, Mafi P, Allard CR, Hull CM, Shi YP*, et al.* Proton block of the pore underlies the inhibition of hERG cardiac K+ channels during acidosis. Am J Physiol Cell Physiol **2012**;302:C1797-806
321. Shi YP, Cheng YM, Van Slyke AC, Claydon TW. External protons destabilize the activated voltage sensor in hERG channels. Eur Biophys J **2014**;43:59-69
322. Shi YP, Thouta S, Cheng YM, Claydon TW. Extracellular protons accelerate hERG channel deactivation by destabilizing voltage sensor relaxation. J Gen Physiol **2019**;151:231-46
323. Shi YP, Thouta S, Claydon TW. Modulation of hERG K(+) Channel Deactivation by Voltage Sensor Relaxation. Front Pharmacol **2020**;11:139
324. Wilson SL, Dempsey CE, Hancox JC, Marrion NV. Identification of a proton sensor that regulates conductance and open time of single hERG channels. Sci Rep **2019**;9:19825
325. Ukachukwu CU, Jimenez-Vazquez EN, Jain A, Jones DK. hERG1 channel subunit composition mediates proton inhibition of rapid delayed rectifier potassium current (I(Kr)) in cardiomyocytes derived from hiPSCs. J Biol Chem **2023**;299:102778
326. Shi W, Wang HS, Pan Z, Wymore RS, Cohen IS, McKinnon D*, et al.* Cloning of a mammalian elk potassium channel gene and EAG mRNA distribution in rat sympathetic ganglia. J Physiol **1998**;511 (Pt 3):675-82
327. Sala-Rabanal M, Nichols CG. Inward rectifying potassium channels. In: Zheng J, Trudeau MC, editors. Handbook of Ion Channels. Boca Raton, FL: CRC Press; 2015. p 241-60.
328. Davies NW. Modulation of ATP-sensitive K+ channels in skeletal muscle by intracellular protons. Nature **1990**;343:375-7
329. Davies NW, Standen NB, Stanfield PR. The effect of intracellular pH on ATP-dependent potassium channels of frog skeletal muscle. J Physiol **1992**;445:549-68
330. Vivaudou M, Forestier C. Modification by protons of frog skeletal muscle KATP channels: effects on ion conduction and nucleotide inhibition. J Physiol **1995**;486 (Pt 3):629-45

331. Forestier C, Pierrard J, Vivaudou M. Mechanism of action of K channel openers on skeletal muscle KATP channels. Interactions with nucleotides and protons. J Gen Physiol **1996**;107:489-502
332. Santa N, Kitazono T, Ago T, Ooboshi H, Kamouchi M, Wakisaka M*, et al.* ATP-sensitive potassium channels mediate dilatation of basilar artery in response to intracellular acidification in vivo. Stroke **2003**;34:1276-80
333. Butt AM, Kalsi A. Inwardly rectifying potassium channels (Kir) in central nervous system glia: a special role for Kir4.1 in glial functions. J Cell Mol Med **2006**;10:33-44
334. Shuck ME, Piser TM, Bock JH, Slightom JL, Lee KS, Bienkowski MJ. Cloning and characterization of two K+ inward rectifier (Kir) 1.1 potassium channel homologs from human kidney (Kir1.2 and Kir1.3). J Biol Chem **1997**;272:586-93
335. Yang Z, Jiang C. Opposite effects of pH on open-state probability and single channel conductance of kir4.1 channels. J Physiol **1999**;520 Pt 3:921-7
336. Xu H, Yang Z, Cui N, Giwa LR, Abdulkadir L, Patel M*, et al.* Molecular determinants for the distinct pH sensitivity of Kir1.1 and Kir4.1 channels. Am J Physiol Cell Physiol **2000**;279:C1464-71
337. Xu H, Cui N, Yang Z, Qu Z, Jiang C. Modulation of kir4.1 and kir5.1 by hypercapnia and intracellular acidosis. J Physiol **2000**;524 Pt 3:725-35
338. Tucker SJ, Imbrici P, Salvatore L, D'Adamo MC, Pessia M. pH dependence of the inwardly rectifying potassium channel, Kir5.1, and localization in renal tubular epithelia. J Biol Chem **2000**;275:16404-7
339. Tanemoto M, Kittaka N, Inanobe A, Kurachi Y. In vivo formation of a proton-sensitive K+ channel by heteromeric subunit assembly of Kir5.1 with Kir4.1. J Physiol **2000**;525 Pt 3:587-92
340. Yang Z, Xu H, Cui N, Qu Z, Chanchevalap S, Shen W*, et al.* Biophysical and molecular mechanisms underlying the modulation of heteromeric Kir4.1-Kir5.1 channels by CO2 and pH. J Gen Physiol **2000**;116:33-45
341. Pessia M, Imbrici P, D'Adamo MC, Salvatore L, Tucker SJ. Differential pH sensitivity of Kir4.1 and Kir4.2 potassium channels and their modulation by heteropolymerisation with Kir5.1. J Physiol **2001**;532:359-67
342. Hibino H, Fujita A, Iwai K, Yamada M, Kurachi Y. Differential assembly of inwardly rectifying K+ channel subunits, Kir4.1 and Kir5.1, in brain astrocytes. J Biol Chem **2004**;279:44065-73
343. Sepulveda FV, Pablo Cid L, Teulon J, Niemeyer MI. Molecular aspects of structure, gating, and physiology of pH-sensitive background K2P and Kir K+-transport channels. Physiol Rev **2015**;95:179-217
344. Hughes BA, Swaminathan A. Modulation of the Kir7.1 potassium channel by extracellular and intracellular pH. Am J Physiol Cell Physiol **2008**;294:C423-31
345. Lesage F, Guillemare E, Fink M, Duprat F, Lazdunski M, Romey G*, et al.* TWIK-1, a ubiquitous human weakly inward rectifying K+ channel with a novel structure. EMBO J **1996**;15:1004-11
346. Lesage F, Lazdunski M. Molecular and functional properties of two-pore-domain potassium channels. Am J Physiol Renal Physiol **2000**;279:F793-801
347. Rajan S, Plant LD, Rabin ML, Butler MH, Goldstein SA. Sumoylation silences the plasma membrane leak K+ channel K2P1. Cell **2005**;121:37-47
348. Feliciangeli S, Chatelain FC, Bichet D, Lesage F. The family of K2P channels: salient structural and functional properties. J Physiol **2015**;593:2587-603
349. Turney TS, Li V, Brohawn SG. Structural Basis for pH-gating of the K(+) channel TWIK1 at the selectivity filter. Nat Commun **2022**;13:3232
350. Chatelain FC, Gilbert N, Bichet D, Jauch A, Feliciangeli S, Lesage F*, et al.* Mechanistic basis of the dynamic response of TWIK1 ionic selectivity to pH. Nat Commun **2024**;15:3849

351. Maingret F, Patel AJ, Lesage F, Lazdunski M, Honore E. Mechano- or acid stimulation, two interactive modes of activation of the TREK-1 potassium channel. J Biol Chem **1999**;274:26691-6
352. Honore E, Maingret F, Lazdunski M, Patel AJ. An intracellular proton sensor commands lipid- and mechano-gating of the K(+) channel TREK-1. EMBO J **2002**;21:2968-76
353. Cohen A, Ben-Abu Y, Hen S, Zilberberg N. A novel mechanism for human K2P2.1 channel gating. Facilitation of C-type gating by protonation of extracellular histidine residues. J Biol Chem **2008**;283:19448-55
354. Sandoz G, Douguet D, Chatelain F, Lazdunski M, Lesage F. Extracellular acidification exerts opposite actions on TREK1 and TREK2 potassium channels via a single conserved histidine residue. Proc Natl Acad Sci U S A **2009**;106:14628-33
355. Ryoo K, Park JY. Two-pore Domain Potassium Channels in Astrocytes. Exp Neurobiol **2016**;25:222-32
356. Nasr N, Faucherre A, Borsotto M, Heurteaux C, Mazella J, Jopling C*, et al.* Identification and characterization of two zebrafish Twik related potassium channels, Kcnk2a and Kcnk2b. Sci Rep **2018**;8:15311
357. Luo Y, Huang L, Liao P, Jiang R. Contribution of Neuronal and Glial Two-Pore-Domain Potassium Channels in Health and Neurological Disorders. Neural Plast **2021**;2021:8643129
358. Duprat F, Lesage F, Fink M, Reyes R, Heurteaux C, Lazdunski M. TASK, a human background K+ channel to sense external pH variations near physiological pH. EMBO J **1997**;16:5464-71
359. Millar JA, Barratt L, Southan AP, Page KM, Fyffe RE, Robertson B*, et al.* A functional role for the two-pore domain potassium channel TASK-1 in cerebellar granule neurons. Proc Natl Acad Sci U S A **2000**;97:3614-8
360. Torborg CL, Berg AP, Jeffries BW, Bayliss DA, McBain CJ. TASK-like conductances are present within hippocampal CA1 stratum oriens interneuron subpopulations. J Neurosci **2006**;26:7362-7
361. Shvetsova AA, Lazarenko VS, Gaynullina DK, Tarasova OS, Schubert R. TWIK-Related Acid-Sensitive Potassium Channels (TASK-1) Emerge as Contributors to Tone Regulation in Renal Arteries at Alkaline pH. Front Physiol **2022**;13:895863
362. Reyes R, Duprat F, Lesage F, Fink M, Salinas M, Farman N*, et al.* Cloning and expression of a novel pH-sensitive two pore domain K+ channel from human kidney. J Biol Chem **1998**;273:30863-9
363. Morton MJ, Abohamed A, Sivaprasadarao A, Hunter M. pH sensing in the two-pore domain K+ channel, TASK2. Proc Natl Acad Sci U S A **2005**;102:16102-6
364. Gonczi M, Szentandrassy N, Johnson IT, Heagerty AM, Weston AH. Investigation of the role of TASK-2 channels in rat pulmonary arteries; pharmacological and functional studies following RNA interference procedures. Br J Pharmacol **2006**;147:496-505
365. Niemeyer MI, Cid LP, Pena-Munzenmayer G, Sepulveda FV. Separate gating mechanisms mediate the regulation of K2P potassium channel TASK-2 by intra- and extracellular pH. J Biol Chem **2010**;285:16467-75
366. Zuniga L, Marquez V, Gonzalez-Nilo FD, Chipot C, Cid LP, Sepulveda FV*, et al.* Gating of a pH-sensitive K(2P) potassium channel by an electrostatic effect of basic sensor residues on the selectivity filter. PLoS One **2011**;6:e16141
367. Cid LP, Roa-Rojas HA, Niemeyer MI, Gonzalez W, Araki M, Araki K*, et al.* TASK-2: a K2P K(+) channel with complex regulation and diverse physiological functions. Front Physiol **2013**;4:198
368. Bustos D, Bedoya M, Ramirez D, Concha G, Zuniga L, Decher N*, et al.* Elucidating the Structural Basis of the Intracellular pH Sensing Mechanism of TASK-2 K(2)P Channels. Int J Mol Sci **2020**;21
369. Khoubza L, Gilbert N, Kim EJ, Chatelain FC, Feliciangeli S, Abelanet S*, et al.* Alkaline-sensitive two-pore domain potassium channels form functional heteromers in pancreatic beta-cells. J Biol Chem **2022**;298:102447

370. Chavez RA, Gray AT, Zhao BB, Kindler CH, Mazurek MJ, Mehta Y*, et al.* TWIK-2, a new weak inward rectifying member of the tandem pore domain potassium channel family. J Biol Chem **1999**;274:7887-92
371. Patel AJ, Maingret F, Magnone V, Fosset M, Lazdunski M, Honore E. TWIK-2, an inactivating 2P domain K+ channel. J Biol Chem **2000**;275:28722-30
372. Rinne S, Schick F, Vowinkel K, Schutte S, Krasel C, Kauferstein S*, et al.* Potassium channel TASK-5 forms functional heterodimers with TASK-1 and TASK-3 to break its silence. Nat Commun **2024**;15:7548
373. Cook DL, Ikeuchi M, Fujimoto WY. Lowering of pHi inhibits Ca2+-activated K+ channels in pancreatic B-cells. Nature **1984**;311:269-71
374. Christensen O, Zeuthen T. Maxi K+ channels in leaky epithelia are regulated by intracellular Ca2+, pH and membrane potential. Pflugers Arch **1987**;408:249-59
375. Kume H, Takagi K, Satake T, Tokuno H, Tomita T. Effects of intracellular pH on calcium-activated potassium channels in rabbit tracheal smooth muscle. J Physiol **1990**;424:445-57
376. Peers C, Green FK. Inhibition of Ca(2+)-activated K+ currents by intracellular acidosis in isolated type I cells of the neonatal rat carotid body. J Physiol **1991**;437:589-602
377. Schubert R, Krien U, Gagov H. Protons inhibit the BK(Ca) channel of rat small artery smooth muscle cells. J Vasc Res **2001**;38:30-8
378. Avdonin V, Tang XD, Hoshi T. Stimulatory action of internal protons on Slo1 BK channels. Biophys J **2003**;84:2969-80
379. Brelidze TI, Magleby KL. Protons block BK channels by competitive inhibition with K+ and contribute to the limits of unitary currents at high voltages. J Gen Physiol **2004**;123:305-19
380. Raingo J, Rebolledo A, Grassi de Gende AO, Sanz N, Tommasi J, Milesi V. pH effects on high conductance Ca2+-activated K+ channels (BK(Ca)) in human internal mammary artery smooth muscle cells. Life Sci **2005**;77:1993-2003
381. Petroff E, Snitsarev V, Gong H, Abboud FM. Acid sensing ion channels regulate neuronal excitability by inhibiting BK potassium channels. Biochem Biophys Res Commun **2012**;426:511-5
382. Petroff EY, Price MP, Snitsarev V, Gong H, Korovkina V, Abboud FM*, et al.* Acid-sensing ion channels interact with and inhibit BK K+ channels. Proc Natl Acad Sci U S A **2008**;105:3140-4
383. Hou S, Horrigan FT, Xu R, Heinemann SH, Hoshi T. Comparative effects of H+ and Ca2+ on large-conductance Ca2+- and voltage-gated Slo1 K+ channels. Channels (Austin) **2009**;3:249-58
384. Yang H, Cui J. BK channels. In: Zheng J, Trudeau MC, editors. Handbook of Ion Channels. Boca Raton, FL: CRC Press; 2015. p 227-39.
385. Guarina L, Vandael DH, Carabelli V, Carbone E. Low pH(o) boosts burst firing and catecholamine release by blocking TASK-1 and BK channels while preserving Cav1 channels in mouse chromaffin cells. J Physiol **2017**;595:2587-609
386. Zhou Y, Xia XM, Lingle CJ. BK channel inhibition by strong extracellular acidification. Elife **2018**;7
387. Dopico AM, Bukiya AN, Jaggar JH. Calcium- and voltage-gated BK channels in vascular smooth muscle. Pflugers Arch **2018**;470:1271-89
388. Sancho M, Kyle BD. The Large-Conductance, Calcium-Activated Potassium Channel: A Big Key Regulator of Cell Physiology. Front Physiol **2021**;12:750615
389. Yang CT, Zeng XH, Xia XM, Lingle CJ. Interactions between beta subunits of the KCNMB family and Slo3: beta4 selectively modulates Slo3 expression and function. PLoS One **2009**;4:e6135
390. Wen D, Cornelius RJ, Yuan Y, Sansom SC. Regulation of BK-alpha expression in the distal nephron by aldosterone and urine pH. Am J Physiol Renal Physiol **2013**;305:F463-76
391. Wen D, Cornelius RJ, Rivero-Hernandez D, Yuan Y, Li H, Weinstein AM*, et al.* Relation between BK-alpha/beta4-mediated potassium secretion and ENaC-mediated sodium reabsorption. Kidney Int **2014**;86:139-45

392. Wang B, Wang-France J, Li H, Sansom SC. Furosemide reduces BK-alphabeta4-mediated K(+) secretion in mice on an alkaline high-K(+) diet. Am J Physiol Renal Physiol **2019**;316:F341-F50
393. Al-Qusairi L, Ferdaus MZ, Pham TD, Li D, Grimm PR, Zapf AM*, et al.* Dietary anions control potassium excretion: it is more than a poorly absorbable anion effect. Am J Physiol Renal Physiol **2023**;325:F377-F93
394. Goodchild SJ, Lamy C, Seutin V, Marrion NV. Inhibition of K(Ca)2.2 and K(Ca)2.3 channel currents by protonation of outer pore histidine residues. J Gen Physiol **2009**;134:295-308
395. Srivastava S, Li Z, Ko K, Choudhury P, Albaqumi M, Johnson AK*, et al.* Histidine phosphorylation of the potassium channel KCa3.1 by nucleoside diphosphate kinase B is required for activation of KCa3.1 and CD4 T cells. Mol Cell **2006**;24:665-75
396. Kee JM, Muir TW. Chasing phosphohistidine, an elusive sibling in the phosphoamino acid family. ACS Chem Biol **2012**;7:44-51
397. Kalagiri R, Hunter T. The many ways that nature has exploited the unusual structural and chemical properties of phosphohistidine for use in proteins. Biochem J **2021**;478:3575-96
398. Ning J, Sala M, Reina J, Kalagiri R, Hunter T, McCullough BS. Histidine Phosphorylation: Protein Kinases and Phosphatases. Int J Mol Sci **2024**;25
399. Yamane T, Furukawa T, Horikawa S, Hiraoka M. External pH regulates the slowly activating potassium current IsK expressed in Xenopus oocytes. FEBS Lett **1993**;319:229-32
400. Freeman LC, Lippold JJ, Mitchell KE. Glycosylation influences gating and pH sensitivity of I(sK). J Membr Biol **2000**;177:65-79
401. Unsold B, Kerst G, Brousos H, Hubner M, Schreiber R, Nitschke R*, et al.* KCNE1 reverses the response of the human K+ channel KCNQ1 to cytosolic pH changes and alters its pharmacology and sensitivity to temperature. Pflugers Arch **2000**;441:368-78
402. Peretz A, Schottelndreier H, Aharon-Shamgar LB, Attali B. Modulation of homomeric and heteromeric KCNQ1 channels by external acidification. J Physiol **2002**;545:751-66
403. Roepke TK, King EC, Purtell K, Kanda VA, Lerner DJ, Abbott GW. Genetic dissection reveals unexpected influence of beta subunits on KCNQ1 K+ channel polarized trafficking in vivo. FASEB J **2011**;25:727-36
404. Dixit G, Dabney-Smith C, Lorigan GA. The membrane protein KCNQ1 potassium ion channel: Functional diversity and current structural insights. Biochim Biophys Acta Biomembr **2020**;1862:183148
405. Abbott GW. KCNQs: Ligand- and Voltage-Gated Potassium Channels. Front Physiol **2020**;11:583
406. Prole DL, Lima PA, Marrion NV. Mechanisms underlying modulation of neuronal KCNQ2/KCNQ3 potassium channels by extracellular protons. J Gen Physiol **2003**;122:775-93
407. Mehrdel B, Villalba-Galea CA. Effect of a sensing charge mutation on the deactivation of KV7.2 channels. J Gen Physiol **2024**;156
408. Jensen HS, Callo K, Jespersen T, Jensen BS, Olesen SP. The KCNQ5 potassium channel from mouse: a broadly expressed M-current like potassium channel modulated by zinc, pH, and volume changes. Brain Res Mol Brain Res **2005**;139:52-62
409. Ruffin VA, Gu XQ, Zhou D, Douglas RM, Sun X, Trouth CO*, et al.* The sodium-activated potassium channel Slack is modulated by hypercapnia and acidosis. Neuroscience **2008**;151:410-8
410. Ruffin VA, Salameh AI, Boron WF, Parker MD. Intracellular pH regulation by acid-base transporters in mammalian neurons. Front Physiol **2014**;5:43
411. Kaczmarek LK. Slack, Slick and Sodium-Activated Potassium Channels. ISRN Neurosci **2013**;2013
412. Kaczmarek LK, Aldrich RW, Chandy KG, Grissmer S, Wei AD, Wulff H. International Union of Basic and Clinical Pharmacology. C. Nomenclature and Properties of Calcium-Activated and Sodium-Activated Potassium Channels. Pharmacol Rev **2017**;69:1-11

413. Schreiber M, Wei A, Yuan A, Gaut J, Saito M, Salkoff L. Slo3, a novel pH-sensitive K+ channel from mammalian spermatocytes. J Biol Chem **1998**;273:3509-16
414. Zhang X, Zeng X, Lingle CJ. Slo3 K+ channels: voltage and pH dependence of macroscopic currents. J Gen Physiol **2006**;128:317-36
415. Zhang X, Zeng X, Xia XM, Lingle CJ. pH-regulated Slo3 K+ channels: properties of unitary currents. J Gen Physiol **2006**;128:301-15
416. Navarro B, Kirichok Y, Clapham DE. KSper, a pH-sensitive K+ current that controls sperm membrane potential. Proc Natl Acad Sci U S A **2007**;104:7688-92
417. Leonetti MD, Yuan P, Hsiung Y, Mackinnon R. Functional and structural analysis of the human SLO3 pH- and voltage-gated K+ channel. Proc Natl Acad Sci U S A **2012**;109:19274-9
418. Brenker C, Zhou Y, Muller A, Echeverry FA, Trotschel C, Poetsch A*, et al.* The Ca2+-activated K+ current of human sperm is mediated by Slo3. Elife **2014**;3:e01438
419. Ludwig MG, Vanek M, Guerini D, Gasser JA, Jones CE, Junker U*, et al.* Proton-sensing G-protein-coupled receptors. Nature **2003**;425:93-8
420. Weiss KT, Fante M, Kohl G, Schreml J, Haubner F, Kreutz M*, et al.* Proton-sensing G protein-coupled receptors as regulators of cell proliferation and migration during tumor growth and wound healing. Exp Dermatol **2017**;26:127-32
421. Hosford PS, Mosienko V, Kishi K, Jurisic G, Seuwen K, Kinzel B*, et al.* CNS distribution, signalling properties and central effects of G-protein coupled receptor 4. Neuropharmacology **2018**;138:381-92
422. Mashiko M, Kurosawa A, Tani Y, Tsuji T, Takeda S. GPR31 and GPR151 are activated under acidic conditions. J Biochem **2019**;166:317-22
423. Klatt W, Wallner S, Brochhausen C, Stolwijk JA, Schreml S. Expression profiles of proton-sensing G-protein coupled receptors in common skin tumors. Sci Rep **2020**;10:15327
424. Sisignano M, Fischer MJM, Geisslinger G. Proton-Sensing GPCRs in Health and Disease. Cells **2021**;10
425. Forch A, Wallner S, Zeman F, Ettl T, Brochhausen C, Schreml S. Expression of Proton-Sensitive GPR31, GPR151, TASK1 and TASK3 in Common Skin Tumors. Cells **2021**;11
426. Imenez Silva PH, Camara NO, Wagner CA. Role of proton-activated G protein-coupled receptors in pathophysiology. Am J Physiol Cell Physiol **2022**;323:C400-C14
427. Imenez Silva PH, Wagner CA. Physiological relevance of proton-activated GPCRs. Pflugers Arch **2022**;474:487-504
428. Kumar NN, Velic A, Soliz J, Shi Y, Li K, Wang S*, et al.* PHYSIOLOGY. Regulation of breathing by CO(2) requires the proton-activated receptor GPR4 in retrotrapezoid nucleus neurons. Science **2015**;348:1255-60
429. Guyenet PG, Bayliss DA. Neural Control of Breathing and CO2 Homeostasis. Neuron **2015**;87:946-61
430. Ramadoss S, Qin J, Tao B, Thomas NE, Cao E, Wu R*, et al.* Bone-marrow macrophage-derived GPNMB protein binds to orphan receptor GPR39 and plays a critical role in cardiac repair. Nat Cardiovasc Res **2024**;3:1356-73
431. Wang J, Simonavicius N, Wu X, Swaminath G, Reagan J, Tian H*, et al.* Kynurenic acid as a ligand for orphan G protein-coupled receptor GPR35. J Biol Chem **2006**;281:22021-8
432. Wang J, Wu X, Simonavicius N, Tian H, Ling L. Medium-chain fatty acids as ligands for orphan G protein-coupled receptor GPR84. J Biol Chem **2006**;281:34457-64

Disclaimer: The statements and opinions are those of the author. The author disclaims responsibility for any injury to people or property resulting from any ideas, methods, instructions, products, or publications cited in the content.

AllE1E70DEG3239Total
7/4/2025

1	E21	A2M
2	E65	AAK1
3	E54	AATK
4	E1	AB113AP
5	E50	ABCA1
6	E54	ABCA12
7	E48	ABCB10
8	E69	Abcb1a
9	E70	Abcc3
10	E31	ABCD1
11	E9	ABHD11
12	E58	AC004019.18
13	E14	AC012501.3
14	E58	AC079602.1
15	E25	AC092162.1
16	E33	ACAA2
17	E21	ACACA
18	E24	ACAN
19	E69	Ace
20	E20	ACSM1
21	E2	ACSM3
22	E29	ACTA2
23	E1	ACTA2
24	E43	ACTA2
25	E66	ACTA2
26	E45	Actb
27	E4	ACTC1
28	E1	ACTG2
29	E21	ACTG2
30	E43	ACTG2
31	E4	ACTN2
32	E16	ACTR3
33	E35	ACTR3
34	E59	Actr3b
35	E1	ACVR2A
36	E70	Acvrl1
37	E38	ADAM12
38	E39	ADAM12
39	E21	ADAM19
40	E38	ADAM19
41	E43	ADAM19
42	E28	ADAM28
43	E49	Adam8

44	E45	Adam9
45	E49	Adamdec1
46	E14	ADAMTS15
47	E1	ADAMTS2
48	E21	ADAMTS4
49	E26	Adarb1
50	E26	Adcy1
51	E4	ADCY2
52	E26	Adcy5
53	E4	ADCY6
54	E4	ADCY8
55	E62	ADCY9
56	E34	ADCYAP1
57	E5	ADCYAP1R1
58	E27	ADD2
59	E21	ADGRG1
60	E34	ADIPOR2
61	E15	ADORA2A
62	E38	ADRA1D
63	E2	ADRA2A
64	E52	ADRA2A
65	E40	AEBP1
66	E30	AFAP1-AS1
67	E2	Afap1l1
68	E25	AFAP1L1
69	E23	AFAP1L2
70	E14	AFMID
71	E21	AGAP2
72	E57	AGBL2
73	E20	AGFG2
74	E50	AGO2
75	E14	AGO3
76	E58	AGPAT9
77	E2	AGR3
78	E42	AGR3
79	E31	AGRN
80	E34	AGT
81	E51	AGT
82	E34	AGTR1
83	E70	Agtr1
84	E26	Ahl1
85	E21	AHRR
86	E37	AICDA

87	E54	AICDA
88	E21	AIFM1
89	E23	AIM2
90	E14	AJ239322.1
91	E70	Ak1
92	E70	Ak5
93	E15	AK8
94	E37	AKAP12
95	E38	AKAP12
96	E31	AKAP13
97	E16	AKR1B1
98	E45	Akr1b10
99	E45	Akr1b3
100	E45	Akr1b8
101	E23	AKR1C2
102	E42	AKR1C3
103	E23	AKR1C4
104	E35	AKT3
105	E52	AL354984.1
106	E21	ALDH18A1
107	E54	ALDH1A1
108	E20	ALDH1A2
109	E49	Aldh1a2
110	E54	ALDH1A2
111	E1	ALDH1A3
112	E69	Aldh1a3
113	E57	ALDH1L1
114	E21	ALDH3B1
115	E44	ALG3
116	E2	ALMS1
117	E43	ALOX5AP
118	E64	ALOX5AP
119	E54	ALPPL2
120	E21	AMDHD2
121	E55	Amhr2
122	E11	AMIG02
123	E13	AMN
124	E58	AMOT
125	E20	AMOTL2
126	E70	Amotl2
127	E2	ANGPT2
128	E1	ANGPTL2
129	E29	ANGPTL4

130	E33	ANGPTL4
131	E43	ANGPTL4
132	E69	Angptl4
133	E65	ANGPTL7
134	E20	ANKRD1
135	E31	ANKRD46
136	E20	ANKRD7
137	E63	ANLN
138	E70	Anln
139	E66	ANP32B
140	E41	ANTXR2
141	E56	ANTXR2
142	E41	ANXA1
143	E70	Anxa1
144	E49	Anxa10
145	E69	Anxa10
146	E42	ANXA13
147	E60	ANXA13
148	E37	ANXA2
149	E45	Anxa2
150	E70	Anxa3
151	E29	ANXA4
152	E16	ANXA6
153	E21	ANXA6
154	E40	ANXA8L2
155	E22	ANXA9
156	E58	AOC1
157	E58	AP001626.1
158	E44	AP2M1
159	E48	APBA2
160	E66	APC2
161	E32	APCDD1
162	E56	APCDD1
163	E34	APLN
164	E37	APOBEC3G
165	E26	Apod
166	E1	APOE
167	E14	APOE
168	E21	APOE
169	E59	Apoe
170	E14	APOL3
171	E2	APP
172	E2	AQP1

173	E51	AQP1
174	E59	Aqp1
175	E25	AQP3
176	E8	AQP3
177	E22	AQP3
178	E58	AQP3
179	E51	AQP4
180	E54	AR
181	E65	AR
182	E70	Arap3
183	E21	ARC
184	E51	ARC
185	E52	AREG
186	E35	ARF4
187	E43	ARF4
188	E21	ARFGEF3
189	E1	ARHGAP20
190	E35	ARHGAP20
191	E1	ARHGAP24
192	E40	ARHGAP25
193	E58	ARHGAP26
194	E43	ARHGDIB
195	E3	ARHGEF16
196	E27	ARHGEF26-AS1
197	E67	Arid5b
198	E41	ARL4C
199	E14	ARL4C
200	E4	ARL6IP5
201	E1	ARMH4
202	E23	ARNTL2
203	E38	ARNTL2
204	E7	ARRB1
205	E62	ARRDC3
206	E31	ARSG
207	E58	ARSI
208	E65	ARX
209	E31	ASAH1
210	E20	ASAP1
211	E12	ASCL1
212	E17	ASCL1
213	E35	ASCL1
214	E65	ASCL1
215	E2	ASCL2

216	E46	ASCL2
217	E15	ASIC4
218	E54	ASNS
219	E2	ASPM
220	E17	ATCAY
221	E60	ATF3
222	E35	ATG14
223	E60	ATM
224	E66	ATN1
225	E26	Atp1a2
226	E4	ATP1A2
227	E5	ATP1A2
228	E51	ATP1A2
229	E29	ATP1B1
230	E19	ATP1B1
231	E51	ATP1B2
232	E15	ATP2B1
233	E58	ATP2C2
234	E66	ATP5D
235	E70	Atp6v0e1
236	E48	ATP6V1C1
237	E42	ATP7B
238	E25	AURKA
239	E67	Auts2
240	E58	AVPI1
241	E34	AVPR2
242	E68	AXIN2
243	E41	AXL
244	E14	B2M
245	E67	B2m
246	E21	B4GALT5
247	E33	B4GALT5
248	E54	B4GALT6
249	E41	BAALC
250	E42	BACE2
251	E56	BACE2
252	E22	BAG1
253	E13	BAIAP2L1
254	E42	BAIAP2L2
255	E63	BAIAP2L2
256	E55	Bambi
257	E62	BANF1
258	E37	BANK1

259	E56	BANK1
260	E46	BARX2
261	E23	BATF3
262	E70	Bbc3
263	E60	BBC3(PUMA)
264	E70	Bbp4
265	E59	BC064078
266	E26	Bc1
267	E60	BCAM
268	E14	BCAN
269	E35	BCAR3
270	E60	BCAS3
271	E63	BCAT1
272	E21	BCAT2
273	E20	BCL11A
274	E12	BCL2
275	E22	BCL2
276	E35	BCL2
277	E70	Bcl2
278	E70	Bcl2l1
279	E1	BCL3
280	E2	BCL7A
281	E14	BCL7A
282	E37	BCL7A
283	E46	BCOR
284	E66	BCORL1
285	E70	Bdnf
286	E65	BEND2
287	E14	BEND3
288	E14	BEND6
289	E26	Bgn
290	E21	BHLHE40
291	E20	BICC1
292	E58	BICC1
293	E1	BIK
294	E49	Birc3
295	E60	BIRC3
296	E20	BIRC5
297	E63	BIRC5
298	E14	BIRC7
299	E39	BIRC7
300	E3	BLNK
301	E15	BLVRA

302	E38	BMP2
303	E41	BMP2
304	E49	Bmp2
305	E60	BMP4
306	E5	BMP7
307	E56	BMX
308	E40	BNC1
309	E29	BNIP3
310	E16	BNIP3
311	E66	BOLA2B
312	E15	BRAF
313	E2	BRCA2
314	E66	BRD4
315	E34	BRN3A
316	E15	BRSK2
317	E33	BSG
318	E11	BSLC18A2
319	E41	BST1
320	E67	Bst2
321	E11	BTBD11
322	E69	Btc
323	E54	BTG2
324	E60	BTG2
325	E66	BTG2
326	E53	BTK
327	E15	BTN2A2
328	E42	BTNL8
329	E54	C10orf10
330	E58	C10orf99
331	E65	C11orf87
332	E14	C11orf96
333	E23	C12orf39
334	E23	C12orf56
335	E41	C12orf75
336	E29	C15orf48
337	E23	C15orf48
338	E41	C16orf45
339	E40	C16orf74
340	E43	C17orf91
341	E14	C1orf115
342	E66	C1orf173
343	E21	C1orf95
344	E34	C1QBP

345	E58	C1QC
346	E56	C1QTNF1
347	E23	C20orf70
348	E58	C2CD4B
349	E34	C3AR1
350	E54	C4orf34
351	E45	C5orf51
352	E11	C6orf192
353	E58	C9orf152
354	E29	CA12
355	E19	CA12
356	E21	CA14
357	E42	CA2
358	E29	CA9
359	E69	Cab39l
360	E58	CACNA1A
361	E4	CACNA1B
362	E34	CACNA1C
363	E4	CACNA1E
364	E11	CACNA2D3
365	E58	CACNB1
366	E3	CACNB3
367	E28	CADM1
368	E29	CADM1
369	E41	CADM1
370	E41	CADM4
371	E58	CADPS
372	E23	CALB1
373	E57	CALB1
374	E26	Calb2
375	E52	CALCA
376	E60	CALD1
377	E21	CALM1
378	E50	CALM1
379	E31	CALM3
380	E30	CALML3-AS1
381	E26	Calml4
382	E42	CALML4
383	E62	CALU
384	E51	CAMK2B
385	E58	CAMK4
386	E26	Campk2a
387	E16	CAP1

388	E21	CAPN5
389	E59	Car2
390	E60	CARD10
391	E26	Cartpt
392	E34	CASK
393	E59	Casp1
394	E37	CASP3
395	E44	CASP4
396	E20	CAT
397	E23	CATSPER1
398	E66	CATSPERD
399	E28	CAV1
400	E41	CAV1
401	E60	CAV1
402	E20	CAVIN2
403	E50	CBL
404	E45	Cbr1
405	E45	Cbr3
406	E69	Cbr4
407	E60	CBS
408	E31	CBX5
409	E2	CC2D2A
410	E20	CCDC114
411	E26	Ccdc136
412	E26	Ccdc153
413	E2	CCDC18
414	E54	CCDC33
415	E54	CCDC46
416	E66	CCDC85B
417	E60	CCDN1
418	E26	Cck
419	E11	CCL1
420	E49	Ccl20
421	E68	CCN3
422	E22	CCND1
423	E35	CCND1
424	E45	Ccnd1
425	E70	Ccnd1
426	E37	CCND2
427	E45	Ccnd2
428	E65	CCND2
429	E53	CCND3
430	E35	CCNE1

431	E60	CCNE2
432	E21	CCNG1
433	E33	CCNL1
434	E66	CCNL2
435	E28	CCR10
436	E18	CCT2
437	E41	CD163L1
438	E14	CD163L1
439	E28	CD19
440	E28	CD22
441	E53	CD22
442	E28	CD24
443	E58	CD247
444	E23	CD274
445	E53	CD36
446	E28	CD38
447	E54	CD4
448	E28	CD40
449	E13	CD44
450	E45	Cd44
451	E34	CD55
452	E29	CD68
453	E23	CD70
454	E28	CD79A
455	E28	CD79B
456	E37	CD86
457	E23	CD8A
458	E41	CD96
459	E11	CD99
460	E23	CDA
461	E14	CDC16
462	E20	CDC20
463	E63	CDC20
464	E21	CDC25B
465	E2	CDC42EP1
466	E60	CDC42EP3
467	E2	CDCA7
468	E14	CDCA7
469	E2	Cdca7l
470	E50	CDCP1
471	E16	CDH1
472	E39	CDH13
473	E40	CDH13

474	E41	CDH13
475	E14	CDH13
476	E42	CDH17
477	E16	CDH2
478	E43	CDH2
479	E70	Cdh2
480	E15	CDH7
481	E39	CDK14
482	E70	Cdk14
483	E20	CDK18
484	E70	Cdk18
485	E14	CDK2
486	E18	CDK4
487	E39	CDK5R1
488	E63	CDK6
489	E65	CDK6
490	E10	CDKN1A
491	E43	CDKN1A
492	E66	CDKN1A
493	E67	Cdkn1a
494	E60	CDKN1A(p21)
495	E65	CDKN1B
496	E18	CDKN2A
497	E46	CDKN2A/B
498	E63	CDKN2C
499	E2	CDO1
500	E46	CDX2
501	E64	CEACAM5
502	E11	CEBPD
503	E33	CEBPD
504	E14	CECR5
505	E31	CELF1
506	E56	CELF6
507	E45	Cend1
508	E2	CENPF
509	E63	CENPF
510	E36	CENPH
511	E31	CEP126
512	E2	CEP192
513	E58	CEP44
514	E14	CEP68
515	E43	CES1
516	E54	CES1

517	E59	Ces2g
518	E35	CFLAR
519	E11	CFR
520	E52	CGA
521	E43	CGB1
522	E43	CGB5
523	E52	CHAC1
524	E58	CHDC2
525	E60	CHECK1
526	E17	CHGA
527	E17	CHGB
528	E54	CHGB
529	E56	CHODL
530	E52	CHRNA2
531	E17	CHRNA3
532	E58	CHRNA5
533	E14	CHRNA9
534	E27	CHST11
535	E56	CHST15
536	E70	Cib1
537	E69	Cidea
538	E54	CIITA
539	E59	Cish
540	E2	CIT
541	E26	Cit
542	E25	CITED1
543	E70	Cited2
544	E2	CKAP2
545	E16	CKAP4
546	E33	CKB
547	E51	CKB
548	E42	CKMT1A
549	E44	CKMT2
550	E61	CLASPIN
551	E41	CLCF1
552	E56	CLCF1
553	E21	CLCN7
554	E26	Cldn11
555	E7	CLDN3
556	E13	CLDN4
557	E59	Clec12a
558	E11	CLEC4D
559	E58	CLEC4E

560	E59	Clec7a
561	E37	CLECSF2
562	E26	Clic6
563	E66	CLIP3
564	E14	CLN6
565	E4	CLN8
566	E31	CLOCK
567	E62	CLSTN1
568	E45	Clu
569	E29	CMBL
570	E67	Cmklr1
571	E11	CMTM8
572	E56	CMTM8
573	E51	CNGA3
574	E1	CNN1
575	E21	CNN2
576	E70	Cnn2
577	E2	CNN3
578	E16	CNN3
579	E18	CNOT2
580	E26	Cnp
581	E35	CNTF
582	E5	CNTN1
583	E40	CNTNAP3B
584	E70	Cobl
585	E37	COBLL1
586	E26	Col11a1
587	E26	Col11a2
588	E39	COL13A1
589	E41	COL13A1
590	E70	Col14a1
591	E1	COL16A1
592	E40	COL17A1
593	E33	COL18A1
594	E70	Col18a1
595	E26	Col19a2
596	E43	COL22A1
597	E1	COL23A1
598	E58	COL26A1
599	E24	COL2A1
600	E26	Col2a1
601	E43	COL4A1
602	E57	COL4A1

603	E70	Col4a1
604	E70	Col4a2
605	E63	COL4A3
606	E21	COL4A3BP
607	E58	COL4A4
608	E40	COL4A6
609	E43	COL5A1
610	E3	COL5A2
611	E33	COL6A1
612	E60	COL6A1
613	E33	COL6A2
614	E14	COL8A1
615	E26	Col9a1
616	E1	COL9A2
617	E58	COLCA1
618	E31	COP1
619	E70	Coro1c
620	E11	COTL1
621	E61	COX4L1
622	E61	COX7B
623	E61	COX7C
624	E59	Cp
625	E29	CP
626	E20	CPA2
627	E11	CPA3
628	E31	CPD
629	E33	CPE
630	E26	Cplx2
631	E18	CPM
632	E2	CPN1
633	E20	CPS1
634	E23	CPS1
635	E11	CR1
636	E45	Creg1
637	E34	CRHR1
638	E20	CRIM1
639	E41	CRIP2
640	E54	CRISPLD2
641	E37	CRY1
642	E23	CSAG2
643	E1	CSDC2
644	E33	CSDE1
645	E67	Csf1

646	E38	CSF2
647	E49	Csf2
648	E69	Csf2
649	E23	CSF2
650	E11	CSF2RB
651	E38	CSF3
652	E70	Csk
653	E40	CSMD2
654	E15	CSNK1A1L
655	E15	CSNK2A
656	E24	CSPG4
657	E51	CSPG5
658	E26	Csrp1
659	E43	CSRP1
660	E41	CSRP2
661	E33	CST3
662	E38	CTBP1
663	E58	CTD-2114J12.1
664	E65	CTD-2192J16.22
665	E25	CTD-2303H24.2
666	E66	CTDNEP1
667	E18	CTDSP2
668	E20	CTGF
669	E43	CTGF
670	E70	Ctgf
671	E17	CTNNA2
672	E70	Ctnna2
673	E13	CTNNB1
674	E50	CTNNB1
675	E37	CTPS
676	E21	CTSA
677	E37	CTSB
678	E42	CTSE
679	E11	CTSH
680	E49	Ctss
681	E43	CTXN1
682	E65	CUX2
683	E21	CX3CL1
684	E17	CXADR
685	E58	CXADR
686	E66	CXADR
687	E8	CXCL1
688	E38	CXCL1

689	E49	Cxcl10
690	E67	Cxcl10
691	E70	Cxcl10
692	E8	CXCL2
693	E20	CXCL8
694	E38	CXCR1
695	E32	CYB5A
696	E68	CYB5A
697	E41	CYB5R2
698	E13	CYBA
699	E70	Cyba
700	E47	CYBB
701	E38	CYGB
702	E11	CYorf15A
703	E32	CYP11B1
704	E32	CYP11B2
705	E32	CYP17A1
706	E29	CYP1B1
707	E57	CYP1B1
708	E18	CYP27B1
709	E38	CYP27B1
710	E42	CYP2C18
711	E58	CYP2C18
712	E58	CYP2C19
713	E45	Cyp2c70
714	E2	CYP2E1
715	E42	CYP2S1
716	E47	CYP2U1
717	E58	CYP4B1
718	E63	CYP4B1
719	E66	CYP4F2
720	E66	CYP4F3
721	E25	CYPP19A1
722	E20	CYR61
723	E41	CYR61
724	E67	Cyr61
725	E58	CYS1
726	E65	DACH2
727	E70	Dact3
728	E14	DAP
729	E14	DAPK1
730	E58	DAPK1
731	E65	DAPK1

732	E2	DAPK2
733	E70	Dapk3
734	E17	DBH
735	E70	Dbn1
736	E31	DBP
737	E58	DCAF12L1
738	E23	DCBLD2
739	E25	DCC
740	E28	DCC
741	E58	DCDC2
742	E2	DCTD
743	E63	DDB2
744	E66	DDB2
745	E17	DDC
746	E42	DDC
747	E54	DDIT3
748	E33	DDIT4
749	E52	DDIT4
750	E54	DDIT4
751	E26	Ddn
752	E65	DDR2
753	E67	Ddx60
754	E33	DEAF1
755	E48	DEDD
756	E29	DEFB1
757	E31	DENND6A
758	E16	DFNA5
759	E30	DGCR5
760	E38	DHRS2
761	E11	DHRS3
762	E59	Diap2
763	E14	DIAPH2-AS1
764	E47	DIRAS1
765	E31	DIXDC1
766	E41	DKK1
767	E52	DKK1
768	E60	DKK1
769	E1	DKK3
770	E40	DKK3
771	E43	DKK3
772	E40	DLC1
773	E14	DLG3
774	E17	DLK1

775	E40	DLK2
776	E12	DLL1
777	E14	DLL3
778	E56	DLX5
779	E63	DLX5
780	E58	DLX6
781	E58	DLX6-AS1
782	E37	DMD
783	E2	DMPK
784	E65	DMRT2
785	E65	DMRT3
786	E65	DMRTA1
787	E65	DMRTA2
788	E59	Dnahc8
789	E58	DNAJC22
790	E17	DNAJC6
791	E66	DNHD1
792	E31	DNLZ
793	E49	Dnmbp
794	E69	Dnmbp
795	E4	DNMT3B
796	E58	DNMT3B
797	E41	DOCK5
798	E55	Dock9
799	E42	DOK4
800	E27	DOK5
801	E42	DPCR1
802	E28	DPEP1
803	E20	DPF3
804	E37	DPP4
805	E51	DPP6
806	E4	DPPA4
807	E62	DPYSL3
808	E43	DPYSL4
809	E60	DRAM1
810	E66	DRAM1
811	E67	Dram1
812	E38	DRAS1
813	E41	DRD2
814	E27	DSCR8
815	E13	DST
816	E2	DTL
817	E21	DTNA

818	E58	DUOX2
819	E38	DUSP10
820	E67	Dusp2
821	E4	DUSP4
822	E8	DUSP4
823	E8	DUSP5
824	E67	Dusp5
825	E59	Dusp6
826	E69	Dusp6
827	E52	DUX4L8
828	E52	DUX4L9
829	E26	Dynlrb2
830	E18	DYRK2
831	E70	Dyrk3
832	E27	DYSF
833	E54	DYSF
834	E56	DYSF
835	E5	ECHDC2
836	E1	ECRG4
837	E26	Ecrg4
838	E20	ECT2
839	E63	ECT2
840	E66	EDA2R
841	E70	Edn1
842	E60	EDN2
843	E28	EDNRB
844	E17	EEF1A2
845	E43	EEF1A2
846	E56	EFCAB4A
847	E20	EFHB
848	E57	EFHB
849	E65	EFHD1
850	E46	EFNA2/3
851	E7	EFNB1
852	E70	Efnb1
853	E27	EGFEM1P
854	E24	EGFLAM
855	E50	EGFR
856	E51	EGFR
857	E29	EGLN3
858	E24	EGR1
859	E21	EGR1
860	E21	EGR2

861	E60	EGR2
862	E21	EGR3
863	E2	EHF
864	E54	EIF4EBP1
865	E58	ELAPOR1
866	E17	ELAVL2
867	E17	ELAVL3
868	E17	ELAVL4
869	E29	ELF3
870	E1	ELF3
871	E46	ELFN2/3
872	E38	ELK3
873	E2	ELL3
874	E57	ELMOD1
875	E59	Elovl7
876	E54	EMID1
877	E55	Emid1
878	E59	Emilin2
879	E41	EML1
880	E69	Emp1
881	E20	EMP2
882	E16	EMP3
883	E67	Emp3
884	E15	EMR1
885	E59	Emr1
886	E46	EN2
887	E59	Enah
888	E26	Enc
889	E26	Enc1
890	E2	ENGASE
891	E54	ENOX1
892	E24	ENPP1
893	E26	Enpp2
894	E1	ENPP2
895	E58	ENPP3
896	E11	ENTPD1
897	E15	ENTPD1
898	E6	EOMES
899	E50	EPB41
900	E1	EPCAM
901	E8	EPHA2
902	E64	EPHA2
903	E70	Epha2

904	E43	EPHB1
905	E27	EPHB2
906	E3	EPHB2
907	E49	Ephb2
908	E2	EPHB3
909	E41	EPHB3
910	E38	EPN3
911	E59	Epx
912	E14	ERAP1
913	E50	ERBB2
914	E60	ERBB4
915	E8	EREG
916	E49	Ereg
917	E54	EREG
918	E69	Ereg
919	E7	ERF
920	E40	ERG
921	E2	ERI2
922	E26	Ermn
923	E58	ERN2
924	E56	ERP27
925	E21	ERRFI1
926	E41	ERRFI1
927	E2	ESAM
928	E2	ESPL1
929	E50	ESR1
930	E58	ESR1
931	E65	ESR1
932	E34	ETV1
933	E49	Etv1
934	E69	Etv1
935	E31	ETV4
936	E69	Etv4
937	E20	ETV5
938	E37	ETV5
939	E49	Etv5
940	E69	Etv5
941	E46	EVX1
942	E27	EXOC6B
943	E16	EXT1
944	E58	EYA2
945	E57	EYA4
946	E70	Eya4

947	E23	F2
948	E44	F2R
949	E39	F2RL1
950	E69	F2rl1
951	E23	F7
952	E14	FABP5
953	E29	FABP6
954	E51	FABP7
955	E2	FADS1
956	E8	FAM107B
957	E50	FAM129B
958	E26	Fam131a
959	E17	FAM163A
960	E2	FAM171A1
961	E14	FAM180B
962	E5	FAM181B
963	E26	Fam183b
964	E70	Fam20a
965	E14	FAM3C2
966	E62	FAM49B
967	E14	FAM69B
968	E14	FAM69C
969	E38	FAM83A
970	E42	FAM83E
971	E41	FAM83G
972	E35	FAM83H
973	E58	FAR2P1
974	E40	FAT3
975	E1	FBLN7
976	E65	FBN3
977	E55	Fbx17
978	E31	FBXL17
979	E56	FBXL21
980	E31	FBXL3
981	E58	FBXO17
982	E38	FBXO32
983	E23	FBXO32
984	E43	FBXO32
985	E56	FBXO43
986	E58	FBXO8
987	E28	FCER2
988	E59	Fcgr2b
989	E10	FCGRT

990	E33	FCGRT
991	E28	FCRL1
992	E28	FCRL2
993	E28	FCRL5
994	E65	FEV
995	E41	FEZ1
996	E67	Ffar2
997	E38	FFRMT1
998	E11	FGD5
999	E68	FGF12
1000	E4	FGF17
1001	E46	FGF18
1002	E46	FGF19
1003	E4	FGF2
1004	E39	FGF2
1005	E60	FGF2
1006	E46	FGF3
1007	E65	FGF5
1008	E4	FGF8
1009	E46	FGF8
1010	E21	FGFBP3
1011	E37	FGFR1
1012	E5	FGFR3
1013	E40	FGFR3
1014	E46	FGFR3
1015	E51	FGFR3
1016	E58	FGFR3
1017	E2	FGFR4
1018	E18	FGFR4
1019	E58	FGFR4
1020	E15	FGFRL1
1021	E68	FGG
1022	E37	FGL2
1023	E67	Fgl2
1024	E2	FHDC1
1025	E40	FHL1
1026	E29	FHL2
1027	E15	FITM10
1028	E40	FJX1
1029	E41	FJX1
1030	E21	FLCN
1031	E54	FLG
1032	E16	FLNA

1033	E41	FLNB
1034	E43	FLNC
1035	E40	FLRT2
1036	E34	FLRT3
1037	E41	FLT1
1038	E54	FLT3
1039	E56	FLT4
1040	E26	Fmod
1041	E1	FMOD
1042	E16	FN1
1043	E33	FN1
1044	E44	FNDC3B
1045	E15	FOCAD
1046	E26	Folr1
1047	E67	Fos
1048	E41	FOSL1
1049	E54	FOSL1
1050	E10	FOSL2
1051	E16	FOSL2
1052	E66	FOSL2
1053	E34	FOXA2
1054	E35	FOXA2
1055	E42	FOXA3
1056	E54	FOXD1
1057	E19	FOXE1S
1058	E41	FOXF1
1059	E4	FOXH1
1060	E40	FOXI1
1061	E26	Foxj1
1062	E54	FOXJ1
1063	E70	Foxj1
1064	E65	FOXL2
1065	E62	FOXM1
1066	E31	FOXO3
1067	E8	FOXQ1
1068	E41	FREM2
1069	E60	FRMD4A
1070	E43	FRMD6
1071	E66	FRMPD2
1072	E14	FRMPD4
1073	E18	FRS2
1074	E20	FSCN1
1075	E63	FSCN1

1076	E39	FST
1077	E43	FST
1078	E27	FTCDNL1
1079	E45	Fth1
1080	E66	FTX
1081	E1	FUT3
1082	E20	FUT5
1083	E37	FUT8
1084	E63	FUT8
1085	E31	FUT9
1086	E5	FXYD1
1087	E51	FXYD1
1088	E29	FXYD2
1089	E43	FXYD5
1090	E65	FXYD7
1091	E58	FYB
1092	E46	FZD10
1093	E70	Fzd2
1094	E42	FZD5
1095	E15	FZD6
1096	E2	FZD7
1097	E21	FZD7
1098	E50	GAB1
1099	E58	GABARAPL1
1100	E31	GABBR1
1101	E65	GABBR1
1102	E67	Gabbr1
1103	E15	GABBR2
1104	E31	GABPA
1105	E49	Gabra3
1106	E55	Gabra5
1107	E51	GABRB1
1108	E4	GABRB3
1109	E34	GABRG1
1110	E4	GABRP
1111	E58	GABRP
1112	E54	GADD45A
1113	E60	GADD45B
1114	E60	GADD45G
1115	E17	GAL
1116	E43	GAL
1117	E42	GAL3ST1
1118	E70	Galk1

1119	E69	Galnt3
1120	E62	GALNT7
1121	E17	GAP43
1122	E14	GAPDHS
1123	E34	GARS
1124	E54	GARS
1125	E51	GAS1
1126	E63	GAS2L3
1127	E41	GAS7
1128	E59	Gas7
1129	E59	Gata1
1130	E59	Gata2
1131	E62	GATA2
1132	E65	GATA2
1133	E17	GATA3
1134	E65	GATA3
1135	E42	GATA6
1136	E54	GATA6
1137	E70	Gbx2
1138	E11	GCA
1139	E20	GCLC
1140	E45	Gclc
1141	E45	Gclm
1142	E42	GCNT3
1143	E45	Gcnt3
1144	E58	GCNT3
1145	E17	GDAP1L1
1146	E59	Gdf10
1147	E8	GDF15
1148	E52	GDF15
1149	E63	GDF15
1150	E66	GDF15
1151	E4	GDF3
1152	E35	GDF3
1153	E25	GDF6
1154	E7	GDPD3
1155	E1	GEM
1156	E38	GEM
1157	E59	Gem
1158	E26	Gfap
1159	E37	GFI1
1160	E49	Gfpt2
1161	E22	GFRA1

1162	E41	GFRA1
1163	E70	Gfra3
1164	E35	GGCX
1165	E20	GGH
1166	E63	GGH
1167	E45	Ggt6
1168	E58	GGT6
1169	E54	GGTLC1
1170	E11	GIMAP1
1171	E40	GIMAP8
1172	E2	GINS1
1173	E70	Gipc1
1174	E38	GJB2
1175	E15	GK5
1176	E2	GKN3
1177	E31	GLCCI1
1178	E21	GLDC
1179	E41	GLI2
1180	E16	GLIPR1
1181	E21	GLIPR1
1182	E43	GLIPR1
1183	E43	GLIPR2
1184	E58	GLRX
1185	E63	GLS
1186	E45	Glt28d2
1187	E26	Glul
1188	E59	Gm14005
1189	E45	Gm34240
1190	E26	Gm42418
1191	E42	GMDS
1192	E48	GMDS
1193	E62	GNA12
1194	E56	GNAO1
1195	E66	GNAO1
1196	E4	GNG13
1197	E17	GNG3
1198	E17	GNG4
1199	E23	GNG4
1200	E26	Gng7
1201	E11	GNPDA1
1202	E61	GNPDA1
1203	E63	GOLGA2B
1204	E56	GOLGA7B

1205	E62	GOPC
1206	E8	GOS2
1207	E32	GOS2
1208	E11	GP1BA
1209	E59	Gp5
1210	E42	GPA33
1211	E1	GPC3
1212	E64	GPD2
1213	E54	GPM6A
1214	E26	Gpnmb
1215	E29	GPNMB
1216	E49	Gpnmb
1217	E58	GPR111
1218	E59	Gpr141
1219	E31	GPR155
1220	E28	GPR160
1221	E41	GPR176
1222	E31	GPR180
1223	E20	GPR35
1224	E42	GPR35
1225	E14	GPR39
1226	E60	GPR39
1227	E56	GPR56
1228	E11	GPR84
1229	E23	GPR84
1230	E15	GPR85
1231	E54	GPR87
1232	E26	Gpr88
1233	E58	GPR97
1234	E21	GPRC5B
1235	E28	GPRC5D
1236	E63	GPT2
1237	E42	GPX2
1238	E19	GPX3
1239	E58	GPX3
1240	E33	GPX4
1241	E58	GR1A2
1242	E54	GRB10
1243	E59	Grb10
1244	E58	GRB14
1245	E50	GRB2
1246	E2	GRB7
1247	E43	GREM1

1248	E17	GRIA2
1249	E66	GRIA2
1250	E4	GRIA4
1251	E34	GRID1
1252	E34	GRID2
1253	E39	GRIM2
1254	E4	GRIN2B
1255	E12	GRIP1
1256	E10	GRK5
1257	E54	GRRP1
1258	E14	GS1-257G1.1
1259	E55	Gsn
1260	E37	GSS
1261	E45	Gsta3
1262	E45	Gstm1
1263	E45	Gstm3
1264	E31	GTF2I
1265	E14	GYG2
1266	E58	GZMA
1267	E23	GZMB
1268	E58	GZMB
1269	E66	H1F0
1270	E31	H2AFX
1271	E67	H2-D1
1272	E67	H2-Dma
1273	E67	H2-Q4
1274	E26	Hap1
1275	E38	HAS2
1276	E2	HAUS4
1277	E58	HAVCR1
1278	E49	Hbegf
1279	E67	Hbegf
1280	E69	Hbegf
1281	E31	HBP1
1282	E57	HCN1
1283	E67	HD-K1
1284	E23	HEPACAM2
1285	E42	HEPH
1286	E38	HEPHL1
1287	E43	HERPUD1
1288	E31	HES1
1289	E33	HES1
1290	E67	Hes1

1291	E70	Hes1
1292	E46	HES2/3/5
1293	E37	HFE
1294	E42	HHLA2
1295	E5	HIF3A
1296	E65	HIF3A
1297	E29	HILPDA
1298	E2	HIRIP3
1299	E66	HIST1H1E
1300	E43	HIST1H2BD
1301	E43	HIST1H2BK
1302	E37	HIST2H2AA
1303	E43	HIST2H2AA3
1304	E66	HK2
1305	E42	HKDC1
1306	E14	HLA-B
1307	E14	HLA-C
1308	E15	HLA-DMA
1309	E54	HLA-DMB
1310	E54	HLA-DPA1
1311	E68	HLA-DQA1
1312	E68	HLA-DRA
1313	E4	HMGA2
1314	E18	HMGA2
1315	E40	HMGA2
1316	E54	HMGA2
1317	E65	HMGA2
1318	E70	Hmga2
1319	E66	HMGCS1
1320	E63	HMMR
1321	E46	HMX1/2
1322	E11	HNRPLL
1323	E58	HOMER2
1324	E54	HOPX
1325	E30	HOXA11-AS
1326	E65	HOXB5
1327	E70	Hoxb9
1328	E23	HOXD11
1329	E23	HOXD13
1330	E26	Hpcal4
1331	E56	HPCAL4
1332	E54	HPN
1333	E37	HPRT1

1334	E22	HR
1335	E41	HRH1
1336	E5	HRSP12
1337	E39	HS3ST3A1
1338	E21	HSD17B14
1339	E52	HSD17B14
1340	E42	HSD17B2
1341	E66	HSD17B7
1342	E32	HSD3B2
1343	E21	HSF4
1344	E66	HSPA5
1345	E11	HSPA6
1346	E31	HSPB1
1347	E70	Hspb1
1348	E11	HSPC159
1349	E65	HTR1E
1350	E58	HTR3A
1351	E28	HVCN1
1352	E21	IARS2
1353	E17	ICA1
1354	E31	ICA1
1355	E60	ICAM1
1356	E67	Icam1
1357	E67	Icosl
1358	E59	Id1
1359	E19	ID4
1360	E49	Ida
1361	E45	Idh1
1362	E53	IDH2
1363	E66	IDI1
1364	E8	IER3
1365	E41	IER3
1366	E54	IER3
1367	E60	IER3
1368	E31	IER5
1369	E67	Ifi30
1370	E59	Ifitm1
1371	E26	Ifitm3
1372	E2	IFITM3
1373	E67	Ifitm3
1374	E7	IGDCC3
1375	E58	IGDCC3
1376	E34	IGF1

1377	E59	Igf1r
1378	E34	IGF2
1379	E62	IGF2
1380	E66	IGF2
1381	E4	IGF2BP1
1382	E23	IGF2BP1
1383	E4	IGF2BP2
1384	E4	IGF2BP3
1385	E11	IGF2R
1386	E34	IGF2R
1387	E59	Igfals
1388	E29	IGFBP1
1389	E70	Igfbp2
1390	E29	IGFBP3
1391	E21	IGFBP3
1392	E38	IGFBP3
1393	E60	IGFBP3
1394	E69	Igfbp3
1395	E19	IGFBP7
1396	E40	IGFBP7
1397	E43	IGFBP7
1398	E60	IGFBP7
1399	E29	IGKC
1400	E29	IGLC2
1401	E14	IGSF11
1402	E58	IGSF9
1403	E41	IL11
1404	E43	IL11
1405	E54	IL11
1406	E11	IL15
1407	E1	IL17B
1408	E70	Il17rc
1409	E15	IL18R1
1410	E11	IL18RAP
1411	E40	IL1A
1412	E38	IL1B
1413	E14	IL1B
1414	E49	Il1b
1415	E54	IL1B
1416	E54	IL1R2
1417	E10	IL1RAP
1418	E15	IL1RAPL1
1419	E25	IL1RL1

1420	E49	Il1rl2
1421	E58	IL20RA
1422	E54	IL2RB
1423	E43	IL32
1424	E40	IL33
1425	E49	Il33
1426	E69	Il33
1427	E38	IL36G
1428	E15	IL4
1429	E28	IL5RA
1430	E24	IL6R
1431	E8	IL8
1432	E43	IL8
1433	E1	ILDR1
1434	E2	ILF3
1435	E37	ILK
1436	E2	IMPDH2
1437	E68	INHA
1438	E38	INHBA
1439	E54	INHBE
1440	E66	INPP5D
1441	E66	INSIG1
1442	E25	INSL3
1443	E23	INSLA4
1444	E12	INSM1
1445	E65	IPO11
1446	E1	IRAG1
1447	E33	IRF1
1448	E7	IRF2
1449	E60	IRF5
1450	E49	Irf8
1451	E67	Irf8
1452	E69	Irf8
1453	E35	IRS2
1454	E65	IRX2
1455	E31	IRX3
1456	E67	Isg15
1457	E67	Isg20
1458	E17	ISL1
1459	E65	ISL1
1460	E25	ISM1
1461	E20	ITCB2
1462	E33	ITGA10

1463	E8	ITGA2
1464	E15	ITGA2
1465	E39	ITGA2
1466	E41	ITGA2
1467	E49	Itga2
1468	E64	ITGA2
1469	E69	Itga2
1470	E59	Itga2b
1471	E64	ITGA2B
1472	E70	Itga3
1473	E70	Itga4
1474	E43	ITGA5
1475	E21	ITGA7
1476	E28	ITGA8
1477	E59	Itga9
1478	E58	ITGAD
1479	E34	ITGAM
1480	E59	Itgam
1481	E24	ITGB1
1482	E13	ITGB1
1483	E49	Itgb2
1484	E38	ITGB3
1485	E67	Itgb3
1486	E33	ITGB4
1487	E64	ITGB6
1488	E41	ITGB8
1489	E39	IVNS1ABP
1490	E42	IYD
1491	E38	JAG1
1492	E40	JAG2
1493	E50	JAK2
1494	E1	JAM2
1495	E70	Jam2
1496	E40	JAM3
1497	E56	JPH2
1498	E17	JPH4
1499	E33	JUNB
1500	E67	Junb
1501	E38	KAL1
1502	E5	KAT2B
1503	E27	KAZN
1504	E6	KCNA1
1505	E12	KCNA1

1506	E34	KCNA1
1507	E47	KCNA3
1508	E58	KCNA5
1509	E21	KCNAB2
1510	E62	KCNAB2
1511	E12	KCNB2
1512	E26	Kcnc2
1513	E34	KCNC3
1514	E58	KCNC3
1515	E65	KCND1
1516	E50	KCND3
1517	E26	Kcne2
1518	E2	KCNE3
1519	E10	KCNE3
1520	E42	KCNE3
1521	E27	KCNE4
1522	E7	KCNF1
1523	E56	KCNF1
1524	E37	KCNG1
1525	E43	KCNG1
1526	E58	KCNG1
1527	E20	KCNG2
1528	E12	KCNG3
1529	E9	KCNH1
1530	E70	Kcnh2
1531	E58	KCNH3
1532	E45	Kcnh7
1533	E12	KCNH8
1534	E58	KCNH8
1535	E51	KCNIP1
1536	E65	KCNIP3
1537	E5	KCNJ10
1538	E31	KCNJ10
1539	E26	Kcnj13
1540	E54	KCNJ13
1541	E19	KCNJ16
1542	E51	KCNJ16
1543	E57	KCNJ16
1544	E58	KCNJ16
1545	E32	KCNJ5
1546	E31	KCNJ8
1547	E48	KCNJ9
1548	E3	KCNK1

1549	E8	KCNK1
1550	E35	KCNK1
1551	E61	KCNK1
1552	E23	KCNK12
1553	E63	KCNK12
1554	E9	KCNK15
1555	E22	KCNK15
1556	E52	KCNK15
1557	E24	KCNK2
1558	E68	KCNK2
1559	E16	KCNK3
1560	E22	KCNK5
1561	E11	KCNK6
1562	E43	KCNK6
1563	E13	KCNMA1
1564	E38	KCNMA1
1565	E39	KCNMA1
1566	E40	KCNMA1
1567	E41	KCNMA1
1568	E60	KCNMA1
1569	E25	KCNMB1
1570	E1	KCNMB1
1571	E12	KCNMB2
1572	E34	KCNMB2
1573	E67	Kcnmb2
1574	E27	KCNMB2-AS1
1575	E44	KCNMB3
1576	E18	KCNMB4
1577	E58	KCNMB4
1578	E51	KCNN2
1579	E28	KCNN3
1580	E4	KCNN3
1581	E5	KCNN3
1582	E34	KCNN3
1583	E8	KCNN4
1584	E36	KCNN4
1585	E41	KCNN4
1586	E49	Kcnn4
1587	E52	KCNN4
1588	E53	KCNN4
1589	E58	KCNN4
1590	E64	KCNN4
1591	E69	Kcnn4

1592	E2	KCNQ1
1593	E55	Kcnq1
1594	E58	KCNQ1
1595	E29	KCNQ1OT1
1596	E33	KCNQ1OT1
1597	E66	KCNQ1OT1
1598	E17	KCNQ2
1599	E46	KCNQ2
1600	E59	Kcnq3
1601	E14	KCNQ5
1602	E17	KCNQ5
1603	E40	KCNQ5
1604	E30	KCNQ5-IT1
1605	E34	KCNS1
1606	E34	KCNS3
1607	E34	KCNT1
1608	E15	KCNT2
1609	E23	KCNU1
1610	E46	KDM2B
1611	E30	KDM4A-AS1
1612	E66	KDM6B
1613	E67	Kdm6b
1614	E6	KHBRBS2
1615	E38	KIAA1644
1616	E2	KIF12
1617	E2	KIF20A
1618	E17	KIF21A
1619	E65	KIF21B
1620	E14	KIF3B
1621	E69	Kif5c
1622	E40	KIRREL
1623	E34	KISS1
1624	E59	Kit
1625	E26	Kl
1626	E59	Klf1
1627	E33	KLF10
1628	E67	Klf10
1629	E31	KLF12
1630	E66	KLF16
1631	E69	Klf4
1632	E67	Klf6
1633	E17	KLHL13
1634	E21	KLHL24

1635	E21	KLHL4
1636	E52	KLK13
1637	E23	KLK14
1638	E37	KLK2
1639	E15	KLRK1
1640	E10	KMO
1641	E64	KRAS
1642	E69	Kras
1643	E22	KRT15
1644	E60	KRT17
1645	E45	Krt18
1646	E24	KRT19
1647	E29	KRT19
1648	E22	KRT19
1649	E60	KRT19
1650	E45	Krt222
1651	E58	KRT23
1652	E7	KRT5
1653	E54	KRT6A
1654	E54	KRT6B
1655	E38	KRT76
1656	E45	Krt8
1657	E38	KRTAP19
1658	E70	L1cam
1659	E58	LAMA1
1660	E57	LAMA2
1661	E56	LAMA4
1662	E33	LAMA5
1663	E33	LAMB2
1664	E41	LAMB3
1665	E54	LAMC2
1666	E20	LAMP5
1667	E37	LASS6
1668	E59	Lass6
1669	E28	LAX1
1670	E54	LBH
1671	E26	Lbp
1672	E31	LBR
1673	E53	LCK
1674	E65	LCN12
1675	E21	LCNL1
1676	E2	LCP1
1677	E43	LCP1

1678	E29	LDHA
1679	E55	Ldha
1680	E66	LDLR
1681	E67	Ldlr
1682	E37	LDOC1
1683	E2	LECT2
1684	E32	LEF1
1685	E55	Lef1
1686	E68	LEF1
1687	E4	LEFTY1
1688	E4	LEFTY2
1689	E27	LEKR1
1690	E34	LEP
1691	E34	LEPR
1692	E31	LFNG
1693	E26	Lgals1
1694	E16	LGALS1
1695	E29	LGALS3
1696	E59	Lgals3
1697	E42	LGALS4
1698	E51	LGI1
1699	E2	LGR5
1700	E36	LGR5
1701	E57	LGR6
1702	E25	LHCGR
1703	E70	Lhfp
1704	E59	Lhfpl2
1705	E46	LHX3
1706	E65	LHX3
1707	E46	LHX3/4
1708	E49	Lif
1709	E54	LIF
1710	E60	LIF
1711	E67	Lif
1712	E69	Lif
1713	E8	LIF
1714	E1	LIFR
1715	E15	LIMK2
1716	E1	LIMS2
1717	E4	LIN28A
1718	E65	LIN28B
1719	E14	LINC00282
1720	E14	LINC00348

1721	E30	LINC00511
1722	E25	LINC00607
1723	E29	LINC00626
1724	E27	LINC00886
1725	E66	LINC01021
1726	E25	LINC01116
1727	E58	LINC01132
1728	E29	LINC01320
1729	E14	LINC01531
1730	E58	LINC01671
1731	E58	LINC02532
1732	E52	LINC02683
1733	E26	Lingo1
1734	E57	LINGO2
1735	E21	LIPG
1736	E1	LIPH
1737	E2	LIPT2
1738	E70	Llgl2
1739	E5	LMO3
1740	E51	LMO3
1741	E1	LMOD1
1742	E65	LMX1A
1743	E43	LOC100132564
1744	E23	LOC100190940
1745	E24	LOC100192378
1746	E66	LOC729966
1747	E17	LONRF2
1748	E16	LOXL2
1749	E39	LOXL2
1750	E41	LOXL2
1751	E65	LPA
1752	E34	LPAR3
1753	E21	LPCAT1
1754	E31	LPGAT1
1755	E37	LPL
1756	E43	LPXN
1757	E11	LRG1
1758	E2	LRIG1
1759	E15	LRP11
1760	E21	LRP4
1761	E14	LRPPRC
1762	E41	LRRC15
1763	E31	LRRC4

1764	E70	Lrrk1
1765	E56	LRRN2
1766	E17	LRRN3
1767	E52	LRRTM1
1768	E58	LRRTM1
1769	E17	LRRTM2
1770	E28	LSAMP
1771	E28	LSR
1772	E21	LSS
1773	E54	LTB
1774	E38	LTB
1775	E60	LTBP1
1776	E40	LTBP2
1777	E70	Ltbp2
1778	E33	LTBP3
1779	E24	LUM
1780	E45	Ly6a
1781	E7	LY6D
1782	E33	LY6E
1783	E50	LYN
1784	E42	LYZ
1785	E54	LZTFL1
1786	E66	LZTS1
1787	E17	MAB21L2
1788	E26	Mag
1789	E26	Mal
1790	E13	MAL2
1791	E57	MAL2
1792	E69	Mall
1793	E14	MAMDC2-AS1
1794	E66	MAMDC4
1795	E11	MANEAL
1796	E17	MAOA
1797	E1	MAOB
1798	E44	MAP1B
1799	E43	MAP1LC3A
1800	E60	MAP2K6
1801	E15	MAP3K14
1802	E58	MAP3K15
1803	E56	MAP3K5
1804	E64	MAP3K5
1805	E64	MAP3K6
1806	E16	MAP4K4

1807	E14	MAP6D1
1808	E50	MAPK1
1809	E59	Mapk13
1810	E50	MAPK14
1811	E38	MAPK6
1812	E21	MAPT
1813	E56	MARCH4
1814	E16	MARCKS
1815	E54	MARK1
1816	E14	MARS2
1817	E2	MARVELD1
1818	E27	MAST4
1819	E70	Matn2
1820	E31	MAZ
1821	E1	MB
1822	E14	MBD5
1823	E59	Mc5r
1824	E70	Mcam
1825	E62	MCFD2
1826	E26	Mcm2
1827	E60	MCM2
1828	E2	MCM8
1829	E68	MCOLN3
1830	E59	Mcpt8
1831	E59	Mdga1
1832	E48	MDH1
1833	E18	MDM2
1834	E2	MECOM
1835	E26	Mef2c
1836	E1	MEF2C
1837	E59	Mefv
1838	E1	MEG3
1839	E26	Melat1
1840	E52	MEP1A
1841	E14	MESDC1
1842	E7	MESP1
1843	E23	MET
1844	E59	Met
1845	E62	MET
1846	E67	Met
1847	E18	METTL1
1848	E18	METTL21B
1849	E66	METTL7A

1850	E21	METTL7B
1851	E21	MFGE8
1852	E58	MFSD2A
1853	E59	Mfsd2b
1854	E14	MGAT4C
1855	E26	Mia
1856	E22	MICB
1857	E2	MIF
1858	E30	MIR205HG
1859	E30	MIR31HG
1860	E65	MKX
1861	E51	MLC1
1862	E25	MLK4
1863	E23	MLLT11
1864	E1	MLPH
1865	E11	MLT11
1866	E69	Mmd
1867	E29	MME
1868	E44	MMP1
1869	E56	MMP1
1870	E64	MMP1
1871	E38	MMP1
1872	E38	MMP10
1873	E44	MMP10
1874	E49	Mmp10
1875	E24	MMP14
1876	E40	MMP3
1877	E54	MMP7
1878	E58	MMP7
1879	E38	MMP9
1880	E59	Mmrn1
1881	E65	MNX1
1882	E46	MNX1
1883	E30	MNX1-AS1
1884	E58	MOB1B
1885	E26	Mobp
1886	E26	Mog
1887	E31	MORC3
1888	E11	MOSC2
1889	E57	MOXD1
1890	E13	MPDZ
1891	E59	Mpl
1892	E2	MPP3

1893	E2	MPZL1
1894	E3	MPZL1
1895	E15	MPZL2
1896	E69	Mpzl2
1897	E21	MRC2
1898	E40	MRC2
1899	E14	MREG
1900	E24	MRGPRX3
1901	E14	MRPL24
1902	E7	MRPL4
1903	E31	MRPS33
1904	E45	Mrps35
1905	E28	MS4A1
1906	E58	MS4A7
1907	E64	MSLN
1908	E66	MSMO1
1909	E21	MSN
1910	E43	MSN
1911	E63	MSN
1912	E15	MSR1
1913	E40	MSRB3
1914	E43	MT1A
1915	E25	MT1F
1916	E43	MT1X
1917	E26	Mt2
1918	E43	MT2A
1919	E21	MT-CYB
1920	E63	MTHFD2
1921	E52	MTND4P12
1922	E58	MTRNR2L12
1923	E1	MUC1
1924	E7	MUC1
1925	E42	MUC13
1926	E42	MUC17
1927	E41	MUC5B
1928	E58	MUC6
1929	E40	MUM1L1
1930	E21	MVD
1931	E23	MYBL1
1932	E14	MYC
1933	E35	MYC
1934	E61	MYC
1935	E17	MYCN

1936	E25	MYH11
1937	E1	MYH11
1938	E38	MYH16
1939	E21	MYH9
1940	E70	Myh9
1941	E1	MYL9
1942	E1	MYLK
1943	E65	MYO18B
1944	E42	MYO1A
1945	E2	MYO1B
1946	E59	Myo1d
1947	E1	MYO5B
1948	E1	MYO5C
1949	E42	MYO7B
1950	E21	MYRF
1951	E18	MYRFL
1952	E17	MYT2L
1953	E21	NAB2
1954	E4	NANOG
1955	E49	Nap1l2
1956	E26	Nap1l5
1957	E2	NAPEPLD
1958	E33	NARF
1959	E14	NAV2
1960	E12	NCAM1
1961	E68	NCAM1
1962	E66	NCAM-AS1
1963	E5	NCAN
1964	E17	NCAN
1965	E51	NCAN
1966	E14	NCL
1967	E14	NCOA3
1968	E26	Ndn
1969	E8	NDRG1
1970	E63	NDRG1
1971	E26	Ndrg2
1972	E38	NDRG4
1973	E51	NDRG4
1974	E29	NDUFA4L2
1975	E66	NDUFB9
1976	E33	NEAT1
1977	E56	NEBL
1978	E37	NEDD9

1979	E34	NEFH
1980	E17	NEFL
1981	E17	NEFM
1982	E41	NEGR1
1983	E25	NELL2
1984	E57	NELL2
1985	E15	NEO1
1986	E60	NEO1
1987	E51	NES
1988	E21	NEU1
1989	E65	NEUROD1
1990	E65	NEUROD4
1991	E34	NF1
1992	E35	NF1B
1993	E24	NFAT5
1994	E31	NFAT5
1995	E2	NFIA
1996	E31	NFIA
1997	E58	NFIA
1998	E12	NFIB
1999	E58	NFIB
2000	E33	NFIC
2001	E66	NFIC
2002	E66	NFIX
2003	E50	NFKB1
2004	E8	NFKBIZ
2005	E31	NFKBIZ
2006	E41	NGEF
2007	E49	Ngf
2008	E1	NGFR
2009	E40	NGFR
2010	E62	NGRN
2011	E31	NHEJ1
2012	E58	NID2
2013	E60	NID2
2014	E15	NINJ1
2015	E25	NIPAL1
2016	E56	NIPAL1
2017	E40	NIPAL4
2018	E23	NKG7
2019	E19	NKX2-1
2020	E35	NKX2-1
2021	E65	NKX2-2

2022	E52	NKX3-1
2023	E46	NKX6-2
2024	E4	NLGN4X
2025	E4	NLGN4Y
2026	E43	NLRP1
2027	E67	Nlrp3
2028	E29	NMB
2029	E17	NMNAT2
2030	E41	NMNAT2
2031	E34	NMU
2032	E60	NMU
2033	E56	NNAT
2034	E29	NNMT
2035	E2	NOD1
2036	E4	NODAL
2037	E70	Nog
2038	E14	NOP56
2039	E2	NOTCH1
2040	E60	NOTCH1
2041	E66	NOTCH1
2042	E66	NOTCH3
2043	E40	NOTCH4
2044	E59	Nov
2045	E70	Nov
2046	E66	NOVA2
2047	E21	NPC2
2048	E65	NPHS1
2049	E34	NPPA
2050	E70	Nppb
2051	E43	NPTX1
2052	E65	NPTX1
2053	E26	Nptxr
2054	E19	NPY1R
2055	E34	NPY1R
2056	E34	NPY2R
2057	E65	NR0B1
2058	E69	Nr1h4
2059	E51	NR2E1
2060	E2	NR2E3
2061	E33	NR2F1
2062	E7	NR4A1
2063	E67	Nr4a2
2064	E67	Nr4a3

2065	E65	NR5A1
2066	E62	NRBF2
2067	E31	NRCAM
2068	E44	NREP
2069	E40	NRG1
2070	E59	Nrg1
2071	E54	NRG2
2072	E26	Nrgn
2073	E58	NRGN
2074	E42	NRIL2
2075	E26	Nrip3
2076	E10	NROB1
2077	E39	NRP1
2078	E41	NRP1
2079	E14	NRP1
2080	E21	NRP2
2081	E17	NRSN1
2082	E41	NRXN3
2083	E60	NT5E
2084	E34	NTF3
2085	E25	NTM
2086	E39	NTM
2087	E41	NTN4
2088	E46	NTNG2
2089	E46	NTSR1
2090	E51	NTSR2
2091	E70	Nuak1
2092	E70	Nuak2
2093	E34	NUCB1
2094	E33	NUCB2
2095	E34	NUCB2
2096	E37	NUDT1
2097	E45	Nupr1
2098	E60	ODC1
2099	E58	OGDHL
2100	E26	Olfm1
2101	E22	OLFM1
2102	E58	OLFM2
2103	E54	OPN1SW
2104	E41	OPRD1
2105	E66	OPRM1
2106	E16	OPTN
2107	E15	OR4K2

2108	E1	ORAI1
2109	E2	ORC1
2110	E39	OSMR
2111	E1	OSR1
2112	E20	OSR1
2113	E46	OTX2
2114	E11	OVOS2
2115	E26	Oxt
2116	E37	P2RX1
2117	E28	P2RX5
2118	E67	P2ry2
2119	E55	P4ha2
2120	E47	PAG1
2121	E68	PAH
2122	E2	PAICS
2123	E37	PAK1
2124	E62	PAK4
2125	E2	PALB2
2126	E21	PALLD
2127	E70	Palld
2128	E54	PALM
2129	E43	PAPPA
2130	E11	PAPSS2
2131	E68	PAPSS2
2132	E42	PAQR8
2133	E28	PARM1
2134	E43	PAT1
2135	E46	PAX2
2136	E51	PAX6
2137	E4	PAX7
2138	E29	PAX8
2139	E31	PBX1
2140	E66	PCBP2
2141	E60	PCCA
2142	E41	PCDH1
2143	E21	PCDH1
2144	E65	PCDH17
2145	E1	PCDH18
2146	E31	PCDH9
2147	E66	PCDHGC3
2148	E60	PCNA
2149	E68	PCP4
2150	E23	PCSK1

2151	E49	Pcsk1n
2152	E66	PCSK1N
2153	E26	Pde10a
2154	E55	Pde11a
2155	E58	PDE11A
2156	E26	Pde1b
2157	E38	PDE2A
2158	E65	PDE3A
2159	E2	PDE3B
2160	E67	Pde4b
2161	E1	PDGFA
2162	E21	PDGFA
2163	E70	Pdgfa
2164	E21	PDGFB
2165	E70	Pdgfb
2166	E39	PDGFC
2167	E43	PDGFC
2168	E70	Pdgfrl
2169	E26	Pdp1
2170	E50	PDP1
2171	E40	PDPN
2172	E60	PDRG1
2173	E29	PDZK1IP1
2174	E16	PEA15
2175	E31	PEA15
2176	E68	PEG10
2177	E49	Peg3
2178	E26	Penk
2179	E67	Per1
2180	E28	PERP
2181	E43	PFKFB4
2182	E16	PFKP
2183	E37	PFKP
2184	E44	PFN2
2185	E58	PGBD5
2186	E54	PGC
2187	E11	PGCP
2188	E66	PGF
2189	E58	PGR
2190	E17	PHACTR3
2191	E63	PHGDH
2192	E66	PHGDH
2193	E10	PHLDA1

2194	E45	Phlda1
2195	E54	PHLDA1
2196	E8	PHLDA2
2197	E41	PHLDA2
2198	E17	PHOX2A
2199	E17	PHOX2B
2200	E58	PI3
2201	E2	PICALM
2202	E66	PIDD
2203	E34	PIEZO2
2204	E49	Pigr
2205	E50	PIK3C2B
2206	E62	PIP4K2A
2207	E52	PIP5K1B
2208	E58	PIP5K1B
2209	E65	PITX2
2210	E1	PKD1
2211	E65	PKD1L1
2212	E21	PKDCC
2213	E58	PKHD1
2214	E55	Pkp4
2215	E9	PLA2G10
2216	E20	PLA2G4E
2217	E11	PLAG1
2218	E57	PLAG1
2219	E65	PLAGL1
2220	E33	PLAT
2221	E64	PLAT
2222	E69	Plat
2223	E49	Plau
2224	E54	PLAU
2225	E64	PLAU
2226	E67	Plau
2227	E38	PLAU
2228	E8	PLAUR
2229	E13	PLAUR
2230	E41	PLAUR
2231	E43	PLAUR
2232	E49	Plaur
2233	E69	Plaur
2234	E2	PLCE1
2235	E47	PLCL2
2236	E52	PLCXD3

2237	E69	Plek2
2238	E29	PLEKHA1
2239	E54	PLEKHA4
2240	E68	PLEKHA5
2241	E14	PLEKHS1
2242	E58	PLEKHS1
2243	E67	Plk2
2244	E16	PLOD2
2245	E26	Plp1
2246	E65	PLP1
2247	E1	PLPP1
2248	E28	PLPP5
2249	E67	Plscr1
2250	E31	PLTP
2251	E70	Plxnbp2
2252	E39	PLXNC1
2253	E25	PMAIP1
2254	E60	PMAIP1(NOXA)
2255	E26	Pmch
2256	E41	PMEPA1
2257	E43	PMEPA1
2258	E16	PML
2259	E35	PNMA2
2260	E51	PNOC
2261	E67	Pnp
2262	E31	PODXL
2263	E42	POF18
2264	E2	POLD1
2265	E2	POLE
2266	E2	POLI
2267	E66	POLR2A
2268	E44	POLR2H
2269	E62	POM121
2270	E23	POPDC3
2271	E1	POSTN
2272	E19	POSTN
2273	E70	Postn
2274	E65	POU1F1
2275	E38	POU2F2
2276	E31	POU3F2
2277	E51	POU3F2
2278	E19	POU3F3
2279	E31	POU3F3

2280	E4	POU5F1
2281	E50	PPARG
2282	E2	PPAT
2283	E49	Ppbp
2284	E13	PPL
2285	E5	PPMiK
2286	E38	PPP1CB
2287	E1	PPP1R14A
2288	E31	PPP1R14C
2289	E49	Ppp1R15a
2290	E67	Ppp1r15a
2291	E26	Ppp1r1b
2292	E58	PPP1R3B
2293	E26	Ppp1r9b
2294	E62	PPP2R1B
2295	E58	PPP2R2C
2296	E41	PRDM1
2297	E27	PRDM16
2298	E65	PRDM8
2299	E45	Prdx6
2300	E2	PRELP
2301	E41	PRICKLE2
2302	E60	PRIM1
2303	E70	Prkaa1
2304	E58	PRKAG2-AS1
2305	E47	PRKAR2B
2306	E24	PRKCB
2307	E26	Prkcd
2308	E27	PRKCE
2309	E70	Prkcq
2310	E50	PRKD1
2311	E59	Prkd2
2312	E49	Prkg2
2313	E69	Prkg2
2314	E5	PRODH
2315	E66	PRODH
2316	E7	PROM1
2317	E11	PROS1
2318	E54	PROS1
2319	E12	PROX1
2320	E66	PRR12
2321	E66	PRR36
2322	E1	PRRX1

2323	E41	PRSS23
2324	E59	Prss34
2325	E31	PRTG
2326	E48	PSAT1
2327	E54	PSAT1
2328	E63	PSAT1
2329	E26	Psd
2330	E5	PSD2
2331	E67	Psmb9
2332	E44	PSMD2
2333	E55	Pstpip2
2334	E60	PSTPIP2
2335	E6	PTEN
2336	E26	Ptgds
2337	E21	PTGDS
2338	E67	Ptger4
2339	E60	PTGES(PIG12)
2340	E52	PTGFR
2341	E65	PTGFR
2342	E49	Ptgs2
2343	E34	PTH1R
2344	E58	PTHLH
2345	E3	PTK7
2346	E50	PTPN1
2347	E50	PTPN12
2348	E50	PTPN21
2349	E66	PTPN23
2350	E50	PTPN6
2351	E13	PTPRC
2352	E1	PTPRE
2353	E15	PTPRE
2354	E67	Ptpre
2355	E50	PTPRJ
2356	E27	PTPRK
2357	E70	Ptprm
2358	E11	PTPRN2
2359	E2	PTPRO
2360	E1	PTPRT
2361	E31	PTPRZ1
2362	E36	PTRH1
2363	E58	PVR
2364	E66	PVRL4
2365	E30	PVT1

2366	E66	PVT1
2367	E13	PXN
2368	E35	PXN
2369	E42	PZDP3
2370	E11	QPCT
2371	E21	QPRT
2372	E1	QRICH2
2373	E2	QSOX2
2374	E16	RAB11FIP5
2375	E35	RAB12
2376	E17	RAB33A
2377	E11	RAB34
2378	E14	RAB38
2379	E54	RAB3B
2380	E56	RAB3C
2381	E16	RAB6IP1
2382	E35	RAC1
2383	E61	RAD51
2384	E26	Ramp3
2385	E34	RAMP3
2386	E56	RAMP3
2387	E44	RAP2B
2388	E59	Rapgef3
2389	E47	RAPGEF5
2390	E22	RAPGEFL1
2391	E59	Raph1
2392	E66	RAPH1
2393	E70	Rarb
2394	E70	Rarg
2395	E26	Rarres2
2396	E29	RARRES2
2397	E2	RASA3
2398	E26	Rasd2
2399	E42	RASEF
2400	E58	RASGRF1
2401	E59	Rasgrf2
2402	E51	RASGRP1
2403	E2	RASL11B
2404	E2	RASSF4
2405	E59	Rassf4
2406	E66	RAVER1
2407	E46	RAX
2408	E65	RAX2

2409	E22	RBBP8
2410	E58	RBBP8NL
2411	E14	RBFA
2412	E56	RBFOX1
2413	E60	RBL1
2414	E6	RBM24
2415	E17	RBMS3
2416	E58	RBP7
2417	E12	RBPJ
2418	E24	RCAN3
2419	E25	RCAN3
2420	E58	RCAN3
2421	E10	RCOR
2422	E55	Rcvm
2423	E14	RDH13
2424	E21	RDH5
2425	E67	Rel
2426	E34	RELN
2427	E57	RELN
2428	E69	Reln
2429	E21	RENBP
2430	E66	RERE
2431	E26	Resp18
2432	E12	RET
2433	E15	RET
2434	E22	RET
2435	E31	REXO1
2436	E65	RFX4
2437	E33	RGCC
2438	E2	RGMB
2439	E49	Rgs16
2440	E20	RGS17
2441	E60	RGS2
2442	E17	RGS4
2443	E56	RGS7
2444	E26	Rgs9
2445	E14	RGS9
2446	E2	RHOBTB3
2447	E33	RHOBTB3
2448	E13	RHOU
2449	E1	RHPN2
2450	E31	RIBC1
2451	E4	RIMS1

2452	E67	Ripk1
2453	E64	RIPK3
2454	E14	RLBP1
2455	E34	RLN1
2456	E52	RLN1
2457	E31	RND2
2458	E67	Rnf144b
2459	E21	RNF145
2460	E2	RNF32
2461	E58	RNF39
2462	E66	RNU1-1
2463	E38	ROBO4
2464	E41	ROBO4
2465	E57	ROPN1L
2466	E65	RORB
2467	E25	RP1
2468	E25	RP11-141M1.3
2469	E65	RP11-192H23.4
2470	E65	RP11-362F19.1
2471	E58	RP11-392E22.10
2472	E58	RP11-392E22.12
2473	E21	RP11-644F5.10
2474	E65	RP11-701P16.2
2475	E14	RP11-79H23.3
2476	E14	RP13-631K18.2
2477	E25	RP1-78014.1
2478	E66	RP3-326I13.1
2479	E65	RP5-842K16.1
2480	E51	RPH3A
2481	E48	RPIA
2482	E65	RPL21
2483	E65	RPL37
2484	E65	RPLP0
2485	E38	RPLPOP2
2486	E60	RPRM
2487	E65	RPS16
2488	E44	RPS23
2489	E65	RPS23
2490	E19	RPS4Y1
2491	E65	RPS5
2492	E60	RRAD

2493	E70	Rras2
2494	E54	RRM2
2495	E66	RRM2B
2496	E24	RRN3P3
2497	E65	RRS1
2498	E67	Rsad2
2499	E26	Rsph1
2500	E65	RSPO2
2501	E32	RSPO3
2502	E66	RTL1
2503	E11	RTN1
2504	E17	RTN1
2505	E21	RTN1
2506	E44	RTP4
2507	E3	RUNX1
2508	E35	RUNX1
2509	E58	RUNX3
2510	E34	RXFP1
2511	E65	RXRG
2512	E65	RYR1
2513	E51	RYR3
2514	E23	S100A2
2515	E60	S100A2
2516	E64	S100A2
2517	E58	S100A3
2518	E64	S100A4
2519	E8	S100A6
2520	E38	S100A6
2521	E38	S100A9
2522	E58	S100A9
2523	E59	S1pr1
2524	E60	SAA1(PIG4)
2525	E5	SALLA
2526	E35	SAMD4A
2527	E44	SAMD9
2528	E5	SAMD9L
2529	E67	Samhd1
2530	E11	SAMSN1
2531	E60	SARDH
2532	E5	SASH1
2533	E59	Satb1
2534	E46	SATB2
2535	E66	SBK1

2536	E50	SCAMP3
2537	E60	SCARA3
2538	E24	SCARA5
2539	E43	SCARNA13
2540	E43	SCARNA8
2541	E61	SCC1
2542	E45	Scd2
2543	E35	SCFD2
2544	E34	SCG2
2545	E54	SCG2
2546	E17	SCG5
2547	E43	SCG5
2548	E49	Scg5
2549	E58	SCGB1D2
2550	E58	SCGB2A1
2551	E16	SCHIP1
2552	E52	SCIN
2553	E59	Scin
2554	E60	SCL4A10
2555	E52	SCML4
2556	E12	SCN3A
2557	E17	SCN3A
2558	E26	Scn4b
2559	E4	SCN5A
2560	E70	Scn5a
2561	E34	SCN7A
2562	E28	SDC1
2563	E8	SDC4
2564	E67	Sdc4
2565	E41	SDK1
2566	E58	SDK2
2567	E59	Sdpr
2568	E70	Sdpr
2569	E14	SEC24D
2570	E2	SECTM1B
2571	E15	SELP
2572	E54	SELPLG
2573	E41	SEMA3B
2574	E44	SEMA3C
2575	E63	SEMA3C
2576	E70	Sema3d
2577	E70	Sema3f
2578	E59	Sema4a

2579	E70	Sema4f
2580	E42	SEMA4G
2581	E21	SEMA7A
2582	E70	Sema7a
2583	E37	SEPT10
2584	E44	SERP1
2585	E59	Serpina3f
2586	E8	SERPINB1
2587	E40	SERPINB13
2588	E8	SERPINB5
2589	E14	SERPINB8
2590	E54	SERPINB8
2591	E67	Serpinb8
2592	E20	SERPINE1
2593	E60	SERPINE1(PAI1)
2594	E38	SERPINE2
2595	E54	SERPINE2
2596	E57	SERPINE2
2597	E1	SERPINF1
2598	E33	SERPINF1
2599	E40	SERPINF1
2600	E41	SERTAD4
2601	E31	SESN3
2602	E60	SESN3
2603	E62	SESN3
2604	E8	SFN
2605	E60	SFN(14-3-3σ)
2606	E4	SFRP1
2607	E41	SFRP1
2608	E70	Sfrp1
2609	E54	SFTPD
2610	E14	SFXN4
2611	E14	SGCB
2612	E1	SGIP1
2613	E21	SGK223
2614	E70	Sgms1
2615	E54	SH2D3C
2616	E40	SH2D5
2617	E42	SH3BGRL2
2618	E16	SH3GLB1
2619	E43	SH3KBP1
2620	E41	SH3PXD2A
2621	E66	SH3PXD2B

2622	E26	Shank1
2623	E58	SHANK1
2624	E50	SHC1
2625	E50	SHC3
2626	E11	SHCBP1
2627	E63	SHCBP1
2628	E1	SHE
2629	E46	SHH
2630	E65	SHH
2631	E70	Shh
2632	E2	SHISA2
2633	E41	SHISA2
2634	E46	SHISA2
2635	E56	SHISA2
2636	E63	SHISA4
2637	E42	SI
2638	E63	SIAE
2639	E45	Sidt2
2640	E20	SIM1
2641	E46	SIM2
2642	E45	Simapos2
2643	E14	SIRPAP1
2644	E20	SIX1
2645	E70	Six4
2646	E66	SKI
2647	E31	SKIL
2648	E44	SKIL
2649	E31	SKIV2L
2650	E35	SKP2
2651	E37	SLAMF1
2652	E28	SLAMF7
2653	E21	SLC04A1
2654	E66	SLC12A4
2655	E31	SLC12A6
2656	E41	SLC14A1
2657	E14	SLC14A1
2658	E58	SLC14A1
2659	E59	Slc16a11
2660	E8	SLC16A3
2661	E43	SLC16A3
2662	E9	SLC16A6
2663	E26	Slc17a6
2664	E26	Slc17a7

2665	E56	SLC18A1
2666	E4	SLC18A2
2667	E59	Slc18a2
2668	E56	SLC18A3
2669	E14	SLC19A2
2670	E58	SLC1A1
2671	E26	Slc1a2
2672	E51	SLC1A2
2673	E58	SLC1A2
2674	E67	Slc1a2
2675	E51	SLC1A3
2676	E58	SLC1A3
2677	E28	SLC1A4
2678	E39	SLC22A4
2679	E51	SLC24A3
2680	E38	SLC25A24
2681	E27	SLC25A26
2682	E14	SLC25A42
2683	E19	SLC26A4
2684	E2	SLC27A2
2685	E14	SLC27A3
2686	E1	SLC28A3
2687	E43	SLC2A3
2688	E3	SLC2A5
2689	E56	SLC30A3
2690	E67	Slc31a2
2691	E18	SLC35E3
2692	E41	SLC35F1
2693	E58	SLC35F5
2694	E58	SLC38A4
2695	E23	SLC38A8
2696	E7	SLC39A2
2697	E19	SLC3A1
2698	E63	SLC3A2
2699	E29	SLC40A1
2700	E42	SLC40A1
2701	E58	SLC40A1
2702	E42	SLC44A4
2703	E27	SLC44A5
2704	E52	SLC45A3
2705	E58	SLC45A4
2706	E67	Slc4a4
2707	E54	SLC4A7

2708	E42	SLC5A1
2709	E34	SLC6A1
2710	E51	SLC6A1
2711	E26	Slc6a11
2712	E24	SLC6A12
2713	E42	SLC6A20
2714	E65	SLC6A7
2715	E67	Slc7a1
2716	E54	SLC7A1
2717	E5	SLC7A11
2718	E62	SLC7A11
2719	E65	SLC7A2
2720	E67	Slc7a2
2721	E63	SLC7A5
2722	E66	SLC7A5
2723	E58	SLC8A1
2724	E58	SLC9A2
2725	E15	SLC9AB
2726	E54	SLCO2B1
2727	E21	SLIT1
2728	E39	SLIT2
2729	E70	Slit2
2730	E1	SLIT3
2731	E41	SLITRK6
2732	E58	SLITRK6
2733	E64	SLK
2734	E43	SLN
2735	E29	SLPI
2736	E54	SLURP1
2737	E41	SMAGP
2738	E31	SMARCA2
2739	E35	SMARCA4
2740	E2	SMARCD3
2741	E20	SMIM5
2742	E2	SMO
2743	E43	SNAI2
2744	E54	SNAI2
2745	E65	SNAI2
2746	E63	SNAP23
2747	E69	Snap25
2748	E17	SNAP91
2749	E49	Snap91
2750	E66	SNHG3

2751	E21	SNN
2752	E43	SNORA12
2753	E61	SNTA1
2754	E2	SNX10
2755	E37	SNX4
2756	E59	Socs2
2757	E33	SOCS3
2758	E60	SOD3
2759	E66	SOGA1
2760	E66	SON
2761	E27	SORCS2
2762	E2	SORD
2763	E53	SORD
2764	E26	Sostdc1
2765	E35	SOX11
2766	E65	SOX11
2767	E4	SOX2
2768	E12	SOX2
2769	E41	SOX2
2770	E46	SOX2
2771	E65	SOX2
2772	E46	SOX2/3/8
2773	E27	SOX2-OT
2774	E46	SOX3/8
2775	E33	SOX4
2776	E24	SOX5
2777	E65	SOX5
2778	E24	SOX6
2779	E59	Sox6
2780	E46	SOX8
2781	E24	SOX9
2782	E51	SOX9
2783	E56	SOX9
2784	E2	SP5
2785	E65	SP5
2786	E2	SPAG5
2787	E43	SPANXB1
2788	E43	SPANXB2
2789	E26	Sparc
2790	E40	SPARC
2791	E14	SPARC
2792	E66	SPATA18
2793	E2	SPATA24

2794	E58	SPDEF
2795	E54	SPDEF
2796	E24	SPDYE1
2797	E54	SPEF1
2798	E66	SPEN
2799	E59	Sphk1
2800	E58	SPI1
2801	E53	SPIB
2802	E2	SPICE1
2803	E33	SPINT2
2804	E21	SPOCD1
2805	E43	SPOCD1
2806	E41	SPOCK1
2807	E19	SPP1
2808	E69	Spp1
2809	E45	Spr2a3
2810	E41	SPRED3
2811	E14	SPRED3
2812	E33	SPRY1
2813	E49	Spry2
2814	E69	Spry2
2815	E51	SPRY4
2816	E31	SPSB4
2817	E26	Sptbn2
2818	E67	Sqstm1
2819	E66	SRCAP
2820	E21	SRGAP1
2821	E27	SRL
2822	E2	SRL
2823	E43	SRPX
2824	E44	SSBP2
2825	E21	SSTR3
2826	E65	ST18
2827	E21	ST3GAL5
2828	E31	ST3GAL5
2829	E42	ST6GALNAC1
2830	E24	ST8SIA1
2831	E16	STAC
2832	E66	STAC
2833	E50	STAM2
2834	E59	Stap2
2835	E32	STAR
2836	E60	STARD4

2837	E66	STARD4
2838	E58	STARD8
2839	E43	STC1
2840	E22	STC2
2841	E38	STC2
2842	E54	STC2
2843	E8	STEAP1
2844	E54	STEAP1
2845	E44	STEAP4
2846	E54	STEAP4
2847	E16	STK17A
2848	E41	STK32B
2849	E13	STK39
2850	E63	STMN1
2851	E17	STMN3
2852	E17	STMN4
2853	E27	STON1-GTF2A1L
2854	E58	STX19
2855	E59	Stxbp6
2856	E3	SULT1C2
2857	E42	SULT1C2
2858	E32	SULT2A1
2859	E68	SULT2A1
2860	E24	SUZ12
2861	E26	Sv2b
2862	E1	SVEP1
2863	E4	SYN2
2864	E40	SYNE1
2865	E41	SYNPO
2866	E12	SYT1
2867	E58	SYT1
2868	E4	SYT2
2869	E26	Tac1
2870	E51	TAC1
2871	E65	TAC4
2872	E34	TACR2
2873	E20	TACR3
2874	E24	TAF13
2875	E1	TAGLN
2876	E40	TAGLN
2877	E43	TAGLN
2878	E70	Tagln

2879	E14	TAP1
2880	E31	TBC1D16
2881	E62	TBC1D16
2882	E17	TBC1D30
2883	E56	TBC1D30
2884	E65	TBX19
2885	E23	TBX21
2886	E24	TBXT
2887	E41	TCAF2
2888	E32	TCF21
2889	E39	TCF4
2890	E4	TCF7L1
2891	E26	Tcf7l2
2892	E27	TCF7L2
2893	E24	TCFL2
2894	E4	TDGF1
2895	E67	Tdrd7
2896	E2	TEAD2
2897	E25	TENM1
2898	E46	TERT
2899	E42	TESC
2900	E35	TFAP2B
2901	E35	TFDP1
2902	E14	TFE3
2903	E22	TFF3
2904	E58	TFF3
2905	E8	TFPI2
2906	E21	TFRC
2907	E19	TG
2908	E41	TGFA
2909	E24	TGFB1
2910	E16	TGFB1
2911	E21	TGFB1
2912	E70	Tgfb2
2913	E70	Tgfb3
2914	E67	Tgif1
2915	E2	TGIF2
2916	E29	TGM2
2917	E33	TGM2
2918	E43	TGM2
2919	E59	Tgm2
2920	E23	TGM4
2921	E17	TH

2922	E60	THBS1
2923	E40	THBS2
2924	E14	THNSL1
2925	E1	THY1
2926	E13	THY1
2927	E27	TIAM1
2928	E2	TIFA
2929	E58	TIMD4
2930	E2	TIMELESS
2931	E14	TIMM50
2932	E21	TIMP1
2933	E31	TIRAP
2934	E63	TK1
2935	E70	Tk1
2936	E31	TLCD1
2937	E46	TLE1
2938	E39	TLE4
2939	E41	TLE4
2940	E67	Tlr3
2941	E41	TLR4
2942	E42	TM4SF20
2943	E65	TMBIM6
2944	E42	TMC5
2945	E58	TMC5
2946	E14	TMC8
2947	E15	TMED1
2948	E1	TMEM125
2949	E23	TMEM156
2950	E43	TMEM158
2951	E43	TMEM166
2952	E31	TMEM170A
2953	E31	TMEM170B
2954	E29	TMEM176A
2955	E49	Tmem176a
2956	E29	TMEM176B
2957	E49	Tmem176b
2958	E26	Tmem212
2959	E54	TMEM22
2960	E26	Tmem30
2961	E17	TMEM35
2962	E65	TMEM38B
2963	E8	TMEM45B
2964	E15	TMEM59

2965	E52	TMEM74
2966	E26	Tmem88b
2967	E2	TMEM9
2968	E29	TMEM91
2969	E15	TMEM98
2970	E56	TMIE
2971	E35	TMIGD2
2972	E1	TMPRSS13
2973	E31	TMPRSS5
2974	E27	TMTC2
2975	E21	TNC
2976	E40	TNC
2977	E57	TNC
2978	E11	TNF
2979	E38	TNFAIP3
2980	E49	Tnfaip3
2981	E66	TNFRSF10B
2982	E42	TNFRSF11A
2983	E8	TNFRSF12A
2984	E21	TNFRSF12A
2985	E28	TNFRSF13B
2986	E28	TNFRSF13C
2987	E21	TNFRSF14
2988	E28	TNFRSF17
2989	E21	TNFRSF19
2990	E55	Tnfrsf19
2991	E67	Tnfrsf1b
2992	E47	TNFRSF21
2993	E37	TNFRSF8
2994	E14	TNFRSF9
2995	E54	TNFRSF9
2996	E2	TNFSF10
2997	E44	TNFSF10
2998	E54	TNFSF4
2999	E67	Tnfsf9
3000	E35	TNIK
3001	E64	TNIK
3002	E65	TNNI1
3003	E58	TNNT1
3004	E49	Tnnt2
3005	E1	TNS1
3006	E1	TNS4
3007	E36	TNS4

3008	E29	TOP2A
3009	E63	TOP2A
3010	E17	TOX
3011	E37	TOX
3012	E42	TOX3
3013	E50	TP53
3014	E43	TP53INP1
3015	E60	TP63
3016	E46	TP73
3017	E60	TP73
3018	E39	TPBG
3019	E41	TPBG
3020	E12	TPH1
3021	E29	TPI1
3022	E70	Tpk1
3023	E41	TPM1
3024	E70	Tpm1
3025	E1	TPM2
3026	E37	TPM2
3027	E43	TPM2
3028	E19	TPO
3029	E60	TPO
3030	E21	TPP1
3031	E54	TPPP3
3032	E37	TPST2
3033	E65	TPT1
3034	E14	TRAM2
3035	E47	TRAM2
3036	E58	TRDC
3037	E26	Trf
3038	E11	TRIAP1
3039	E25	TRIB1
3040	E69	Trib1
3041	E49	Trib2
3042	E69	Trib2
3043	E24	TRIL
3044	E7	TRIM29
3045	E2	TRIM37
3046	E4	TRIM71
3047	E51	TRIM9
3048	E67	Trip10
3049	E12	TRIT1
3050	E1	TRO

3051	E16	TRPC1
3052	E54	TRPC1
3053	E15	TRPC6
3054	E14	TRPM1
3055	E34	TRPV4
3056	E70	Trpv4
3057	E7	TRPV6
3058	E38	TRPV8
3059	E60	TSC2
3060	E33	TSC22D3
3061	E18	TSFM
3062	E57	TSGA10
3063	E19	TSHR
3064	E20	TSHZ1
3065	E59	Tshz2
3066	E65	TSHZ2
3067	E68	TSPAN12
3068	E43	TSPAN13
3069	E69	Tspan13
3070	E69	Tspan3
3071	E18	TSPAN31
3072	E15	TSPAN8
3073	E42	TSPAN8
3074	E63	TSPYL3
3075	E33	TTC3
3076	E35	TTC3
3077	E26	Ttr
3078	E51	TTYH1
3079	E11	TUBA4A
3080	E25	TUBB2B
3081	E17	TUBB2B
3082	E58	TUBB2B
3083	E65	TUBB4A
3084	E66	TUBB4A
3085	E2	TXNDC16
3086	E21	TXNIP
3087	E33	TXNIP
3088	E45	Txnip
3089	E31	TYW1
3090	E48	UAP1
3091	E21	UAP1L1
3092	E50	UBASH3B
3093	E35	UBB

3094	E67	Ube216
3095	E14	UBE2E3
3096	E14	UBE2H
3097	E31	UBL3
3098	E23	UCHL1
3099	E34	UCN2
3100	E45	Ugdh
3101	E45	Ugt2b34
3102	E23	UGT3A1
3103	E14	ULBP2
3104	E4	UNC13C
3105	E20	UNC5A
3106	E62	UNC5A
3107	E17	UNC5C
3108	E6	UNC5D
3109	E46	UNCX
3110	E2	UNG
3111	E54	UPP1
3112	E31	USB1
3113	E42	USH1C
3114	E62	VAMP7
3115	E26	Vat1l
3116	E2	VAV3
3117	E26	Vcan
3118	E16	VCAN
3119	E43	VCAN
3120	E56	VCAN
3121	E21	VCL
3122	E35	VCL
3123	E2	VDR
3124	E60	VDR
3125	E29	VEGFA
3126	E19	VEGFA
3127	E54	VEGFA
3128	E21	VGF
3129	E21	VGLL4
3130	E33	VGLL4
3131	E42	VIL1
3132	E16	VIM
3133	E66	VIM
3134	E65	VIPR1
3135	E1	VIT
3136	E31	VKORC1L1

3137	E31	VMAC
3138	E29	VMP1
3139	E30	VPS9D1-AS1
3140	E32	VSNL1
3141	E40	VSNL1
3142	E65	VSTM2A
3143	E52	VTCN1
3144	E66	VWA1
3145	E58	VWA2
3146	E54	VWA5A
3147	E66	VWA5B2
3148	E56	VWDE
3149	E26	Vxn
3150	E27	WASF3
3151	E4	WDFY2
3152	E14	WDR43
3153	E16	WDR47
3154	E68	WDR63
3155	E23	WDR72
3156	E58	WDR72
3157	E2	WDR90
3158	E70	Wee1
3159	E25	WFDC1
3160	E2	WFDC15B
3161	E29	WFDC2
3162	E70	Wisp1
3163	E54	WISP2
3164	E70	Wisp2
3165	E65	WNT16
3166	E46	WNT3A
3167	E39	WNT5A
3168	E46	WNT5A
3169	E54	WNT6
3170	E58	WNT6
3171	E40	WNT7A
3172	E49	Wnt7a
3173	E46	WNT7B
3174	E10	WRN
3175	E37	WSB2
3176	E70	Wwc1
3177	E24	WWP2
3178	E37	XBP1
3179	E60	XBP1

3180	E47	XBP1
3181	E58	XCL2
3182	E66	XIST
3183	E14	XKRX
3184	E24	XYLB
3185	E35	YAP1
3186	E54	YARS
3187	E18	YEATS4
3188	E33	YPEL3
3189	E58	YWHAEP7
3190	E37	ZA20D3
3191	E35	ZADH2
3192	E37	ZAP70
3193	E54	ZBED2
3194	E65	ZBED2
3195	E67	Zbp1
3196	E37	ZBT20
3197	E2	ZBTB12
3198	E26	Zbtb18
3199	E31	ZBTB41
3200	E35	ZBTB7A
3201	E21	ZCCHC12
3202	E33	ZCCHC24
3203	E62	ZCCHC3
3204	E39	ZEB1
3205	E33	ZFAND5
3206	E66	ZFHX3
3207	E2	ZFP566
3208	E65	ZFPM2
3209	E26	Zic1
3210	E65	ZIC2
3211	E46	ZIC5
3212	E65	ZIC5
3213	E2	ZKSCAN17
3214	E43	ZMAT3
3215	E66	ZMAT3
3216	E23	ZMAT4
3217	E65	ZMAT4
3218	E66	ZMIZ1
3219	E54	ZMYND10
3220	E27	ZMYND8
3221	E60	ZNF185
3222	E65	ZNF385B

3223	E31	ZNF396
3224	E66	ZNF428
3225	E65	ZNF536
3226	E14	ZNF704
3227	E35	ZNF704
3228	E65	ZNF750
3229	E14	ZNF75D
3230	E61	ZNF791
3231	E65	ZNF804A
3232	E4	ZSCAN10
3233	E21	ZYX
3234	E43	ZYX
3235	E26	1110017D15Rik
3236	E45	1700030C14Rik
3237	E45	1700031L13Rik
3238	E26	1700094D03Rik
3239	E26	2900040C04Rik